Precise Orbit Determination

Adrian Jäggi

AIUB

Astronomical Institute

University of Bern

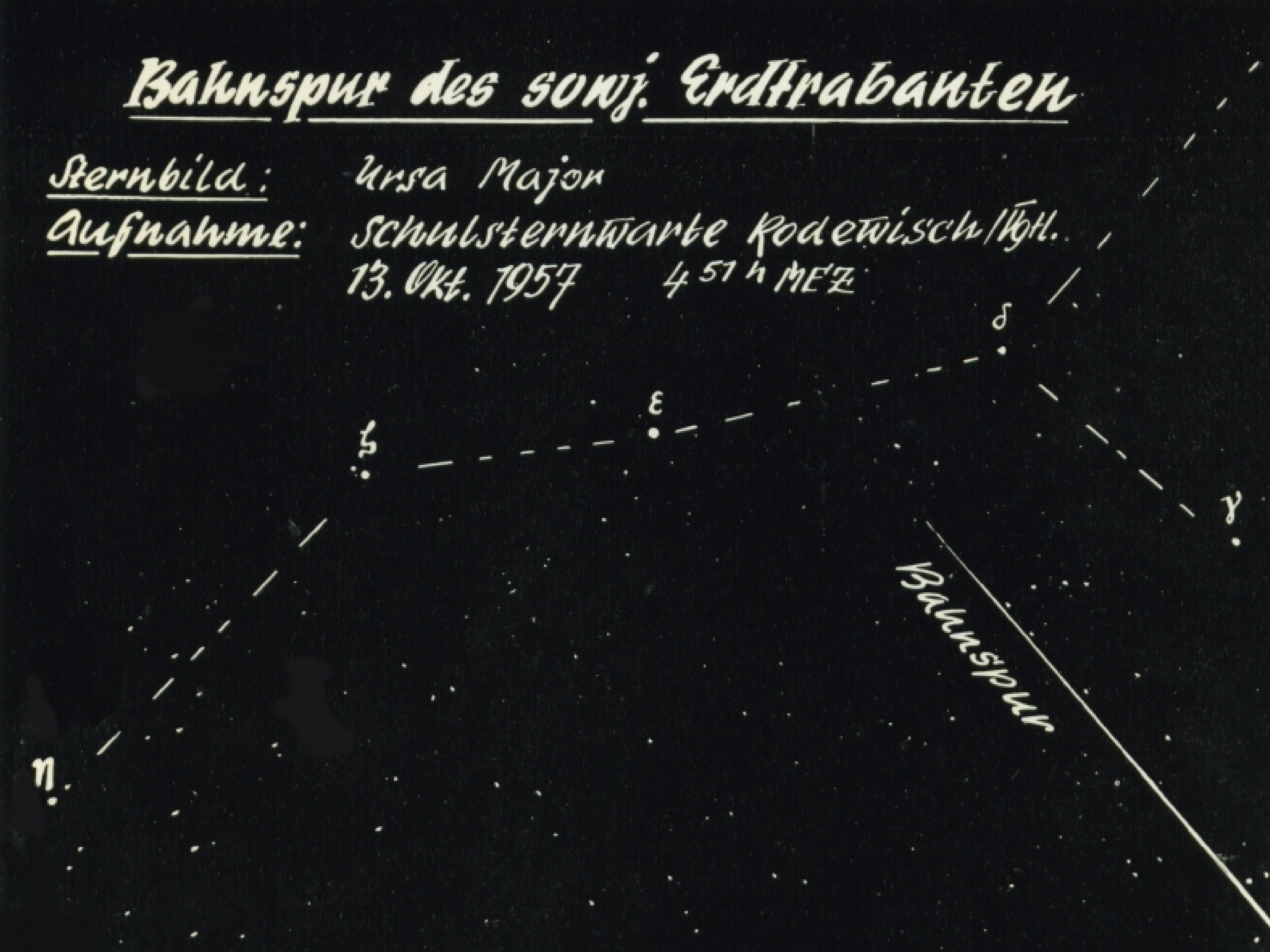
Bahnspur des sowj. Erdtrabanten
Sternbild: Ursa Major
Aufnahme: Schulsternwarte Rodewisch/Vgtl.
13. Okt. 1957 4 57 h MEZ
δ
ε
ζ
γ
η
Bahnspur

Low Earth Orbiters (LEOs)

CHAMP

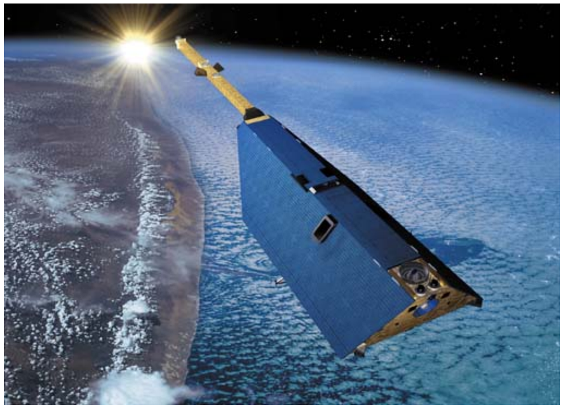

CHA**llenging**
Minisatellite **P**ayload

GRACE

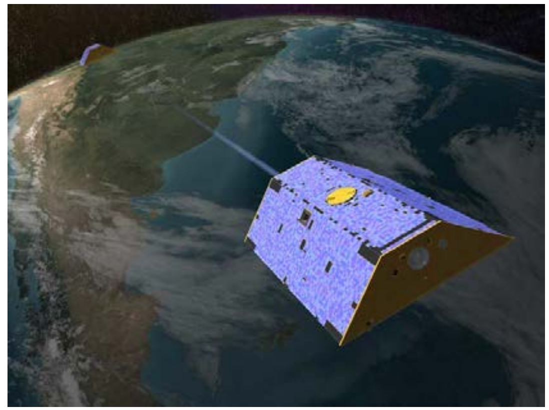

Gravity **R**ecovery **A**nd
Climate **E**xperiment

GOCE

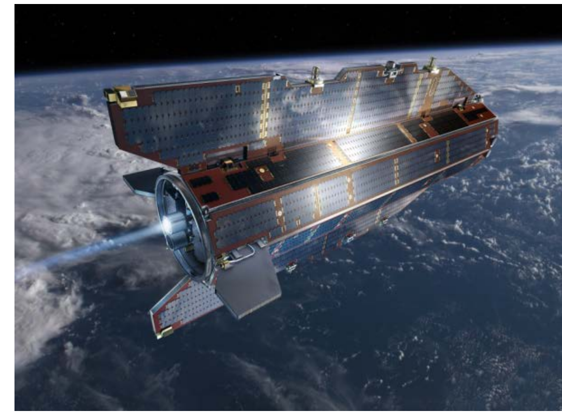

Gravity and
steady-state **O**cean
Circulation **E**xplorer

Of course, there are many more missions equipped with GPS receivers

Jason

Jason-2

MetOp-A

Icesat

COSMIC

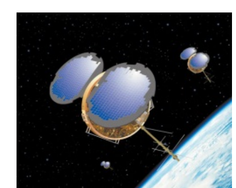

LEO Constellations

TanDEM-X

Swarm

Sentinel

and of course, in the future

Spherical SLR Satellites

Starlette

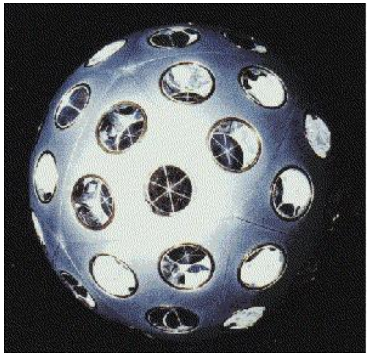

Stella

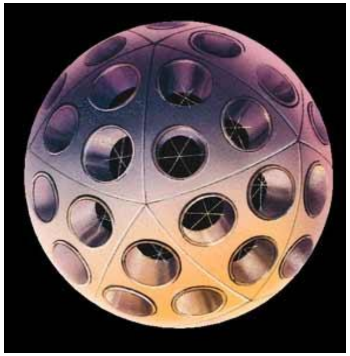

LARES

Ajisai

LAGEOS

Etalon

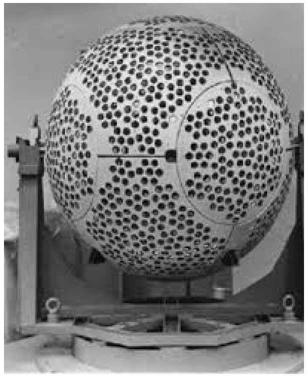

Wilhelm und Else Heraeus Autumn School
Global Gravity Field Modeling
from Satellite-to-Satellite Tracking Data

Satellite Laser Ranging

Introduction to SLR

SLR: **S**atellite **L**aser **R**anging

Characteristics:

- Satellites equipped with **retro-reflectors**
- **Global** whenever satellites are **visible**
- **Small** number of scientific users
- **Weather-dependent** (optical signals are passing through the atmosphere)
- **1-dimensional distance** information

Wilhelm und Else Heraeus Autumn School
Global Gravity Field Modeling
from Satellite-to-Satellite Tracking Data

SLR Space Segment

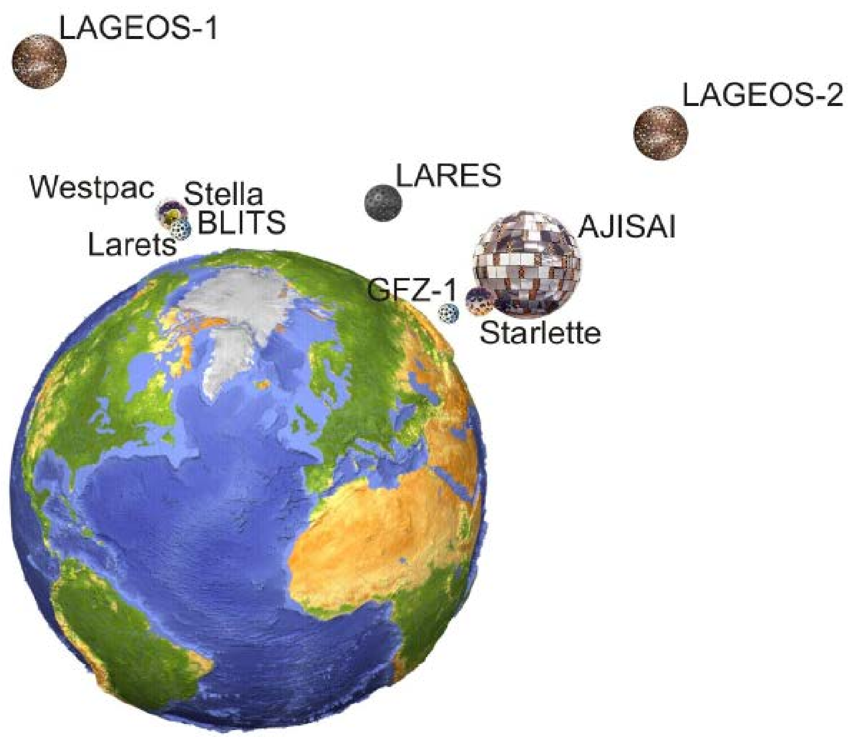

- The space segment is rather **small**, but **long lasting** (passive satellites)

- Apart from GFZ-1, Westpac and BLITS, **all** satellites are still actively used for SLR activities

SLR Ground Segment

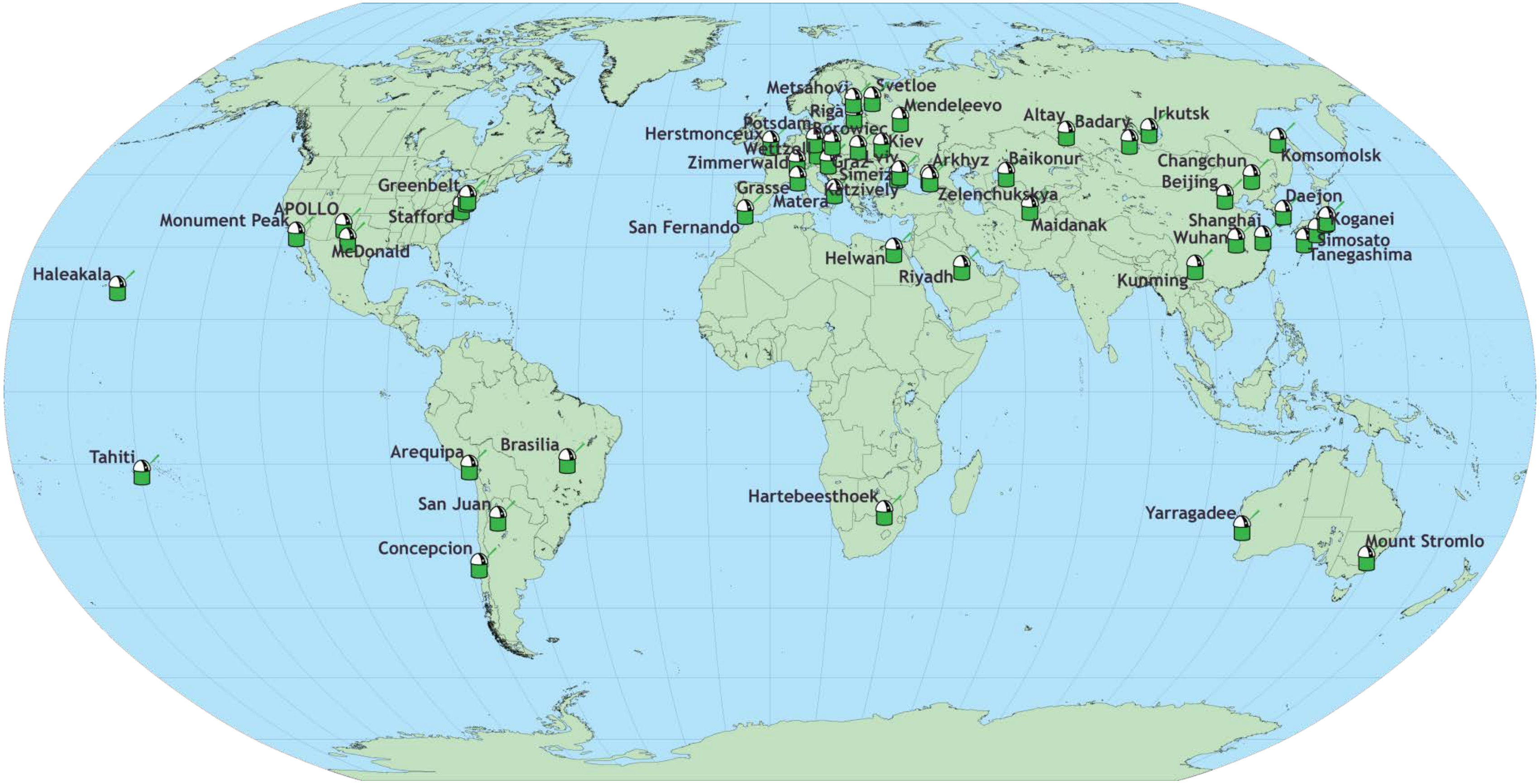

ILRS stations, http://ilrs.gsfc.nasa.gov/

SLR Ground Segment

Each SLR station consists of:

- **Laser Oscillator**: Neodym-YAG (532 nm) or Titanium-Saphir (423 nm) lasers to generate ultra-short, high-energetic laser pulses

- **Optical Telescope**: targeted emission of the laser pulses

- **Reception System**: Optical telescope and detectors to register the incoming photons

- **Timing Facility**: Epoch registration and time of flight measurement

Most of the SLR stations within the ILRS are unique prototypes

The Zimmerwald SLR Station

The Zimmerwald SLR Station

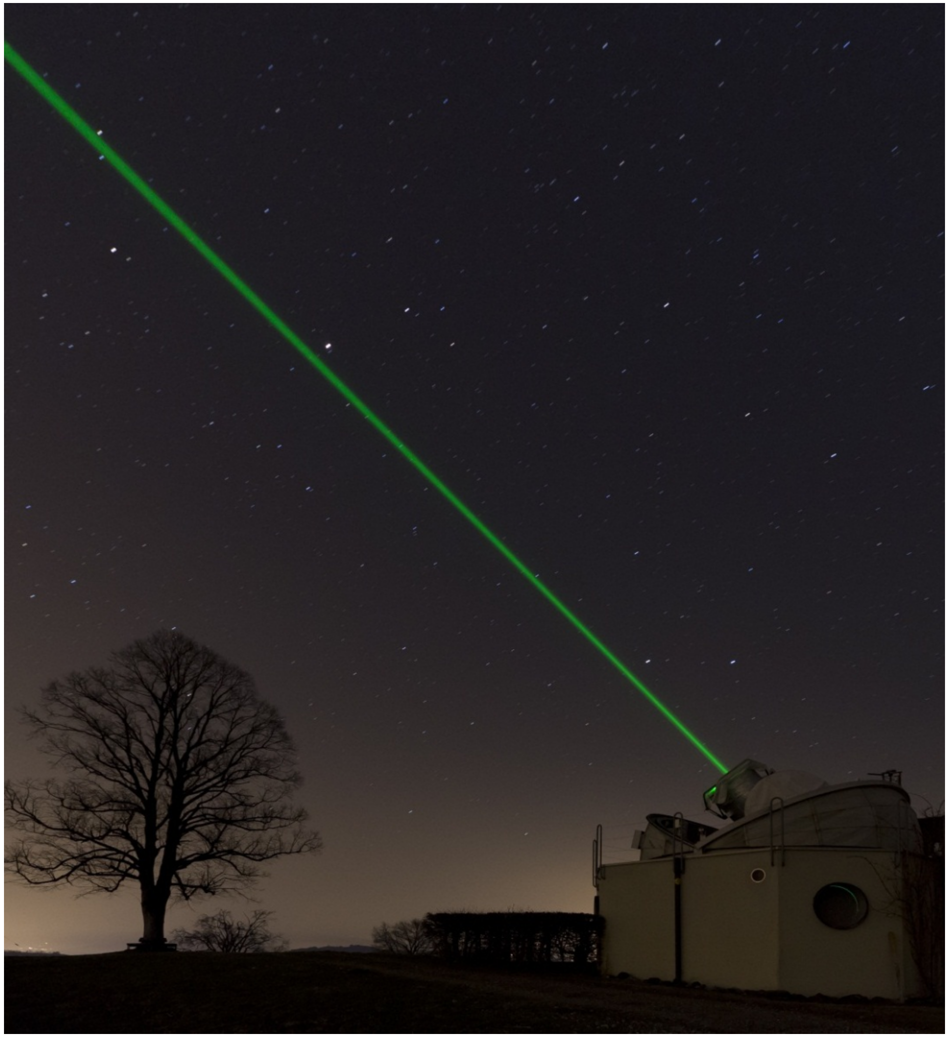

Wilhelm und Else Heraeus Autumn School
Global Gravity Field Modeling
from Satellite-to-Satellite Tracking Data

ILRS Station Performance (1)

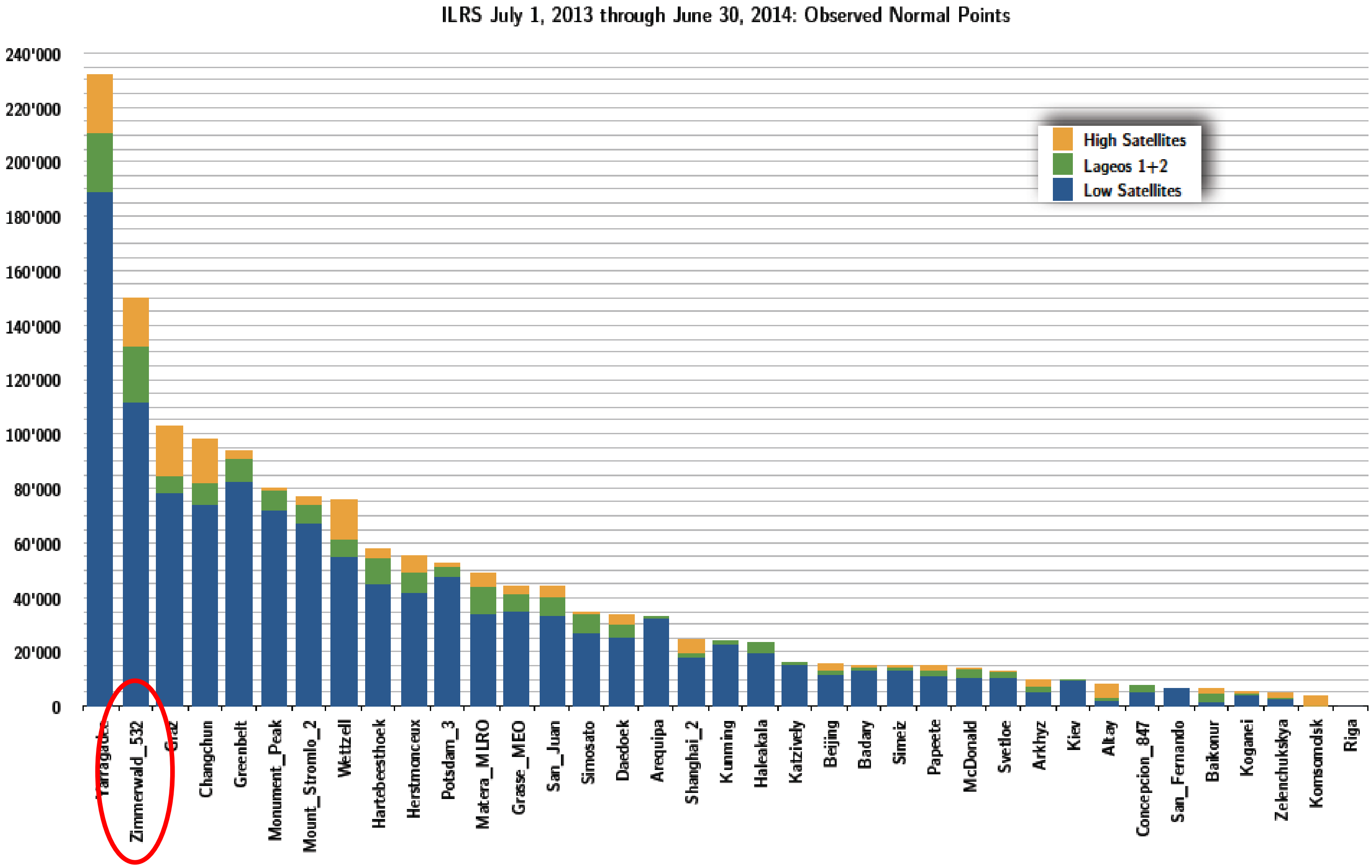

ILRS Station Performance (2)

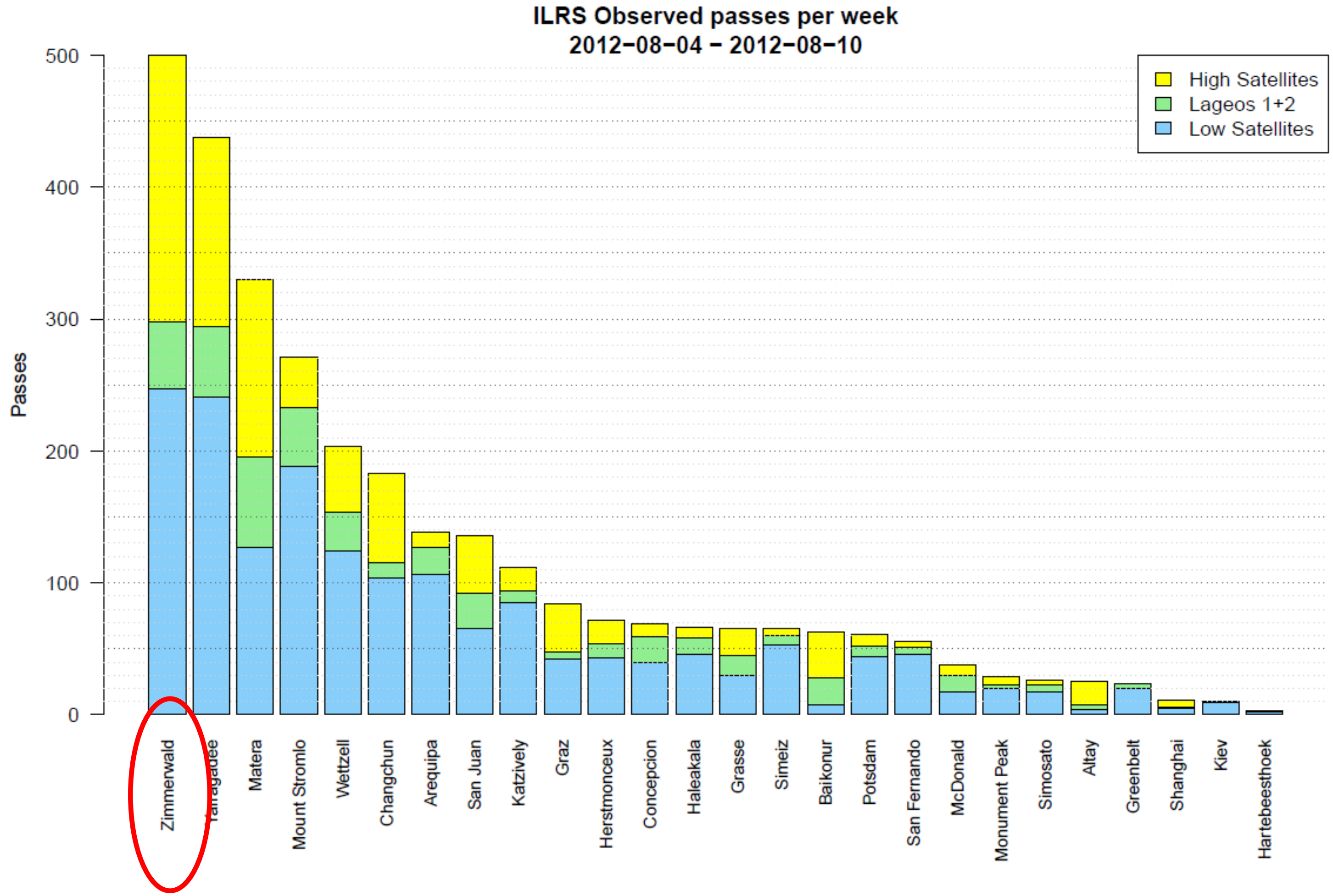

Spatial Coverage of SLR Measurements

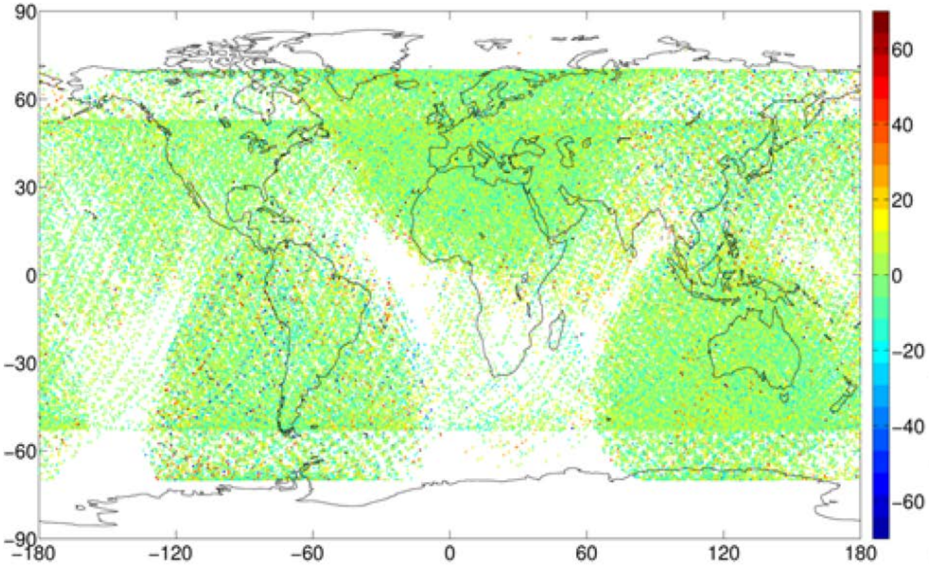

LAGEOS-1/2 (year 2009)

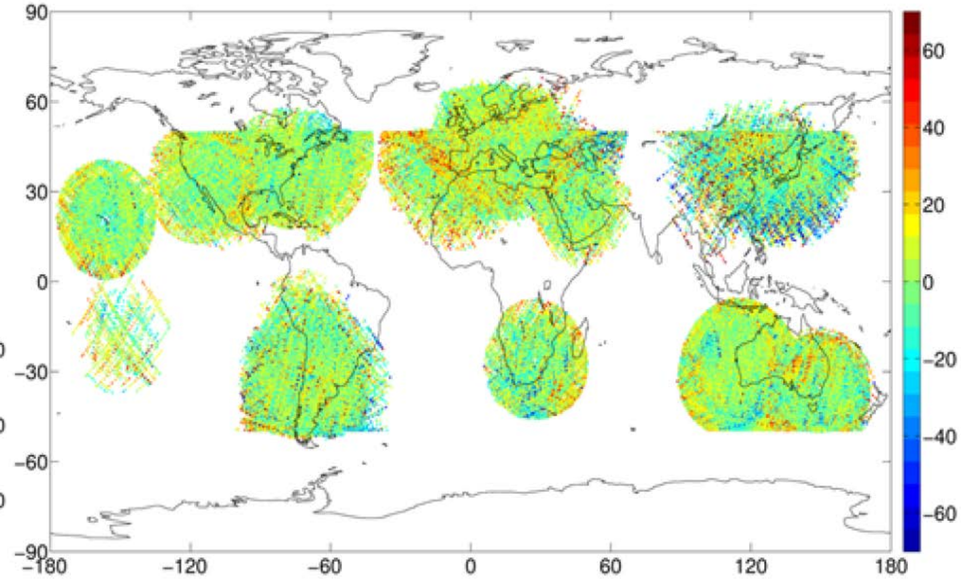

Stella, Starlette, AJISAI (year 2009)

SLR Measurements

SLR Observations Δt_i^k are defined as:

$$\Delta t_i^k = \tau_{i,up}^k + \tau_{i,down}^k$$

Δt_i^k Round-trip time of flight

$\tau_{i,up}^k$ Time of flight from the laser station to the satellite

$\tau_{i,down}^k$ Time of flight from the satellite back to the laser station

- SLR observations are unbiased „**range**“ (distance) measurements

- **Measurement noise**: mm to cm for single-shot measurements

Relation to Position Vectors

Neglecting atmospheric delays, Δt_i^k may be expressed by:

$$\Delta t_i^k = \frac{1}{c}\left(|\boldsymbol{r}_i(t_{sat} - \tau_{i,up}^k) - \boldsymbol{r}^k(t_{sat})| + |\boldsymbol{r}_i(t_{sat} + \tau_{i,down}^k) - \boldsymbol{r}^k(t_{sat})|\right)$$

$\boldsymbol{r}_i$ Inertial position of the SLR station at pulse emission and reception time

$\boldsymbol{r}^k$ Inertial position of the satellite at pulse reflection time

For terrestrial SLR, Δt_i^k may be approximated by:

$$\Delta t_i^k = \frac{2}{c}\,|\boldsymbol{r}_i(t_{sat}) - \boldsymbol{r}^k(t_{sat})|$$

Global Positioning System

Introduction to GPS

GPS

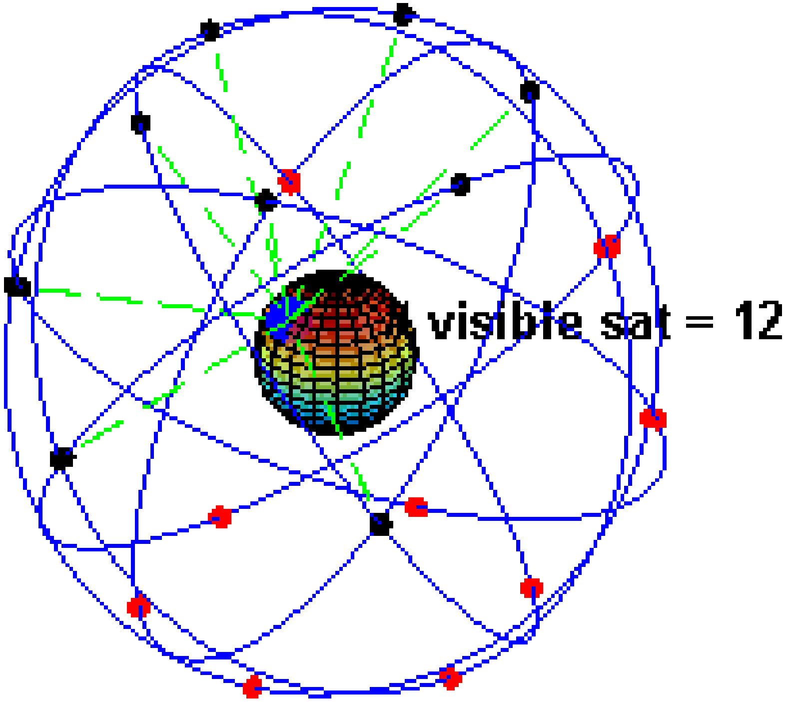

Galileo

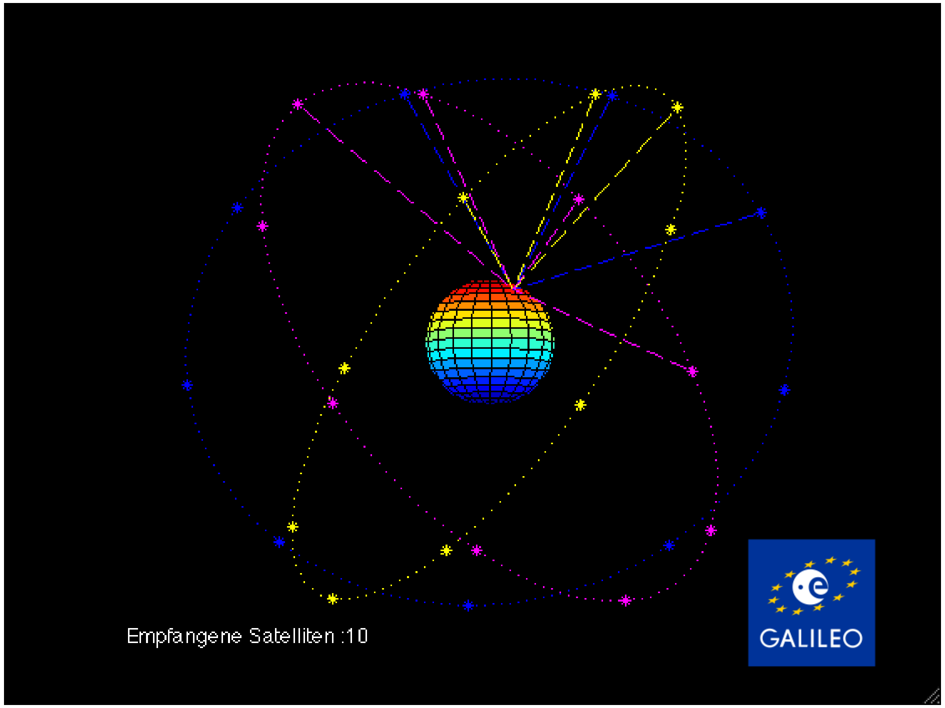

Other GNSS are already existing (GLONASS) or being built up (Galileo), but so far there are no multi-GNSS spaceborne receivers in orbit.

Introduction to GPS

GPS: **G**lobal **P**ositioning **S**ystem

Characteristics:

- Satellite system for (real-time) **Positioning** and **Navigation**
- **Global** (everywhere on Earth, up to altitudes of 5000km) and **at any time**
- **Unlimited** number of users
- **Weather-independent** (radio signals are passing through the atmosphere)
- **3-dimensional position**, **velocity** and **time** information

Wilhelm und Else Heraeus Autumn School
Global Gravity Field Modeling
from Satellite-to-Satellite Tracking Data

GPS Segments

The GPS consists of **3 main segments**:

- **Space Segment**: the satellites and the constellation of satellites
- **Control Segment**: the ground stations, infrastructure and software for operation and monitoring of the GPS
- **User Segment**: all GPS receivers worldwide and the corresponding processing software

We should add an important **4th segment**:

- **Ground Segment**: all civilian permanent networks of reference sites and the international/regional/local services delivering products for the users

Wilhelm und Else Heraeus Autumn School
Global Gravity Field Modeling
from Satellite-to-Satellite Tracking Data

Space Segment

- The space segment nominally consists of **24 satellites**, presently: 32 active GPS satellites

- Constellation design: at least **4 satellites** in view from **any location** on the Earth at **any time**

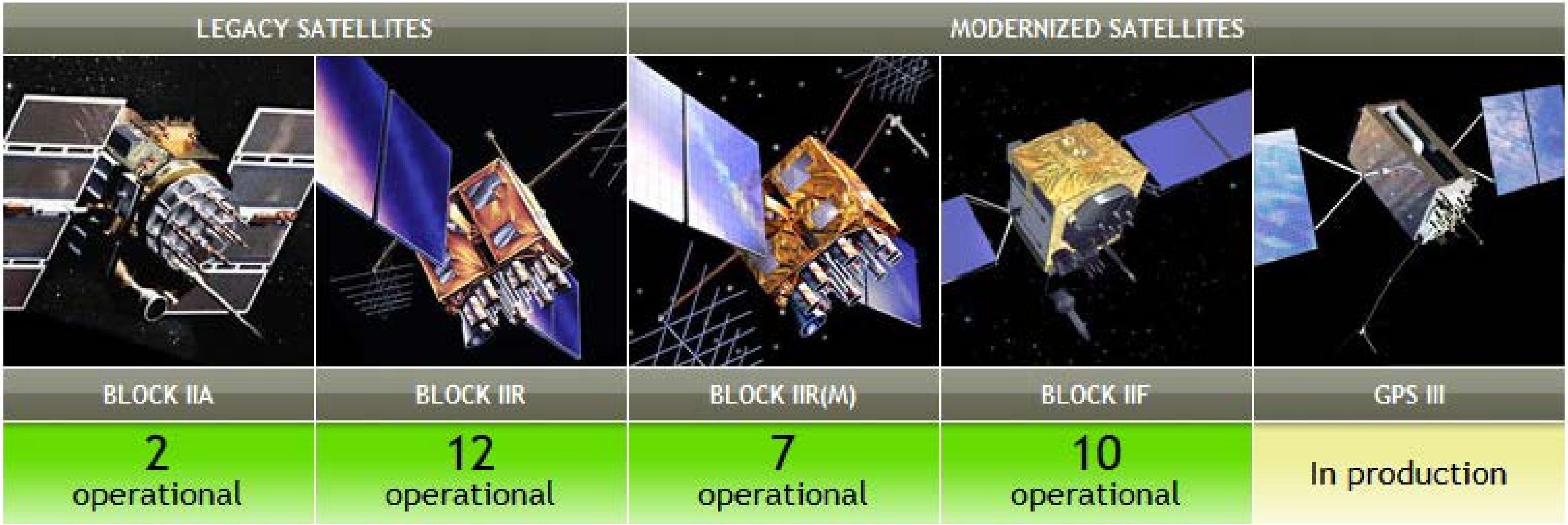

Global Network of the IGS

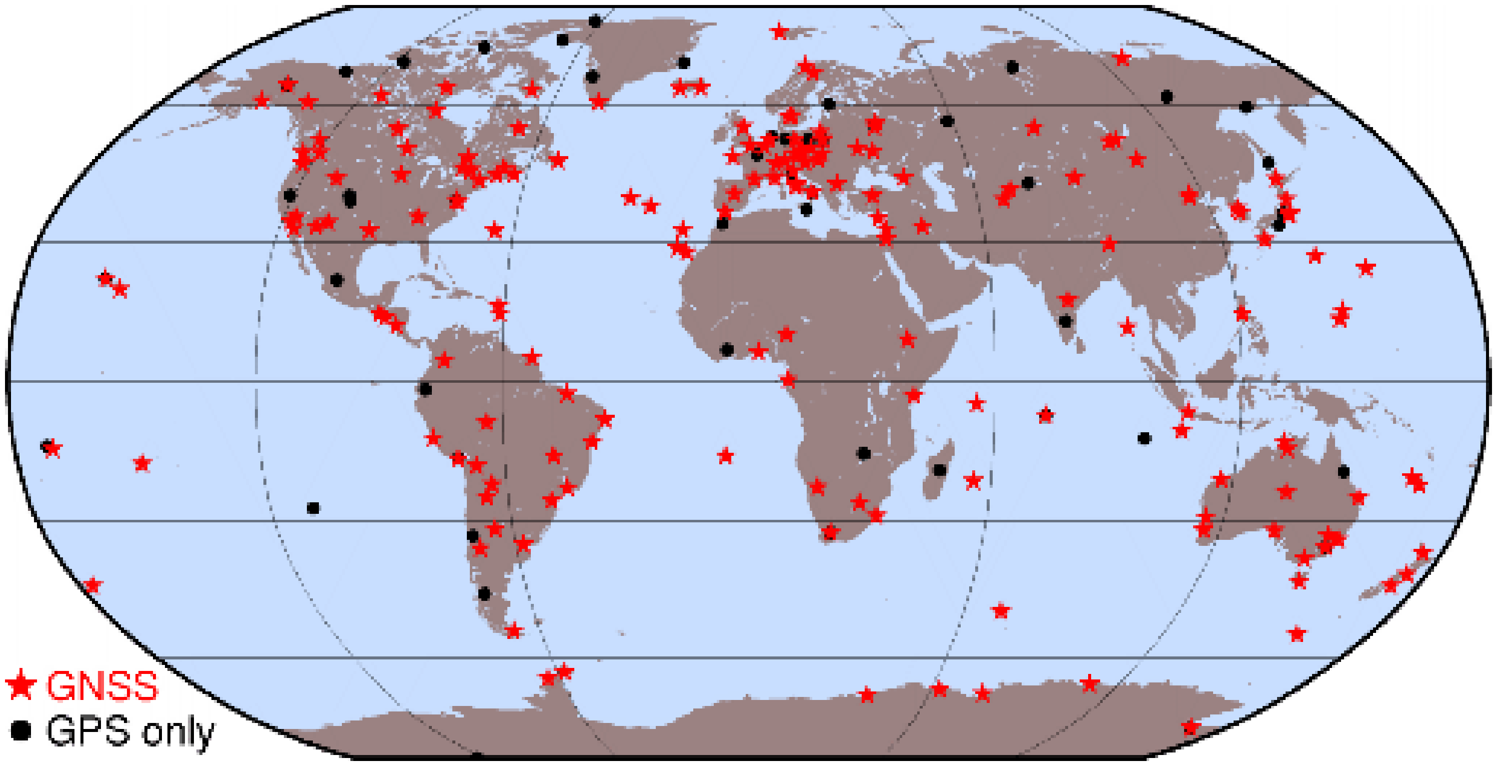

IGS stations used for computation of final orbits at CODE (Dach et al., 2009)

Parameters of a Global IGS Solution

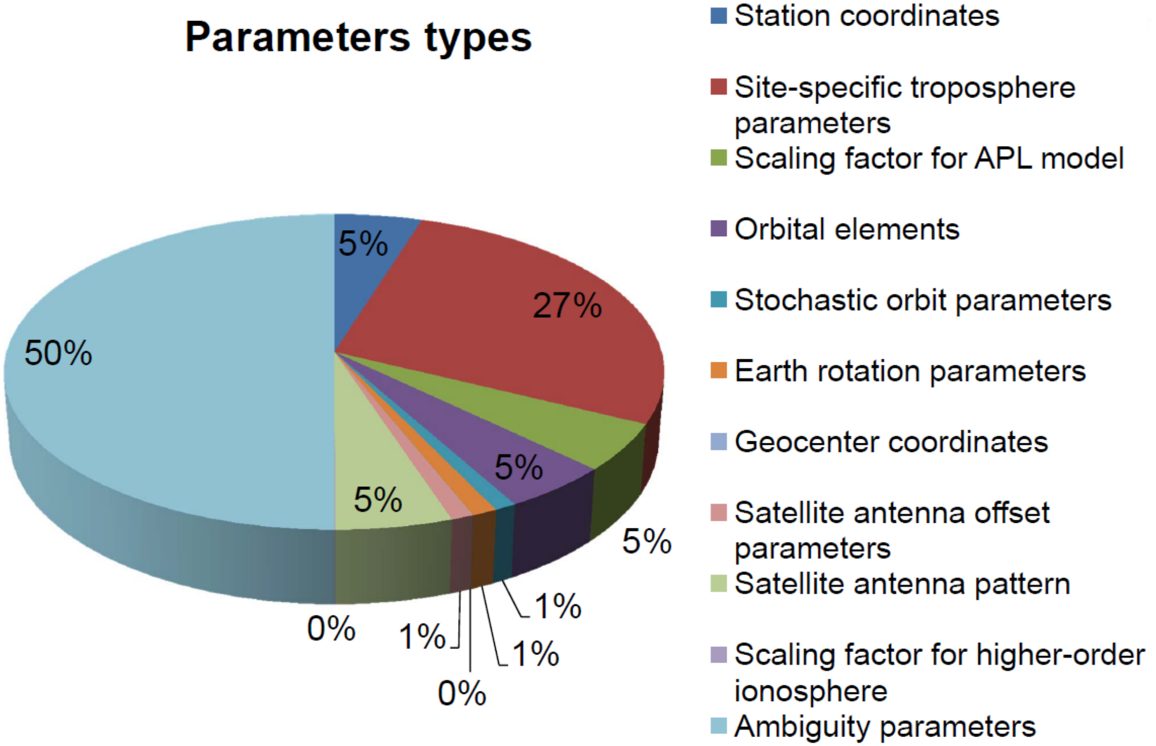

- Large number of **measurement type specific parameters**
- Rather small number of **orbital parameters**

Performance of IGS Final Orbits

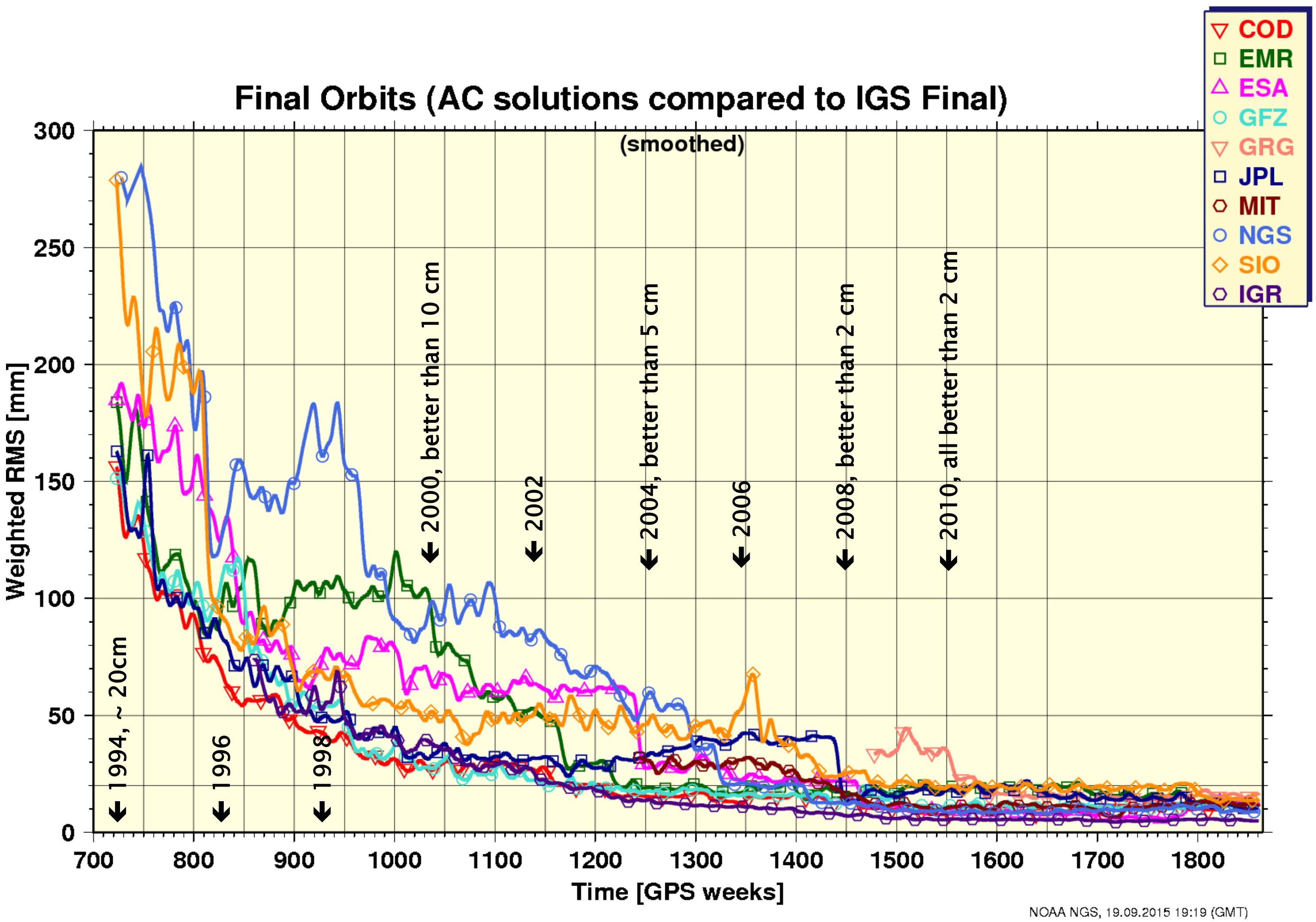

Computation of Final Clocks at CODE

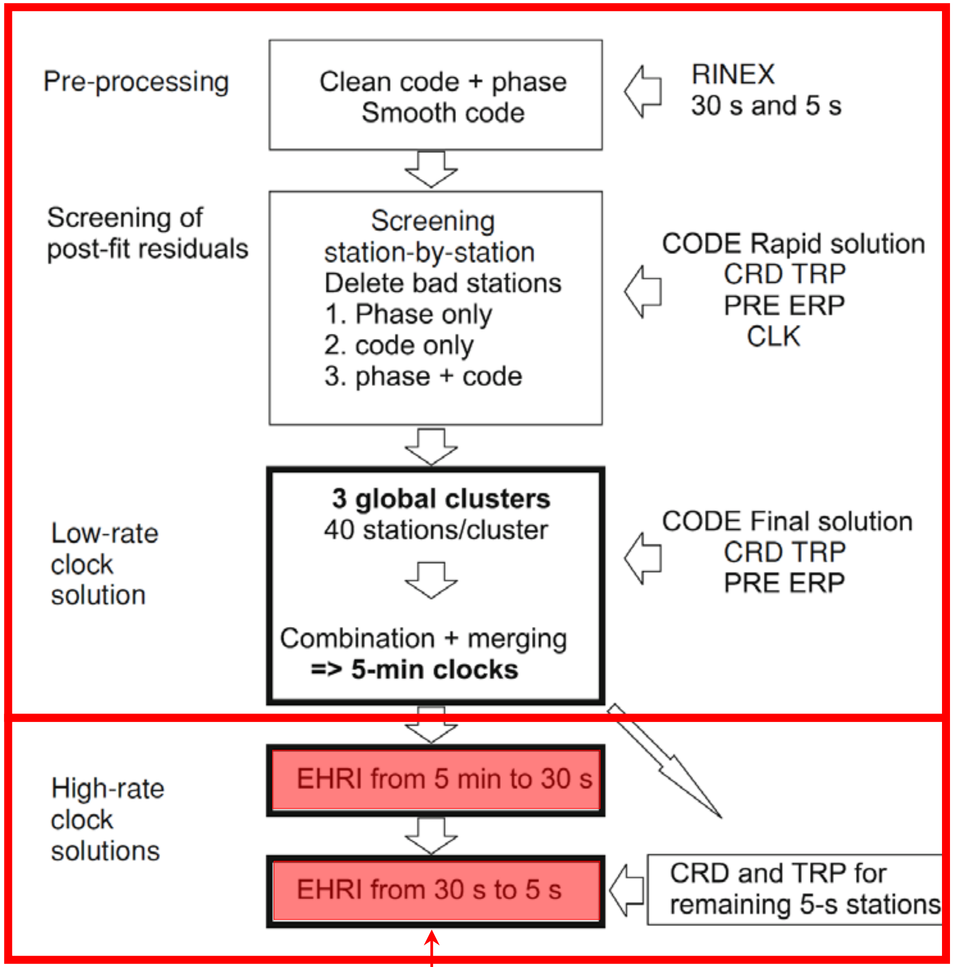

(Bock et al., 2009)

The final clock product with 5 min sampling is based on undifferenced GPS data of typically 120 stations of the IGS network

The IGS 1 Hz network is finally used for clock densification to 5 sec

The 5 sec clocks are interpolated to 1 sec as needed for 1 Hz LEO GPS data

GPS Signals

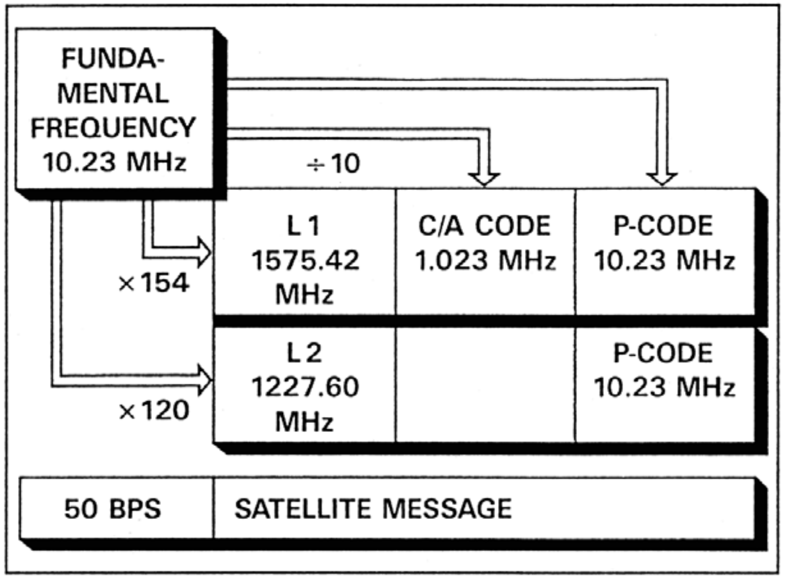

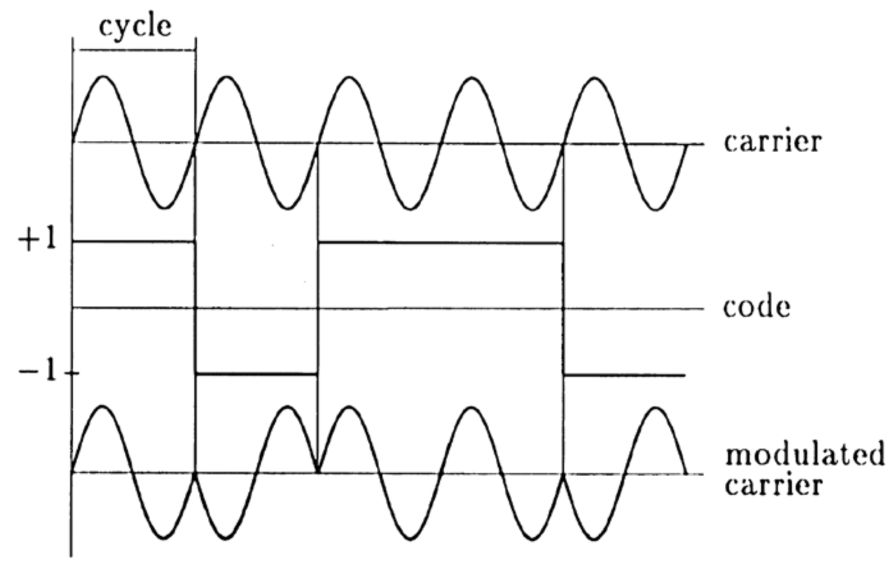

Signals driven by an **atomic clock**

Two **carrier signals** (sine waves):

- **L1**: f = 1575.43 MHz, λ = 19 cm
- **L2**: f = 1227.60 MHz, λ = 24 cm

Bits encoded on carrier by phase modulation:

- **C/A-code** (Clear Access / Coarse Acquisition)
- **P-code** (Protected / Precise)
- **Broadcast/Navigation Message**

Pseudorange / Code Measurements

Code Observations P_i^k are defined as:

$$P_i^k \doteq c\,(T_i - T^k)$$

c Spee

T_i Recei

T^k GPS ... ne)

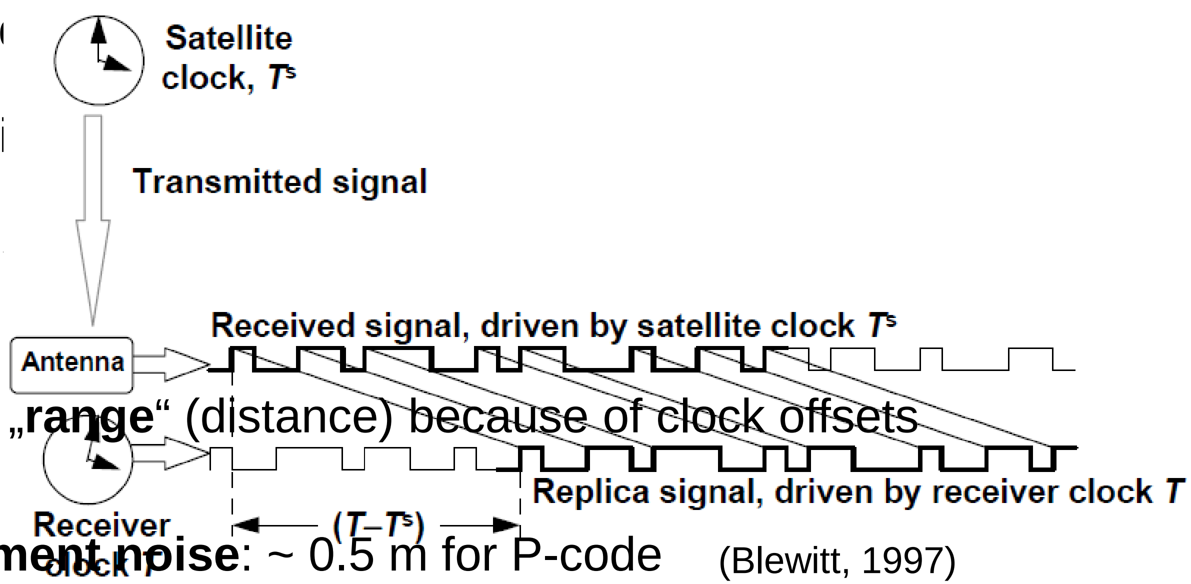

- No actual „**range**“ (distance) because of clock offsets

- **Measurement noise**: ~ 0.5 m for P-code (Blewitt, 1997)

Code Observation Equation

$$P_i^k = \rho_i^k - c \cdot \Delta t^k + c \cdot \Delta t_i$$

t_i, t^k	GPS time of reception and emission
Δt^k	Satellite clock offset $T^k - t^k$
Δt_i	Receiver clock offset $T_i - t_i$
ρ_i^k	Distance between receiver and satellite $c\,(t_i - t^k)$

Known from ACs or IGS:

- satellite positions $(x^{k_j}, y^{k_j}, z^{k_j})$
- satellite clock offsets Δt^{k_j}

4 unknown parameters:

- receiver position (x_i, y_i, z_i)
- receiver clock offset Δt_i

Carrier Phase Measurements (1)

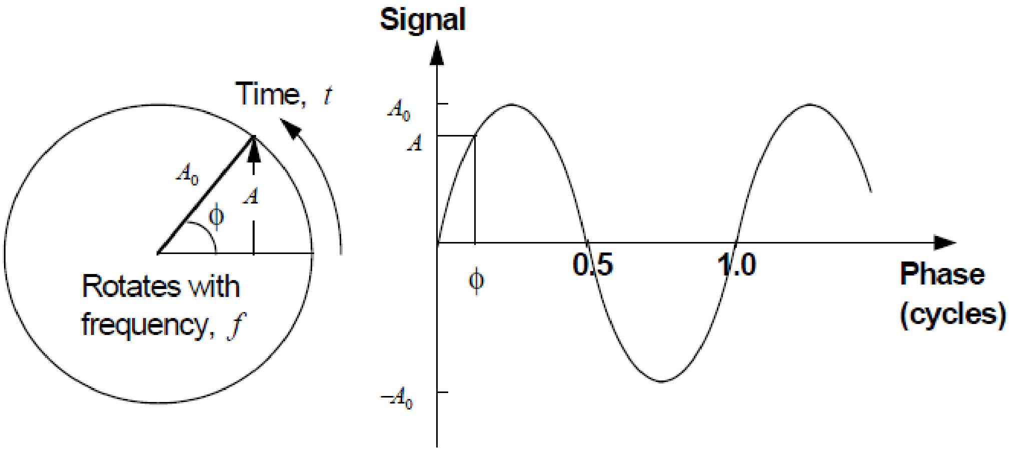

Phase ϕ (in cycles) increases linearly with time t:

$$\phi = f \cdot t$$

where f is the frequency

The **satellite** generates with its clock the phase signal ϕ^k. At emission time T^k (in satellite clock time) we have

$$\phi^k = f \cdot T^k$$

The same phase signal, e.g., a wave crest, propagates from the satellite to the receiver, but the receiver measures only the fractional part of the phase and does not know the **integer number of cycles** N_i^k (phase ambiguity):

$$\phi_i^k = \phi^k - N_i^k = f \cdot T^k - N_i^k$$

Carrier Phase Measurements (2)

The **receiver** generates with its clock a **reference phase.** At time of reception T_i of the satellite phase ϕ_i^k (in receiver clock time) we have:

$$\phi_i = f \cdot T_i$$

The actual **phase measurement** is the difference between receiver reference phase ϕ_i and satellite phase ϕ_i^k:

$$\psi_i^k = \phi_i - \phi_i^k = f \cdot T_i - (f \cdot T^k - N_i^k) = f \cdot (T_i - T^k) + N_i^k$$

Multiplication with the wavelength $\lambda = c/f$ leads to the **phase observation equation** in meters:

$$\begin{aligned} L_i^k &= \lambda \cdot \psi_i^k = c \cdot (T_i - T^k) + \lambda \cdot N_i^k \\ &= \rho_i^k - c \cdot \Delta t^k + c \cdot \Delta t_i + \lambda \cdot N_i^k \end{aligned}$$

Difference to the pseudorange observation: **integer ambiguity term** N_i^k

Improved Observation Equation

$$L_i^k = \rho_i^k - c \cdot \Delta t^k + c \cdot \Delta t_i + \cancel{T_i^k} + \cancel{I_i^k} + \lambda \cdot N_i^k$$
$$+ \Delta_{rel} - c \cdot b^k + c \cdot b_i + m_i^k + \epsilon_i^k$$

ρ_i^k	Distance between satellite and receiver ←	Satellite positions and clocks
Δt^k	Satellite clock offset wrt GPS time ←	are known from ACs or IGS
Δt_i	Receiver clock offset wrt GPS time	
$\cancel{T_i^k}$	~~Tropospheric delay~~ ←	Not existent for LEOs
$\cancel{I_i^k}$	~~Ionospheric delay~~ ←	Cancels out (first order only) when forming the ionosphere-free linear combination:
N_i^k	Phase ambiguity	
Δ_{rel}	Relativistic corrections	
b^k	Delays in satellite (cables, electronics)	
b_i	Delays in receiver and antenna	
m_i^k	Multipath, scattering, bending effects	
ϵ_i^k	Measurement error	

$$L_c = \frac{f_1^2}{f_1^2 - f_2^2} L_1 - \frac{f_2^2}{f_1^2 - f_2^2} L_2$$

Geometric Distance

Geometric distance ρ_{leo}^{k} is given by:

$$\rho_{leo}^{k} = \left|\boldsymbol{r}_{leo}(t_{leo}) - \boldsymbol{r}^{k}(t_{leo} - \tau_{leo}^{k})\right|$$

$\boldsymbol{r}_{leo}$ Inertial position of LEO antenna phase center at reception time

$\boldsymbol{r}^{k}$ Inertial position of GPS antenna phase center of satellite k at emission time

τ_{leo}^{k} Signal traveling time between the two phase center positions

Different ways to represent $\boldsymbol{r}_{leo}$:

- **Kinematic** orbit representation
- **Dynamic** or **reduced-dynamic** orbit representation

Orbit Representation

Kinematic Orbit Representation (1)

Satellite position $\boldsymbol{r}_{leo}(t_{leo})$ (in inertial frame) is given by:

$$\boldsymbol{r}_{leo}(t_{leo}) = \boldsymbol{R}(t_{leo}) \cdot (\boldsymbol{r}_{leo,e,0}(t_{leo}) + \delta\boldsymbol{r}_{leo,e,ant}(t_{leo}))$$

$\boldsymbol{R}$	Transformation matrix from Earth-fixed to inertial frame
$\boldsymbol{r}_{leo,e,0}$	LEO center of mass position in Earth-fixed frame
$\delta\boldsymbol{r}_{leo,e,ant}$	LEO antenna phase center offset in Earth-fixed frame

Kinematic positions $\boldsymbol{r}_{leo,e,0}$ are estimated for each **measurement epoch**:

- Measurement epochs **need not** to be identical with nominal epochs
- Positions are **independent** of models describing the LEO dynamics. Velocities cannot be provided

Kinematic Orbit Representation (2)

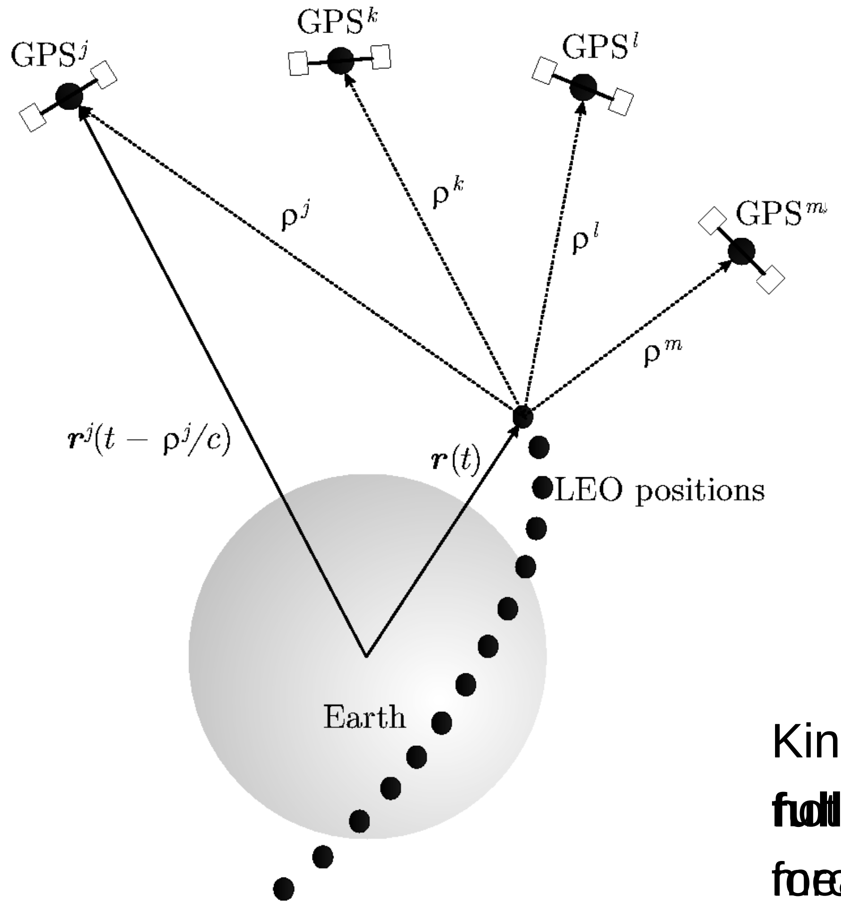

A kinematic orbit is an ephemeris at **discrete** measurement epochs

Kinematic positions are **fully independent** of the force models used for LEO orbit determination (Svehla and Rothacher, 2004)

Kinematic positions are **not uncorrelated** if phase measurements are used (due to ambiguities) (Jäggi et al., 2011)

Kinematic Orbit Representation (3)

Measurement epochs
(in GPS time)

Positions (km)
(Earth-fixed)

```
*  2009 11  2  0  0  0.80678020
PL15  -390.612059  6623.987679   73.104149 193219.797196
*  2009 11  2  0  0  1.80678020
PL15  -389.240315  6624.166512   65.402457 193219.799413
*  2009 11  2  0  0  2.80678020
PL15  -387.868014  6624.336133   57.700679 193219.801634
*  2009 11  2  0  0  3.80678020
PL15  -386.495163  6624.496541   49.998817 193219.803855
*  2009 11  2  0  0  4.80678019
PL15  -385.121760  6624.647724   42.296889 193219.806059
*  2009 11  2  0  0  5.80678019
PL15  -383.747819  6624.789703   34.594896 193219.808280
*  2009 11  2  0  0  6.80678019
PL15  -382.373332  6624.922464   26.892861 193219.810495
*  2009 11  2  0  0  7.80678019
PL15  -380.998306  6625.046003   19.190792 193219.812692
*  2009 11  2  0  0  8.80678019
PL15  -379.622745  6625.160329   11.488692 193219.814899
*  2009 11  2  0  0  9.80678018
PL15  -378.246651  6625.265448    3.786580 193219.817123
```

Clock correction to nominal epoch (μs), e.g., to epoch 00:00:03

Excerpt of kinematic GOCE positions at begin of 2 Nov, 2009

GO_CONS_SST_PKI_2__20091101T235945_20091102T235944_0001 Times in UTC

Dynamic Orbit Representation (1)

Satellite position $\boldsymbol{r}_{leo}(t_{leo})$ (in inertial frame) is given by:

$$\boldsymbol{r}_{leo}(t_{leo}) = \boldsymbol{r}_{leo,0}(t_{leo}; a, e, i, \Omega, \omega, u_0; Q_1, ..., Q_d) + \delta\boldsymbol{r}_{leo,ant}(t_{leo})$$

$\boldsymbol{r}_{leo,0}$	LEO center of mass position
$\delta\boldsymbol{r}_{leo,ant}$	LEO antenna phase center offset
$a, e, i, \Omega, \omega, u_0$	LEO initial osculating orbital elements
$Q_1, ..., Q_d$	LEO dynamical parameters

Satellite trajectory $\boldsymbol{r}_{leo,0}$ is a particular solution of an **equation of motion**

- One set of **initial conditions** (orbital elements) is estimated per arc. Dynamical parameters of the force model on request

Dynamic Orbit Representation (2)

Equation of motion (in inertial frame) is given by:

$$\ddot{\boldsymbol{r}} = -GM\frac{\boldsymbol{r}}{r^3} + \boldsymbol{f}_1(t, \boldsymbol{r}, \dot{\boldsymbol{r}}, Q_1, ..., Q_d)$$

with initial conditions

$$\boldsymbol{r}(t_0) = \boldsymbol{r}(a, e, i, \Omega, \omega, u_0; t_0)$$
$$\dot{\boldsymbol{r}}(t_0) = \dot{\boldsymbol{r}}(a, e, i, \Omega, \omega, u_0; t_0)$$

The **acceleration** $\boldsymbol{f}_1$ consists of **gravitational** and **non-gravitational** perturbations taken into account to model the satellite trajectory. Unknown parameters $Q_1, ..., Q_d$ of force models may appear in the equation of motion together with deterministic (known) accelerations given by analytical models.

Wilhelm und Else Heraeus Autumn School
Global Gravity Field Modeling
from Satellite-to-Satellite Tracking Data

Perturbing Accelerations of a LEO Satellite

Force	**Acceleration** (m/s²)
Central term of Earth's gravity field	8.42
Oblateness of Earth's gravity field	0.015
Atmospheric drag	0.00000079
Higher order terms of Earth's gravity field	0.00025
Attraction from the Moon	0.0000054
Attraction from the Sun	0.0000005
Direct solar radiation pressure	0.000000097
...	...

Osculating Orbital Elements (1)

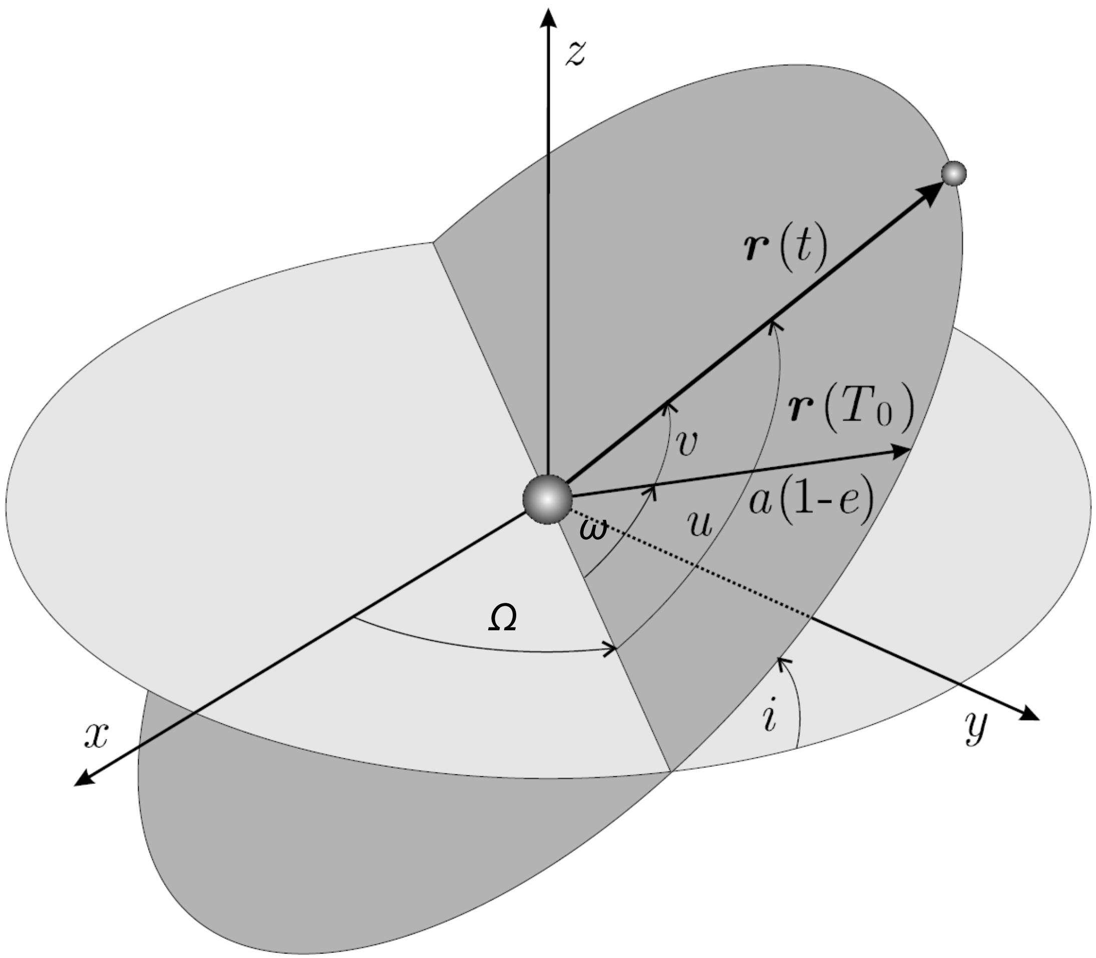

Osculating Orbital Elements of GOCE (2)

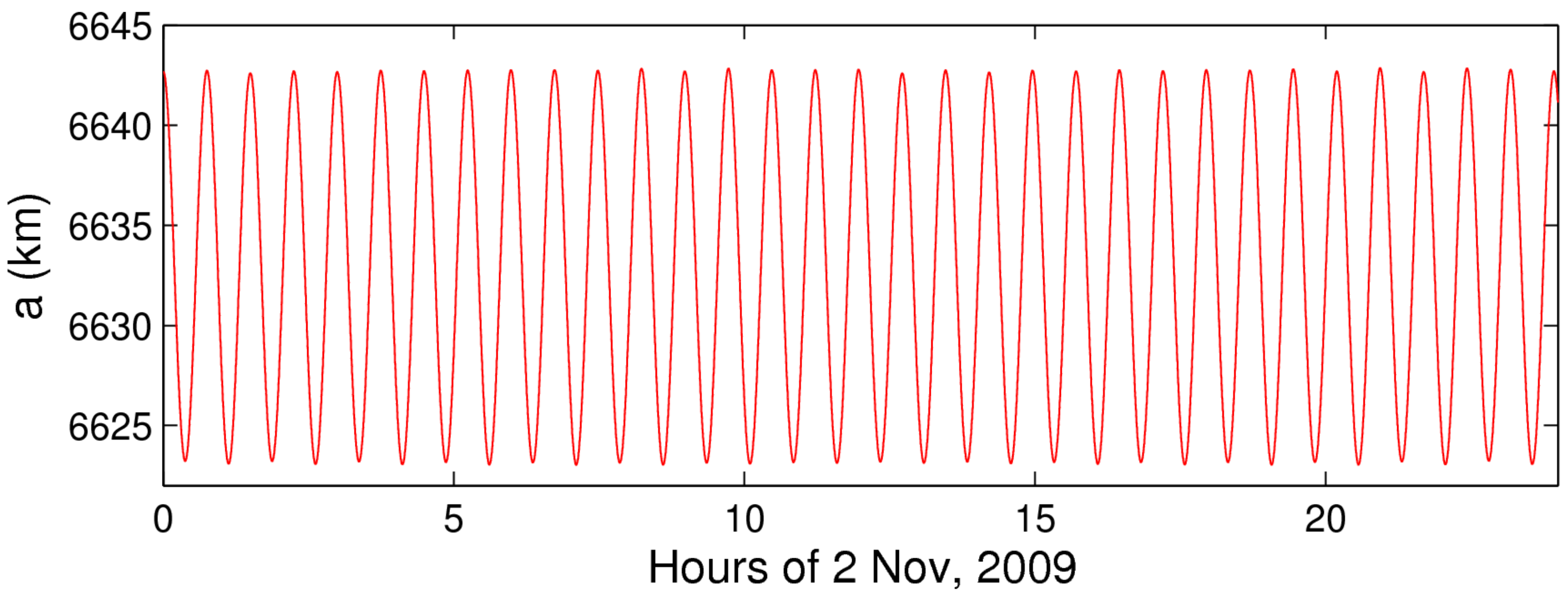

Semi-major axis:

Twice-per-revolution variations of about ±10 km around the mean semi-major axis of 6632.9km, which corresponds to a mean altitude of 254.9 km

Osculating Orbital Elements of GOCE (3)

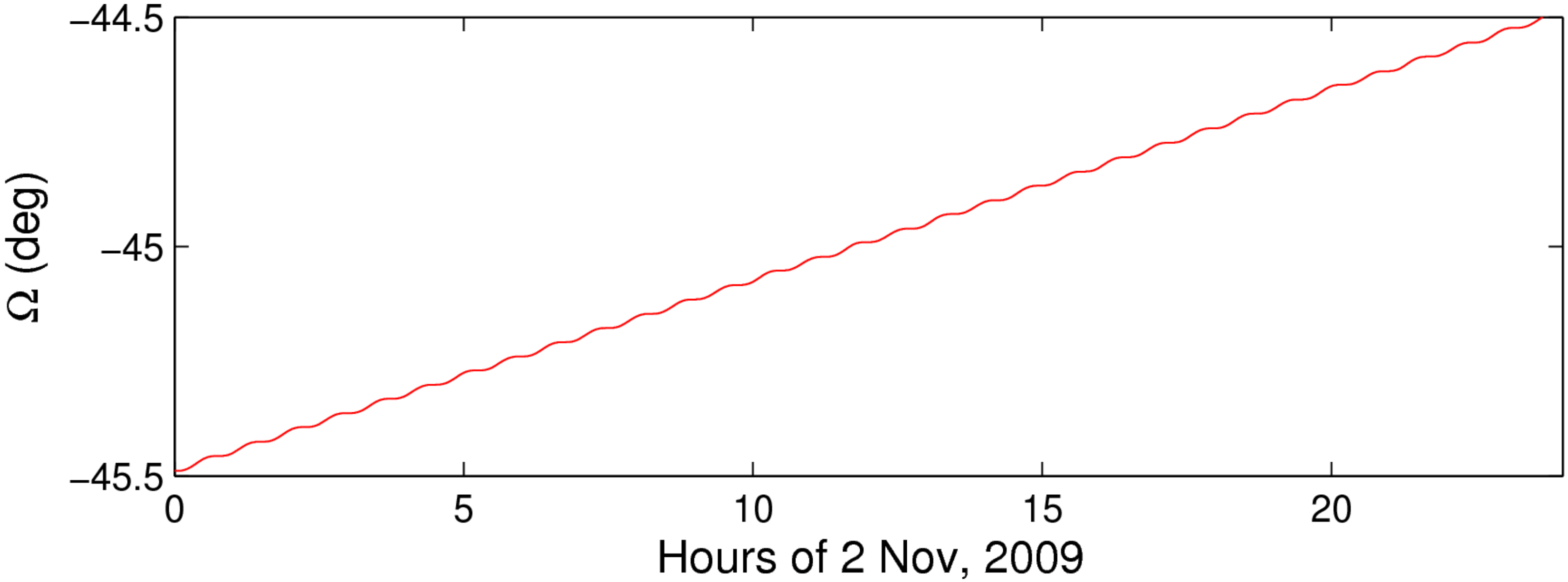

Right ascension of ascending node:

Twice-per-revolution variations and linear drift of about +1°/day (360°/365days) due to the sun-synchronous orbit

Dynamic Orbit Representation (3)

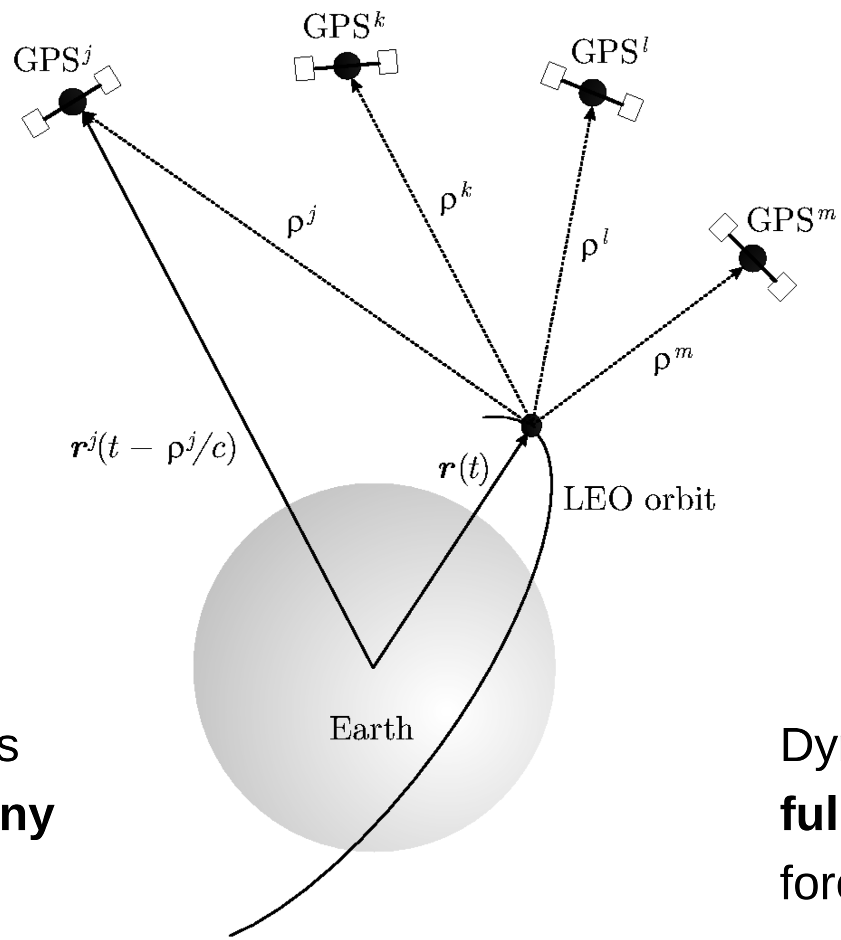

Dynamic orbit positions may be computed at **any epoch** within the arc

Dynamic positions are **fully dependent** on the force models used, e.g., on the gravity field model

Reduced-Dynamic Orbit Representation (1)

Equation of motion (in inertial frame) is given by:

$$\ddot{\boldsymbol{r}} = -GM\frac{\boldsymbol{r}}{r^3} + \boldsymbol{f}_1(t, \boldsymbol{r}, \dot{\boldsymbol{r}}, Q_1, ..., Q_d, P_1, ..., P_s)$$

$P_1, ..., P_s$ Pseudo-stochastic parameters

Pseudo-stochastic parameters are:

- additional empirical parameters characterized by a priori known **statistical properties**, e.g., by expectation values and a priori variances
- useful to **compensate** for deficiencies in dynamic models, e.g., deficiencies in models describing non-gravitational accelerations
- often set up as **piecewise constant accelerations** to ensure that satellite trajectories are continuous and differentiable at any epoch

Wilhelm und Else Heraeus Autumn School
Global Gravity Field Modeling
from Satellite-to-Satellite Tracking Data

Reduced-Dynamic Orbit Representation (2)

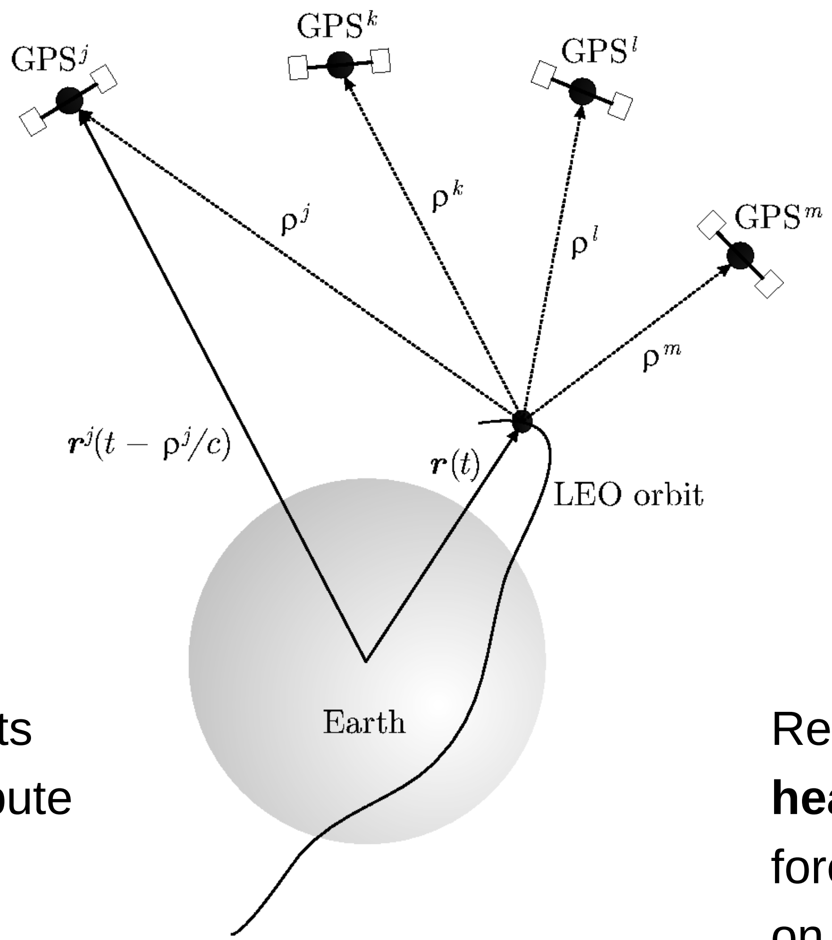

Reduced-dynamic orbits are well suited to compute LEO orbits of **highest quality**

(Jäggi et al., 2006; Jäggi, 2007)

Reduced-dynamic orbits **heavily depend** on the force models used, e.g., on the gravity field model

Reduced-dynamic Orbit Representation (3)

Position epochs
(in GPS time)

Positions (km) &
Velocities (dm/s)
(Earth-fixed)

Clock corrections
are not provided

```
*  2009 11  2  0  0  0.00000000
PL15   -391.718353   6623.836682     79.317661 999999.999999
VL15  13710.157683   1908.731015 -77015.601314 999999.999999
*  2009 11  2  0  0 10.00000000
PL15   -377.980705   6625.284690      2.298385 999999.999999
VL15  13764.602016    987.250587 -77021.193676 999999.999999
*  2009 11  2  0  0 20.00000000
PL15   -364.190222   6625.811136    -74.721213 999999.999999
VL15  13815.825127     65.631014 -77016.232293 999999.999999
*  2009 11  2  0  0 30.00000000
PL15   -350.350131   6625.415949   -151.730567 999999.999999
VL15  13863.820409   -855.995477 -77000.719734 999999.999999
*  2009 11  2  0  0 40.00000000
PL15   -336.463660   6624.099187   -228.719134 999999.999999
VL15  13908.581905  -1777.497047 -76974.660058 999999.999999
*  2009 11  2  0  0 50.00000000
PL15   -322.534047   6621.861041   -305.676371 999999.999999
VL15  13950.104280  -2698.741871 -76938.058807 999999.999999
*  2009 11  2  0  1  0.00000000
PL15   -308.564533   6618.701833   -382.591743 999999.999999
VL15  13988.382807  -3619.598277 -76890.923043 999999.999999
```

Excerpt of reduced-dynamic GOCE positions at begin of 2 Nov, 2009

GO_CONS_SST_PRD_2__20091101T235945_20091102T235944_0001

Orbit Determination

Principle of Orbit Determination

The **actual orbit** $\boldsymbol{r}(t)$ is expressed as a truncated Taylor series:

$$\boldsymbol{r}(t) = \boldsymbol{r}_0(t) + \sum_{i=1}^{n} \frac{\partial \boldsymbol{r}_0}{\partial P_i}(t) \cdot (P_i - P_{0,i})$$

$\boldsymbol{r}_0(t)$	A priori orbit
$\frac{\partial \boldsymbol{r}_0}{\partial P_i}(t)$	Partial derivative of the a priori orbit $\boldsymbol{r}_0(t)$ w.r.t. parameter P_i
$P_{0,i}$	A priori parameter values of the a priori orbit $\boldsymbol{r}_0(t)$
P_i	Parameter values of the improved orbit $\boldsymbol{r}(t)$

A **least-squares** adjustment of spacecraft tracking data yields **corrections** to the a priori parameter values $P_{0,i}$. Using the above equation, the improved (linearized) orbit $\boldsymbol{r}(t)$ may be eventually computed.

A priori orbit generation: Keplerian Orbit

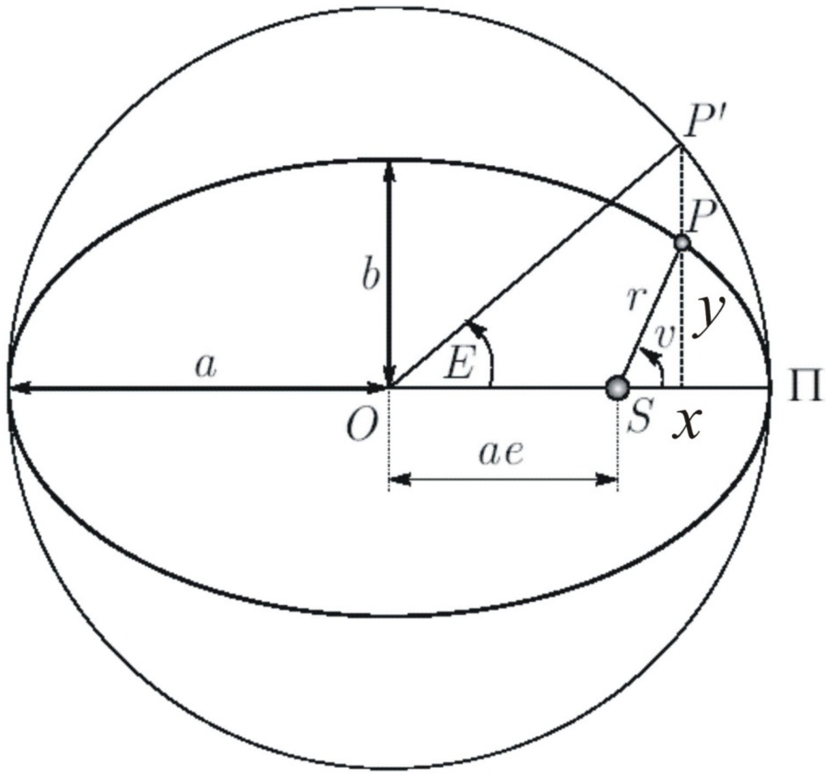

Coordinates in orbital system:

n = mean motion

$$n^2 a^3 = GM$$

M = mean anomaly

$$M(t) = n\,(t - T_0)$$

Kepler's equation:

E = eccentric anomaly

$$E(t) = M(t) + e \sin E(t)$$

$$x = a(\cos E - e)$$

$$y = a\sqrt{1-e^2}\,\sin E$$

A priori orbit generation: Keplerian Orbit

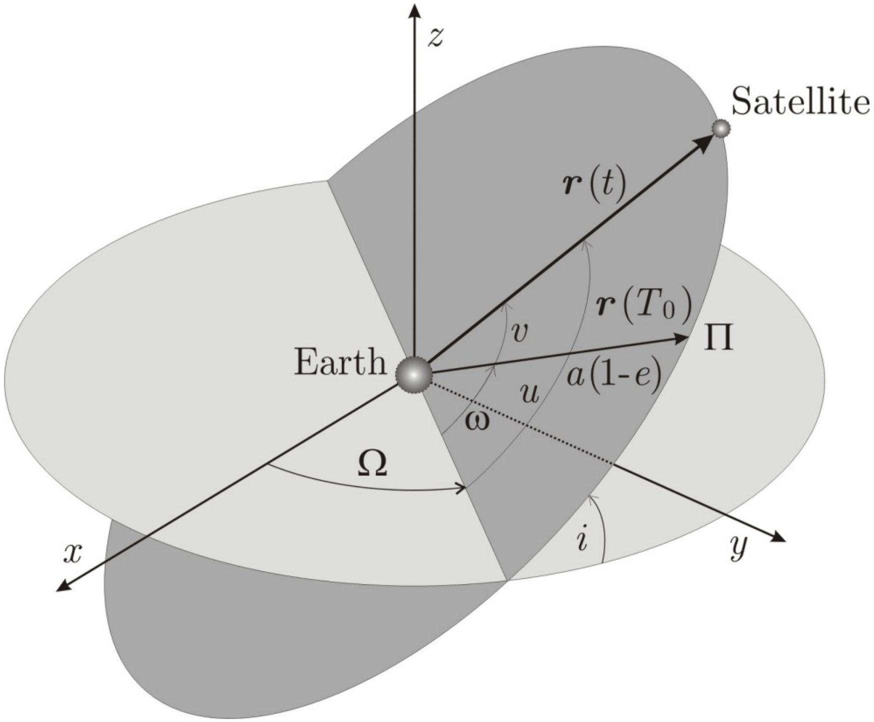

The resulting formulas are those used in the two-body problem for ephemerides calculations. They are coded in the SR ephem which is used for the exercises.

Positions in equatorial system:

They follow from the coordinates in the orbital system by adopting three particular rotations:

$$\begin{pmatrix} x_a \\ y_a \\ z_a \end{pmatrix} = \mathbf{R}_3(-\Omega)\cdot\mathbf{R}_1(-i)\cdot\mathbf{R}_3(-\omega)\cdot\begin{pmatrix} x \\ y \\ 0 \end{pmatrix}$$

The same holds for the velocities:

$$\begin{pmatrix} \dot{x}_a \\ \dot{y}_a \\ \dot{z}_a \end{pmatrix} = \mathbf{R}_3(-\Omega)\cdot\mathbf{R}_1(-i)\cdot\mathbf{R}_3(-\omega)\cdot\begin{pmatrix} \dot{x} \\ \dot{y} \\ 0 \end{pmatrix}$$

Numerical Integration (1)

Collocation algorithms (one particular class of numerical integration techniques) are subsequently used to briefly illustrate the principles of numerical integration:

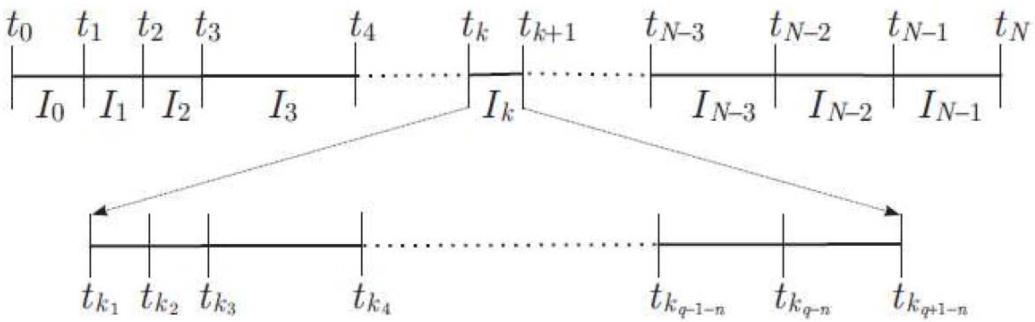

The original intervall is divided into N integration intervals. For each interval I_k a further subdivision is performed according to the order q of the adopted method. At these points t_{k_j} the numerical solution is requested to solve the differential equation system of order n.

(Beutler, 2005)

Numerical Integration (2)

Initial value problem in the interval I_k is given by:

$$\ddot{\mathbf{r}}_k = \mathbf{f}(t, \mathbf{r}_k, \dot{\mathbf{r}}_k)$$

with initial conditions

$$\mathbf{r}_k(t_k) \doteq \mathbf{r}_{k0} \qquad \text{and} \qquad \dot{\mathbf{r}}_k(t_k) \doteq \dot{\mathbf{r}}_{k0}$$

where the initial values are defined as

$$\mathbf{r}_{k0}^{(i)} = \begin{cases} \mathbf{r}_0^{(i)} & ;\ k = 0 \\ \mathbf{r}_{k-1}^{(i)}(t_k) & ;\ k > 0 \end{cases}$$

Numerical Integration (3)

The **collocation method** approximates the solution in the interval I_k by:

$$\mathbf{r}_k(t) \doteq \sum_{l=0}^{q} \frac{1}{l!}(t-t_k)^l\,\mathbf{r}_{k0}^{(l)}$$

The coefficients $\mathbf{r}_{k0}^{(l)}$, $l = 0,\ldots,q$ are obtained by requesting that the numerical solution assumes the initial values and solves the differential equation system at $q-1$ different epochs $t_{k_j},\ j = 1,\ldots,q-1$. This leads to the conditions

$$\sum_{l=2}^{q} \frac{(t_{k_j}-t_k)^{l-2}}{(l-2)!}\,\mathbf{r}_{k0}^{(l)} = \mathbf{f}(t_{k_j},\mathbf{r}_k(t_{k_j}),\dot{\mathbf{r}}_k(t_{k_j}))\ , \quad j = 1,\ldots,q-1\,.$$

They are non-linear but can be solved efficiently by an iterative procedure.

(Beutler, 2005)

Pocket Guide of Least-Squares Adjustment (1)

The system of **Observation Equations** is given by:

$$\boldsymbol{L}' + \boldsymbol{\epsilon} = \boldsymbol{F}(\boldsymbol{X})$$

or, if $\boldsymbol{F}$ is a non-linear function of the parameters, in its **linearized** form:

$$\boldsymbol{L}' + \boldsymbol{\epsilon} = \boldsymbol{F}(\boldsymbol{X}_0) + \boldsymbol{A}\,\boldsymbol{x}$$

$\boldsymbol{L}'$	Tracking observations	$\boldsymbol{X}_0$	A priori parameter values
$\boldsymbol{\epsilon}$	Observation corrections	$\boldsymbol{x}$	Parameter corrections
$\boldsymbol{F}$	Functional model	$\boldsymbol{X}$	Improved parameter values, i.e., $\boldsymbol{X} = \boldsymbol{X}_0 + \boldsymbol{x}$

$$\boldsymbol{A} \doteq \left.\frac{\partial \boldsymbol{F}(\boldsymbol{X})}{\partial \boldsymbol{X}}\right|_{\boldsymbol{X}=\boldsymbol{X}_0}$$ First design matrix

Wilhelm und Else Heraeus Autumn School
Global Gravity Field Modeling from Satellite-to-Satellite Tracking Data

Pocket Guide of Least-Squares Adjustment (2)

The system of **Normal Equations** is obtained by minimizing $\boldsymbol{\epsilon}^T \, P \, \boldsymbol{\epsilon}$:

$$\left(\boldsymbol{A}^T \boldsymbol{P} \boldsymbol{A}\right) \boldsymbol{x} - \boldsymbol{A}^T \boldsymbol{P} \boldsymbol{l} = \boldsymbol{N} \boldsymbol{x} - \boldsymbol{b} = \boldsymbol{0}$$

$\boldsymbol{N} \doteq \boldsymbol{A}^T \boldsymbol{P} \boldsymbol{A}$ Normal equation matrix

$\boldsymbol{b} \doteq \boldsymbol{A}^T \boldsymbol{P} \boldsymbol{l}$ Right-hand side with "O-C" term $\boldsymbol{l} \doteq \boldsymbol{L}' - \boldsymbol{F}(\boldsymbol{X}_0)$

$\boldsymbol{P} = \sigma_0^2 \, \boldsymbol{C}_{ll}^{-1}$ Weight matrix, from covariance matrix $\boldsymbol{C}_{ll}$ of observations

For a **regular** normal equation matrix the parameter corrections follow as:

$$\boldsymbol{x} = \left(\boldsymbol{A}^T \boldsymbol{P} \boldsymbol{A}\right)^{-1} \boldsymbol{A}^T \boldsymbol{P} \boldsymbol{l} = \boldsymbol{N}^{-1} \boldsymbol{b}$$

Pocket Guide of Least-Squares Adjustment (3)

The **a posteriori standard deviation of unit weight** is computed as:

$$m_0 = \sqrt{\frac{\boldsymbol{\epsilon}^T \, P \, \boldsymbol{\epsilon}}{f}}$$

f Degree of freedom (number of observations minus number of parameters)

The **covariance matrix** of the adjusted parameters is given by

$$\boldsymbol{C_{xx}} = m_0^2 \, \boldsymbol{Q_{xx}} = m_0^2 \, \boldsymbol{N}^{-1}$$

and their a posteriori standard deviations follow from the diagonal elements:

$$m_x = \sqrt{C_{xx}} = m_0 \, \sqrt{Q_{xx}}$$

Pocket Guide of Least-Squares Adjustment (4)

Parameter constraints may be introduced by artificial observations with a user-specified variance σ^2_{abs}. These observations have to be appended to the system of observation equations. If the change with respect to the a priori value is used as the actual parameter in the artificial observation equation, the weight

$$W = \frac{\sigma_0^2}{\sigma^2_{abs}}$$

has to be only added to the corresponding diagonal element of the normal equation matrix $\boldsymbol{N}$, because the value O–C is zero in this special case.

Example of Filter Approaches (1)

Assuming that measurement data are uncorrelated between measurement epochs, and that the epoch-wise weight matrix is denoted by P_j, the normal equation system at epoch no. j reads as

$$N_j \Delta x_{0\,j} = b_j$$

$$N_j = (A^T P A)_j = \sum_{k=0}^{j} A_k^T P_k A_k \doteq \sum_{k=0}^{j} \Delta N_k$$

$$b_j = (A^T P \Delta l)_j = \sum_{k=0}^{j} A_k^T P_k \Delta l_k \doteq \sum_{k=0}^{j} \Delta b_k$$

$$\Delta x_{0\,j} = Q_j b_j$$

$$Q_j = N_j^{-1}$$

The index j indicates that for the solution all measurements up to epoch t_j are used

Example of Filter Approaches (2)

The recursion formula for the non-inverted normal equation system is trivial:

$$N_{j+1} \Delta x_{0,j+1} = b_{j+1}$$

$$N_{j+1} = N_j + \Delta N_{j+1}$$

$$b_{j+1} = b_j + \Delta b_{j+1}$$

Solution vectors, error estimates, and covariance matrices can be computed at every measurement epoch if required. If the dimension of N_j is large, however, a frequent inversion will not be a preferred solution strategy.

Example of Filter Approaches (3)

A recursion formula can also be derived for the inverted normal equation system:

$$N_{j+1}\Delta x_{0,j+1} = b_{j+1}$$

$$\Delta x_{0,j+1} = Q_{j+1}\left(b_j + \Delta b_{j+1}\right) = Q_{j+1}\left(N_j \Delta x_{0j} + \Delta b_{j+1}\right)$$

$$\Delta x_{0,j+1} = Q_{j+1}\left(\left\{N_{j+1} - \Delta N_{j+1}\right\}\Delta x_{0j} + \Delta b_{j+1}\right)$$

$$\Delta x_{0,j+1} = \Delta x_{0j} + Q_{j+1}A_{j+1}^T P_{j+1}\boxed{\left\{\Delta l_{j+1} - A_{j+1}\Delta x_{0j}\right\}}$$

resubstitution term

$$\Delta x_{0,j+1} = \Delta x_{0j} + \boxed{K_{j+1}}\left\{\Delta l_{j+1} - A_{j+1}\Delta x_{0j}\right\}$$

gain matrix

The formulas are well suited for real-time applications as it is straightforward to check the results for plausibility. They are also closely related to the Kalman filter formulas. Aspects not presented here are the transformation of the parameters to a new set of parameters at every epoch and stochastic system equations.

Example of Filter Approaches (4)

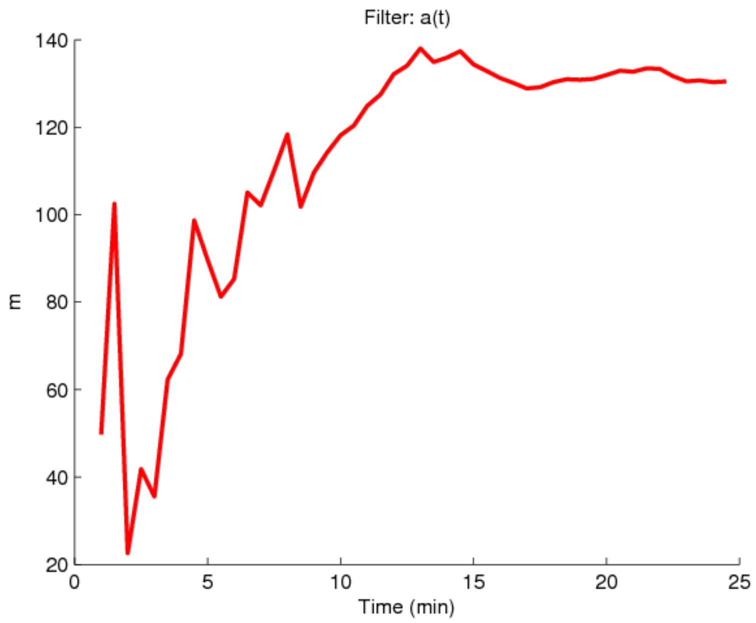

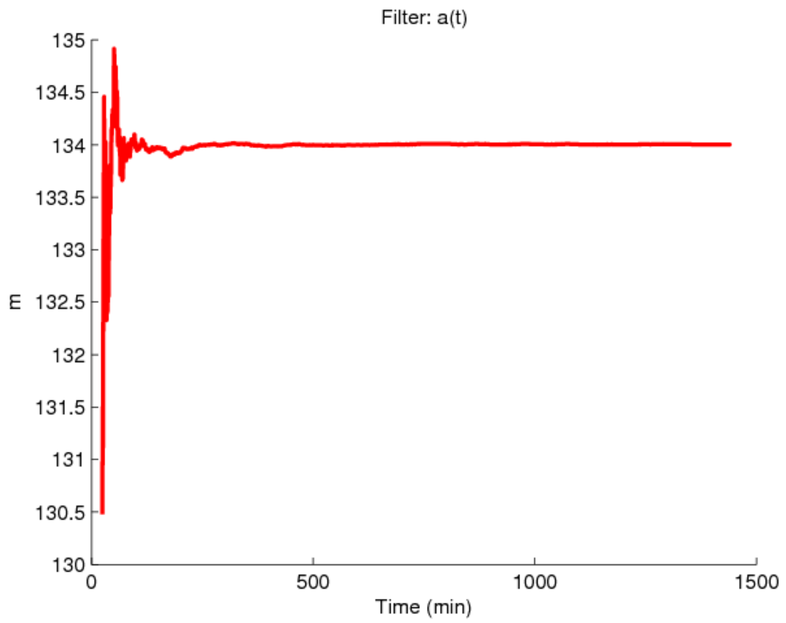

Example from the exercise: Semi-major axis refering to t_0 from a filter solution.

Left: epochs 3 – 50, Right: epochs 50 until end of the day.

Even with only a few epochs the solution is much better than the “quick and dirty” polynomial fit. After about 500 min the solution is stable.

Wilhelm und Else Heraeus Autumn School
Global Gravity Field Modeling
from Satellite-to-Satellite Tracking Data

Example of Filter Approaches (5)

For the recursion formula developed so far the following relations may be used:

$$N_{j+1} = N_j + \Delta N_{j+1}\,, \quad Q_{j+1} = \left(N_{j+1}\right)^{-1}$$

If the dimension of N_{j+1} is large, the following recursion formula, following from a rather laborious derivation, is preferred:

$$Q_{j+1} = Q_j - Q_j A_{j+1}^T P_{j+1} \left(E + A_{j+1} Q_j A_{j+1}^T P_{j+1}\right)^{-1} A_{j+1} Q_j$$

$$Q_{j+1} = Q_j - Q_j A_{j+1}^T \left(P_{j+1}^{-1} + A_{j+1} Q_j A_{j+1}^T\right)^{-1} A_{j+1} Q_j$$

The matrix to be inverted is of the size of the number of measurements to be processed per epoch.

Partial Derivatives

The partial of the r -th observation w.r.t. orbit parameter P_i may be expressed as

$$\frac{\partial F_r(\boldsymbol{X})}{\partial P_i} = \left(\boldsymbol{\nabla}\left(F_r(\boldsymbol{X})\right)\right)^T \cdot \; \frac{\partial \boldsymbol{r}_0}{\partial P_i}(t)$$

with the gradient given by

$$\left(\boldsymbol{\nabla}\left(F_r(\boldsymbol{X})\right)\right)^T = \left(\frac{\partial F_r(\boldsymbol{X})}{\partial r_{0,1}} \; \frac{\partial F_r(\boldsymbol{X})}{\partial r_{0,2}} \; \frac{\partial F_r(\boldsymbol{X})}{\partial r_{0,3}} \right)$$

if the observations only depend on the geocentric position vector and are referring to only one epoch. The gradient only depends on the type of observations used, whereas the second term is independent of the observation type and related to the **variational equations**. This separates the observation-specific (**geometric**) part from the **dynamic** part.

Variational Equations (1)

For each orbit parameter P_i the corresponding **variational equation** reads as

$$\ddot{\boldsymbol{z}}_{P_i} = \boldsymbol{A}_0 \cdot \boldsymbol{z}_{P_i} + \boldsymbol{A}_1 \cdot \dot{\boldsymbol{z}}_{P_i} + \frac{\partial \boldsymbol{f}_1}{\partial P_i}$$

with the 3 x 3 matrices defined by

$$A_{0[i;k]} \doteq \frac{\partial f_i}{\partial r_{0,k}} \quad \text{and} \quad A_{1[i;k]} \doteq \frac{\partial f_i}{\partial \dot{r}_{0,k}}$$

f_i i -th component of the total acceleration $\boldsymbol{f}$

$r_{0,k}$ k-th component of the geocentric position $\boldsymbol{r}_0$

For each orbit parameter P_i the **variational equation** is a linear differential equation system of second order in time. Their solutions are all needed for orbit determination.

Variational Equations (2)

The variational equation is a linear, **homogeneous** system with initial values

$$\boldsymbol{z}_{P_i}(t_0) \neq \boldsymbol{0} \quad \text{and} \quad \dot{\boldsymbol{z}}_{P_i}(t_0) \neq \boldsymbol{0} \quad \text{for} \quad P_i \in \{a, e, i, \Omega, \omega, u_0\}$$

and a linear, **inhomogeneous** system with initial values

$$\boldsymbol{z}_{P_i}(t_0) = \boldsymbol{0} \quad \text{and} \quad \dot{\boldsymbol{z}}_{P_i}(t_0) = \boldsymbol{0} \quad \text{for} \quad P_i \in \{Q_1, ..., Q_d\}$$

Let us assume that the functions $\boldsymbol{z}_{O_j}(t), j = 1, ..., 6$ are the partials w.r.t. the six parameters $O_j, j = 1, ..., 6$ defining the initial conditions at time t_0. The ensemble of these six functions forms one **complete system** of solutions of the homogeneous part of the variational equation, which allows to obtain the solution of the inhomogeneous system by the method of "**variation of constants**".

Variational Equations (3)

The solution and its first time derivative may be written as

$$\boldsymbol{z}_{P_i}^{(k)}(t) = \sum_{j=1}^{6} \alpha_{O_j P_i}(t) \cdot \boldsymbol{z}_{O_j}^{(k)}(t) \; ; \quad k = 0, 1$$

with the coefficient functions defined by

$$\boldsymbol{\alpha}_{P_i}(t) \doteq \int_{t_0}^{t} \boldsymbol{Z}^{-1}(t') \cdot \boldsymbol{h}_{P_i}(t') \cdot dt'$$

$\boldsymbol{\alpha}_{P_i}$ column array defined by $(\alpha_{O_1 P_i}, \ldots, \alpha_{O_6 P_i})^T$

$\boldsymbol{Z}$ 6 x 6 matrix defined by $\boldsymbol{Z}_{[1,\ldots,3;j]} \doteq \boldsymbol{z}_{O_j}, \boldsymbol{Z}_{[4,\ldots,6;j]} \doteq \dot{\boldsymbol{z}}_{O_j}$

$\boldsymbol{h}_{P_i}$ column array defined by $(\mathbf{0}^T, \; \partial \boldsymbol{f}_1^T / \partial P_i)^T$

Variational Equations (4)

Note that the solutions $\boldsymbol{z}_{P_i}(t)$ of the variational equation and its time derivative may be expressed with the **same** functions $\alpha_{O_j P_i}(t)$ as a linear combination with the homogeneous solutions $\boldsymbol{z}_{O_j}(t)$ and $\dot{\boldsymbol{z}}_{O_j}(t)$, respectively.Therefore, only the six initial value problems associated with the initial conditions have to be actually treated as differential equation systems. Their solutions have to be either obtained approximately, or by numerical integration techniques.

All variational equations related to dynamical orbit parameters may be reduced to **definite integrals**. They can be efficiently solved numerically, e.g., by a Gaussian quadrature technique.

It must be emphasized that each additional orbit parameter requires an additional numerical solution of a definite integral. In view of the potentially large number of orbit parameters, it is advantagous that for **pseudo-stochastic orbit parameters** an explicit numerical quadrature of the definite integrals can be avoided.

(Jäggi, 2007)

Partial Derivatives for Keplerian Orbits

The partial derivatives wrt the orbital elements can be explicitly derived for Keplerian orbits by using the formulas of the two-body problem:

$$\begin{pmatrix} x_e \\ y_e \\ z_e \end{pmatrix} = \mathbf{R}_3(-\Omega) \cdot \mathbf{R}_1(-i) \cdot \mathbf{R}_3(-\omega) \cdot \begin{pmatrix} a(\cos E - e) \\ a\sqrt{1-e^2} \cdot \sin E \\ 0 \end{pmatrix}$$

As an example, for the partial derivative wrt the inclination *i* we obtain

$$\frac{\partial}{\partial i}\begin{pmatrix} x_e \\ y_e \\ z_e \end{pmatrix} = \mathbf{R}_3(-\Omega) \cdot \frac{\partial}{\partial i}\left\{\mathbf{R}_1(-i)\right\} \cdot \mathbf{R}_3(-\omega) \cdot \begin{pmatrix} a(\cos E - e) \\ a\sqrt{1-e^2} \cdot \sin E \\ 0 \end{pmatrix}$$

Similar expressions are also obtained for the other partial derivatives. Note that the partials wrt *a* and *e* are more complicated as *E* depends on them, as well.

Pulses (1)

The special case of instantaneous velocity changes (pulses) V_i at times t_i in predetermined directions $\boldsymbol{e}(t_i)$ is particularly simple. The contribution of this parameter $P_i = V_i$ to $\boldsymbol{f}_1$ may be formally written as $V_i \cdot \delta(t - t_i) \cdot \boldsymbol{e}(t)$ and the corresponding variational equation reads as

$$\ddot{\boldsymbol{z}}_{V_i} = \boldsymbol{A}_0 \cdot \boldsymbol{z}_{V_i} + \boldsymbol{A}_1 \cdot \dot{\boldsymbol{z}}_{V_i} + \delta(t - t_i) \cdot \boldsymbol{e}(t)$$

The coefficients $\boldsymbol{\alpha}_{V_i}(t)$ read for this special case as

$$\boldsymbol{\alpha}_{V_i}(t) \doteq \int_{t_0}^{t} \delta(t' - t_i) \cdot \boldsymbol{Z}^{-1}(t') \cdot \boldsymbol{h}_{V_i}(t') \cdot dt' = \boldsymbol{Z}^{-1}(t_i) \cdot \boldsymbol{h}_{V_i}(t_i) \doteq \beta_{V_i}$$

Subsequently, an alternative, more intuitive derivation is given.

Pulses (2)

Let us assume that we want to allow for an instantaneous velocity change of the orbit $\boldsymbol{r}(t)$ at the epoch t_i in the direction of the unit vector $\boldsymbol{e}$. We want the resulting orbit to be continuous. The difference of the new – old orbit at t_i obviously is given for $t = t_i$ by:

$$\delta\dot{\boldsymbol{r}}(t_i) = \delta v\,\boldsymbol{e}$$

$$\delta\boldsymbol{r}(t_i) = \boldsymbol{0}\ .$$

The difference of the new – old orbit for $t \geq t_i$ obviously is given by:

$$\delta\boldsymbol{r}(t) = \left(\frac{\partial\boldsymbol{r}}{\partial\left(\delta v\right)}\right)(t)\ \delta v$$

Pulses (2)

where

$$\left(\frac{\partial \boldsymbol{r}}{\partial\left(\delta v\right)}\right)(t_i) = \boldsymbol{0}$$
$$\left(\frac{\partial \dot{\boldsymbol{r}}}{\partial\left(\delta v\right)}\right)(t_i) = \boldsymbol{e}$$

As the partial derivative is a solution of the homogeneous variational equations, we may write

$$\left(\frac{\partial \boldsymbol{r}}{\partial\left(\delta v\right)}\right)(t) = \sum_{k=1}^{6} \beta_k \left(\frac{\partial \boldsymbol{r}}{\partial I_k}\right)(t) \stackrel{\text{def}}{=} \sum_{k=1}^{6} \beta_k \, \boldsymbol{z}_k(t)$$

The time independent coefficients β_k still have to be determined.

Pulses (3)

To solve for the unknown coefficients, the linear combination of the six partial derivatives w.r.t. the osculating elements at time t_0 have to be inserted into the equations defining the partial derivatives w.r.t. δv at time t_i:

$$\sum_{k=1}^{6} \beta_k \, z_k(t_i) = 0$$

$$\sum_{k=1}^{6} \beta_k \, \dot{z}_k(t_i) = e$$

There is one set of coefficients for each pulse. Even if a huge number of pulses are introduced, there is no necessity to solve additional variational equations.

Short-Arc Approach

It is as well possible to not only allow for a discontinuous velocity vector, but also for a discontinuous position vector by setting up instantaneous position changes in addition. In analogy to the instantaneous velocity changes, the coefficients of the linear combination of the six partial derivatives w.r.t. the osculating elements at time t_0 may be found by solving a system of linear equations:

Position changes:

$$\sum_{j=1}^{6} \beta_{O_j X_i} \cdot \mathbf{z}_{O_j}(t_i) = \mathbf{e}(t_i)$$

$$\sum_{j=1}^{6} \beta_{O_j X_i} \cdot \dot{\mathbf{z}}_{O_j}(t_i) = \mathbf{0}$$

Velocity changes:

$$\sum_{j=1}^{6} \beta_{O_j V_i} \cdot \mathbf{z}_{O_j}(t_i) = \mathbf{0}$$

$$\sum_{j=1}^{6} \beta_{O_j V_i} \cdot \dot{\mathbf{z}}_{O_j}(t_i) = \mathbf{e}(t_i)$$

(Mayer-Gürr et al., 2005)

GPS-based LEO POD

Wilhelm und Else Heraeus Autumn School
Global Gravity Field Modeling
from Satellite-to-Satellite Tracking Data

LEO Sensor Offsets

Phase center offsets $\delta \boldsymbol{r}_{leo,ant}$:

- are needed in the inertial or Earth-fixed frame and have to be transformed from the satellite frame using **attitude data** from the star-trackers

- consist of a frequency-independent **instrument offset**, e.g., defined by the center of the instrument‘s mounting plane (CMP) in the satellite frame

- consist of frequency-dependent **phase center offsets** (PCOs), e.g., defined wrt the center of the instrument‘s mounting plane in the antenna frame (ARF)

- consist of frequency-dependent **phase center variations** (PCVs) varying with the direction of the incoming signal, e.g., defined wrt the PCOs in the antenna frame

Example: GOCE Sensor Offsets (1)

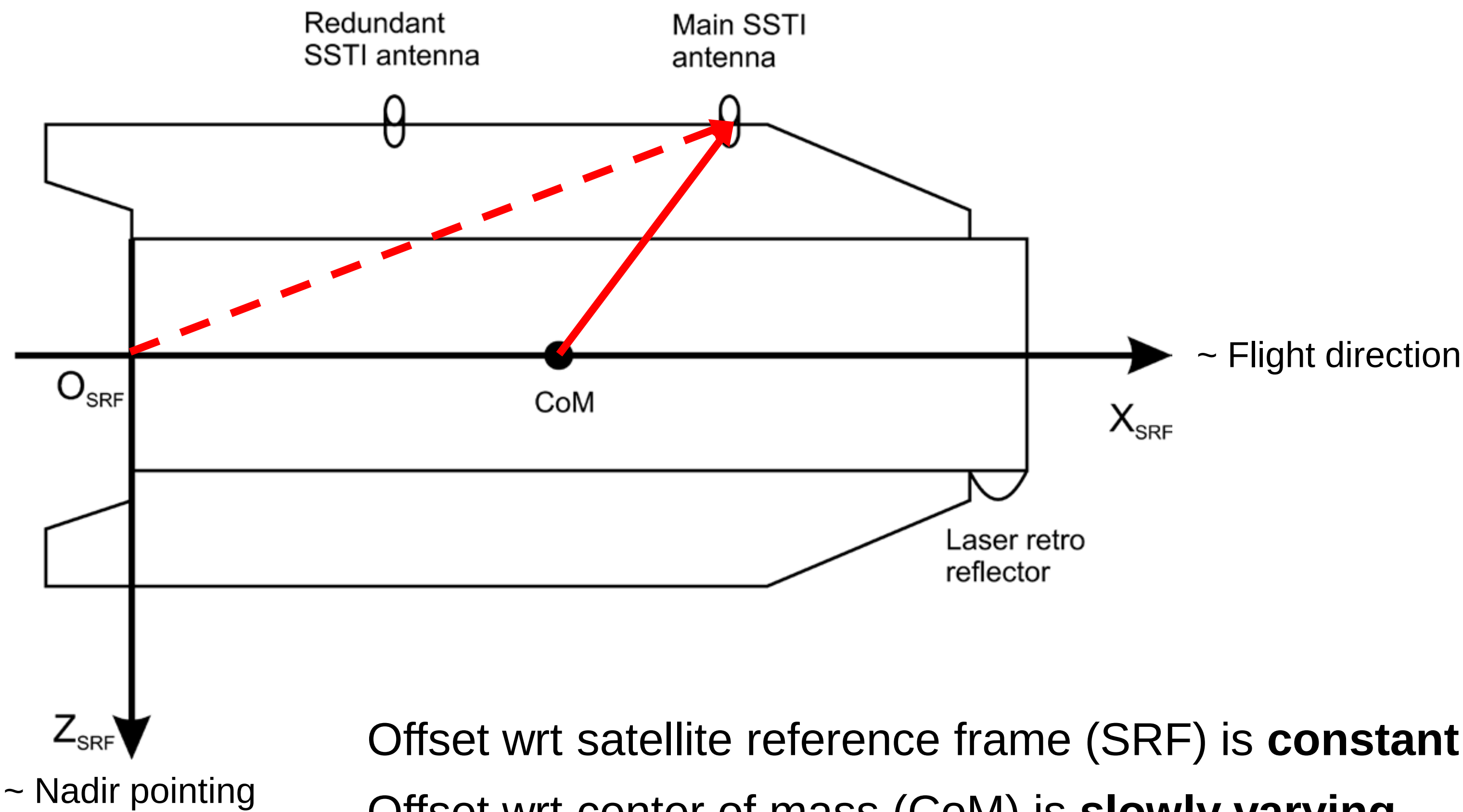

Offset wrt satellite reference frame (SRF) is **constant**

Offset wrt center of mass (CoM) is **slowly varying**

Wilhelm und Else Heraeus Autumn School
Global Gravity Field Modeling
from Satellite-to-Satellite Tracking Data

Example: GOCE Sensor Offsets (2)

Table 1: CoM coordinates in SRF system

CoM	X_{SRF}[m]	Y_{SRF}[m]	Z_{SRF}[m]
Begin of Life (BoL)	2.4990	0.0036	0.0011
End of Life (EoL)	2.5290	0.0038	0.0012

Table 2: SSTI antenna CMP coordinates in SRF system

CMP coordinates	X_{SRF} [m]	Y_{SRF}[m]	Z_{SRF}[m]
Main	3.1930	0.0000	-1.0922
Redundant	1.3450	0.0000	-1.0903

Table 3: SSTI antenna CMP coordinates wrt to CoM (BoL)

CMP coordinates	X_{CoM} [m]	Y_{CoM}[m]	Z_{CoM}[m]
Main	0.6940	-0.0036	-1.0933
Redundant	-1.1540	-0.0036	-1.0914

Table 4: SSTI antenna phase center offsets in ARF system

Phase center offsets	X_{ARF}[mm]	Y_{ARF}[mm]	Z_{ARF}[mm]
Main: L1	-0.18	3.51	-81.11
Main: L2	-1.22	-1.00	-84.18
Redundant: L1	-0.96	3.14	-81.33
Redundant: L2	-1.48	-1.20	-84.18

Derived from Bigazzi and Frommknecht (2010)

Example: GOCE GPS Antenna

L1, L2, Lc phase center offsets

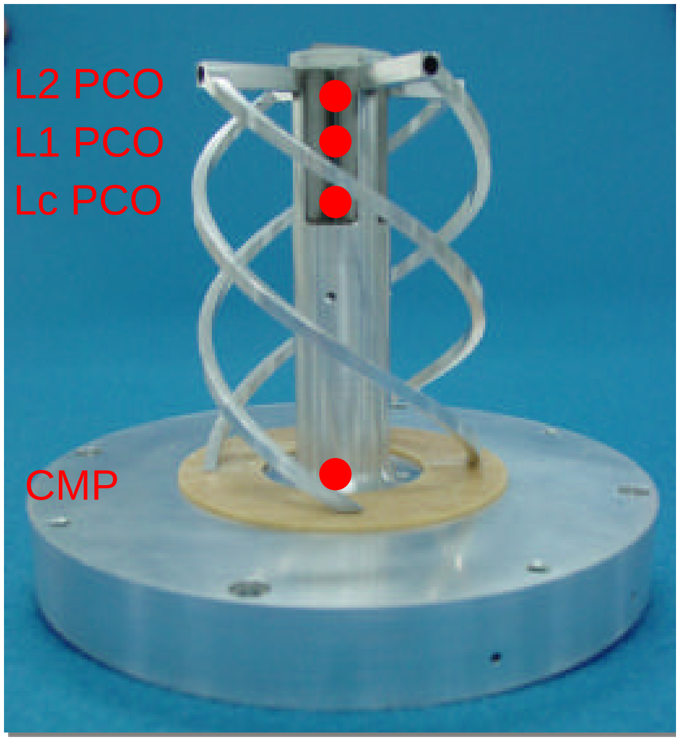

Measured from ground calibration in anechoic chamber

Lc phase center variations

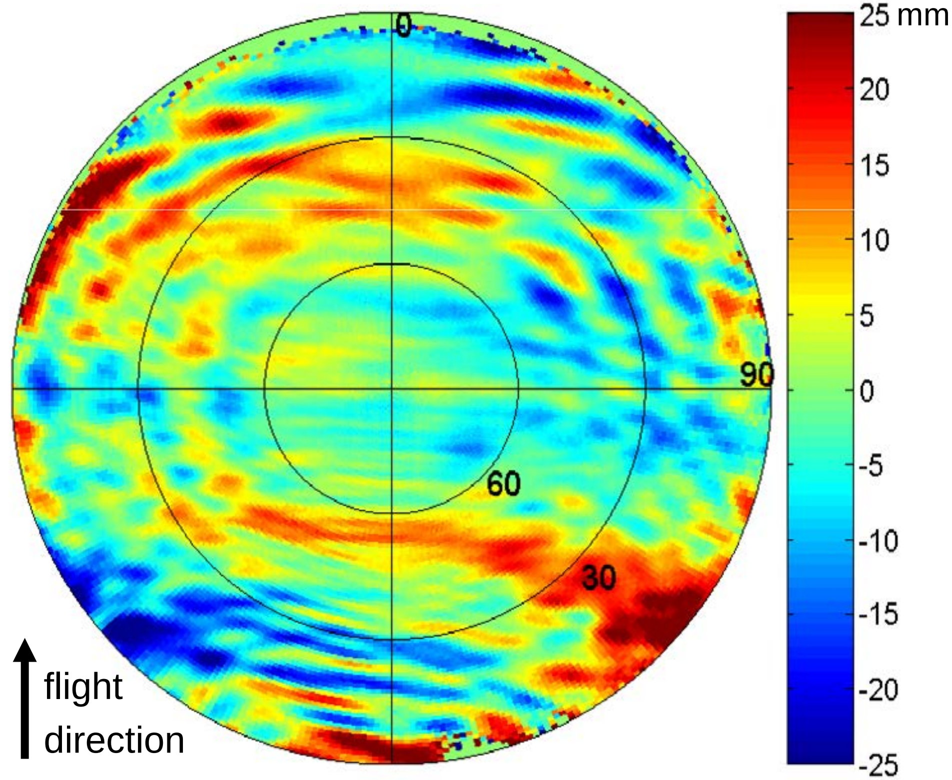

Empirically derived during orbit determination according to Jäggi et al. (2009)

Wilhelm und Else Heraeus Autumn School
Global Gravity Field Modeling
from Satellite-to-Satellite Tracking Data

Visualization of Orbit Solutions

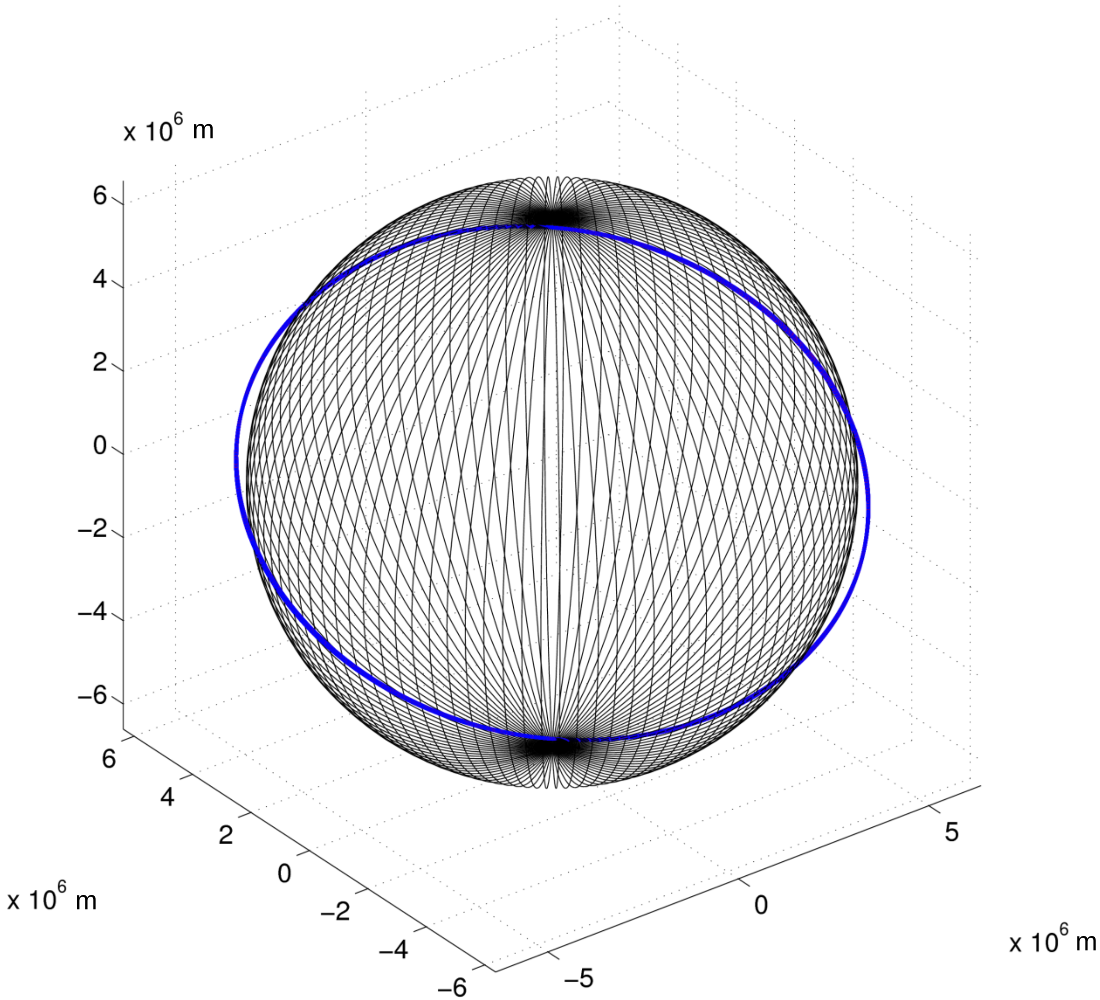

It is more instructive to look at differences between orbits in well suited coordinate systems …

Co-Rotating Orbital Frames

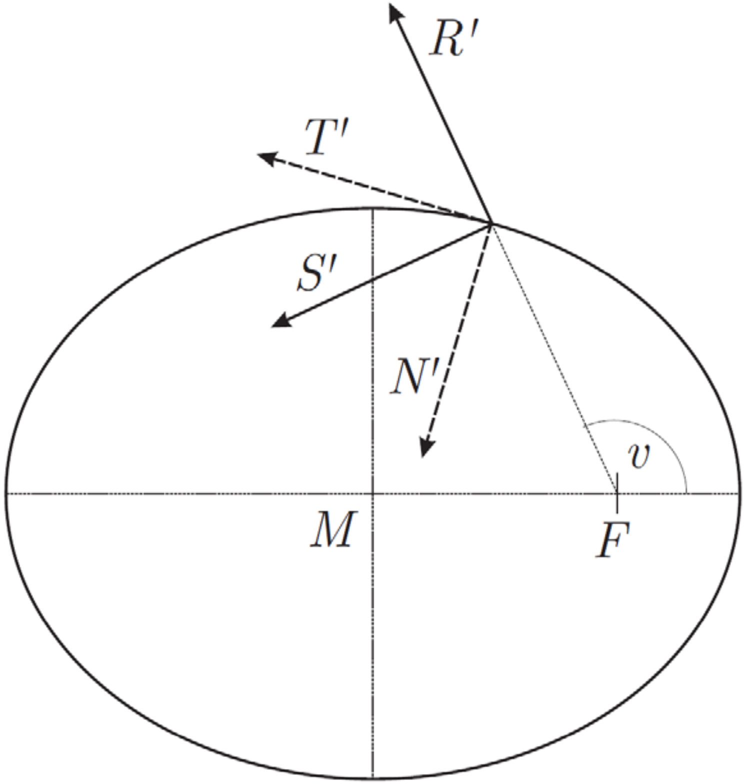

R, S, C unit vectors are pointing:
- into the radial direction
- normal to **R** in the orbital plane
- normal to the orbital plane (cross-track)

T, N, C unit vectors are pointing:
- into the tangential (along-track) direction
- normal to **T** in the orbital plane
- normal to the orbital plane (cross-track)

Small eccentricities: **S**~**T** (velocity direction)

Orbit Differences KIN-RD (GOCE: begin of mission)

Differences at epochs of kin. positions

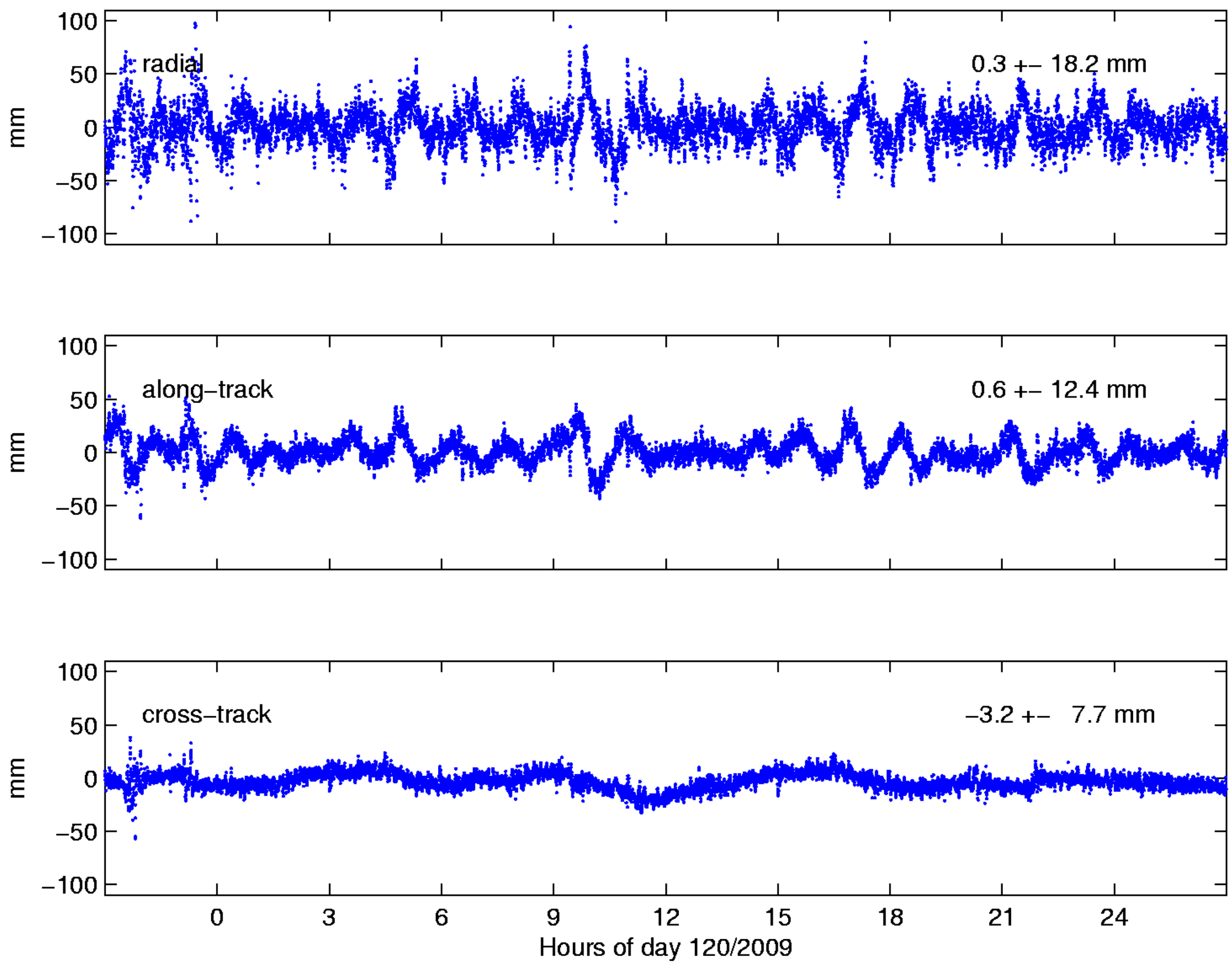

Orbit Differences KIN-RD, Time-Differenced

Largest scatter of kin. positions

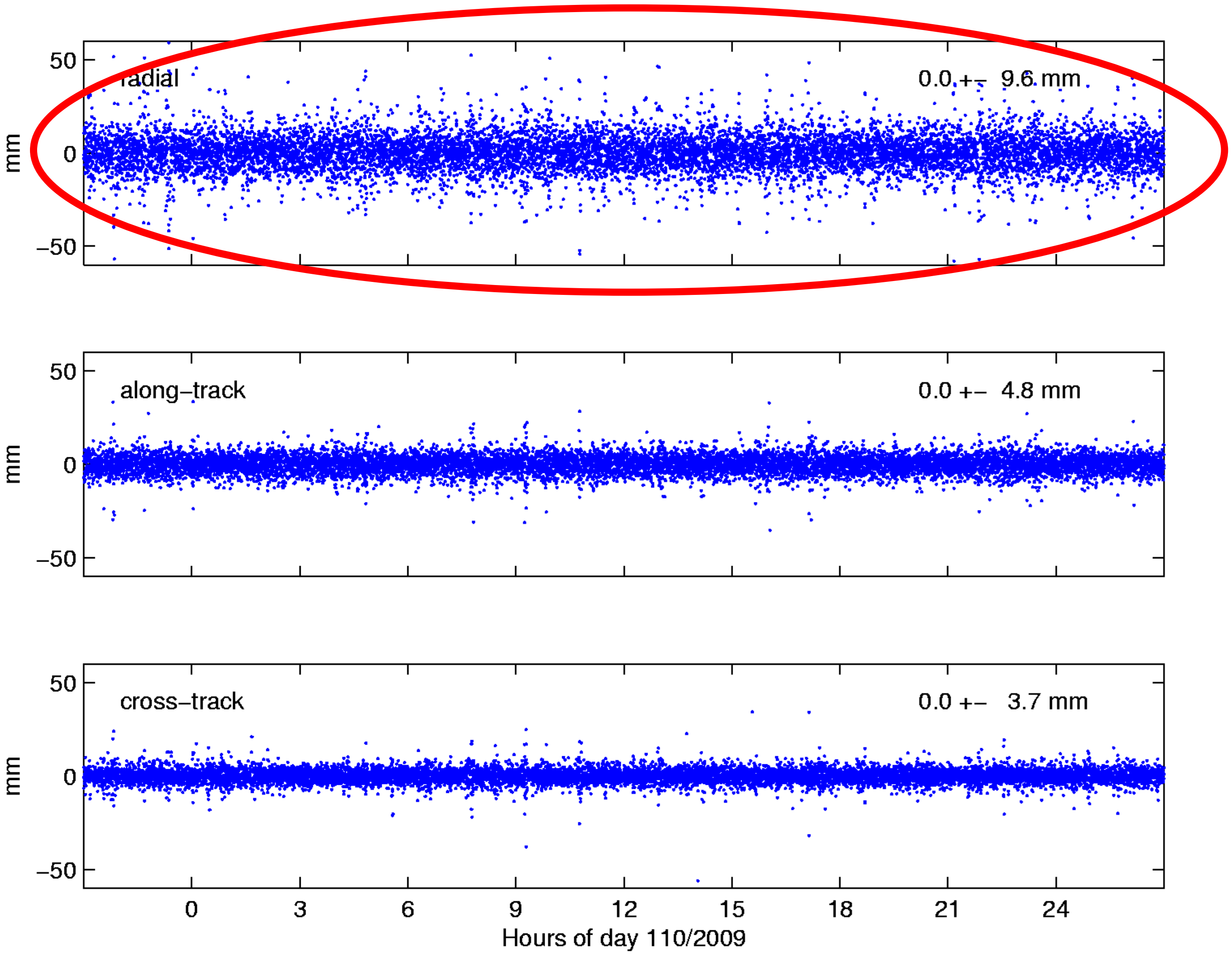

Pseudo-Stochastic Accelerations (GOCE: Begin of Mission)

First drag-free
flight on 7-May

Largest signal
due to air-drag

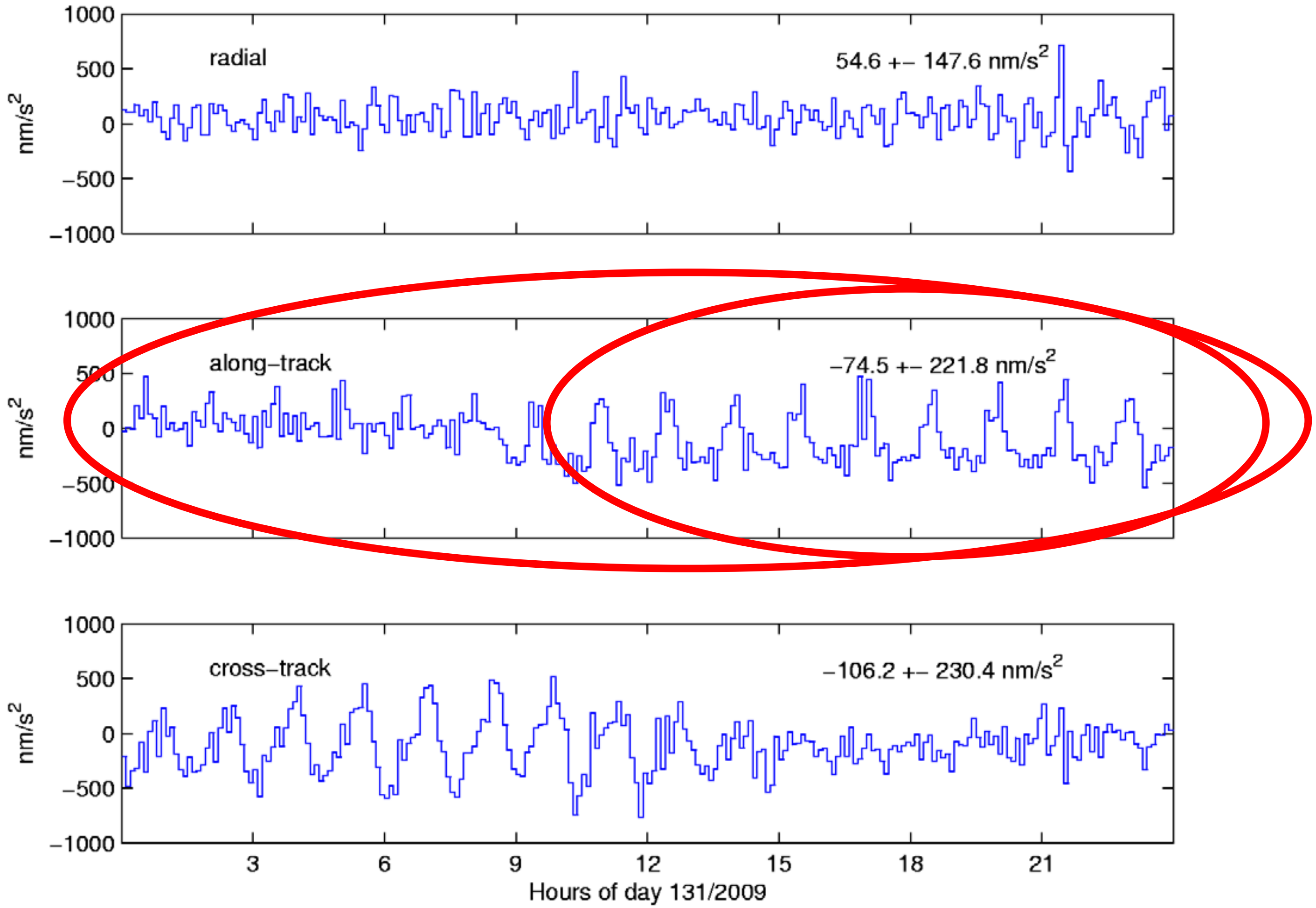

Improving LEO Orbit Determination (1)

PCV modeling is one of the limiting factors for most precise LEO orbit determination. Unmodeled PCVs are systematic errors, which

- **directly** propagate into kinematic orbit determination and severly degrade the position estimates

- propagate into reduced-dynamic orbit determination to a smaller, **but still large extent**

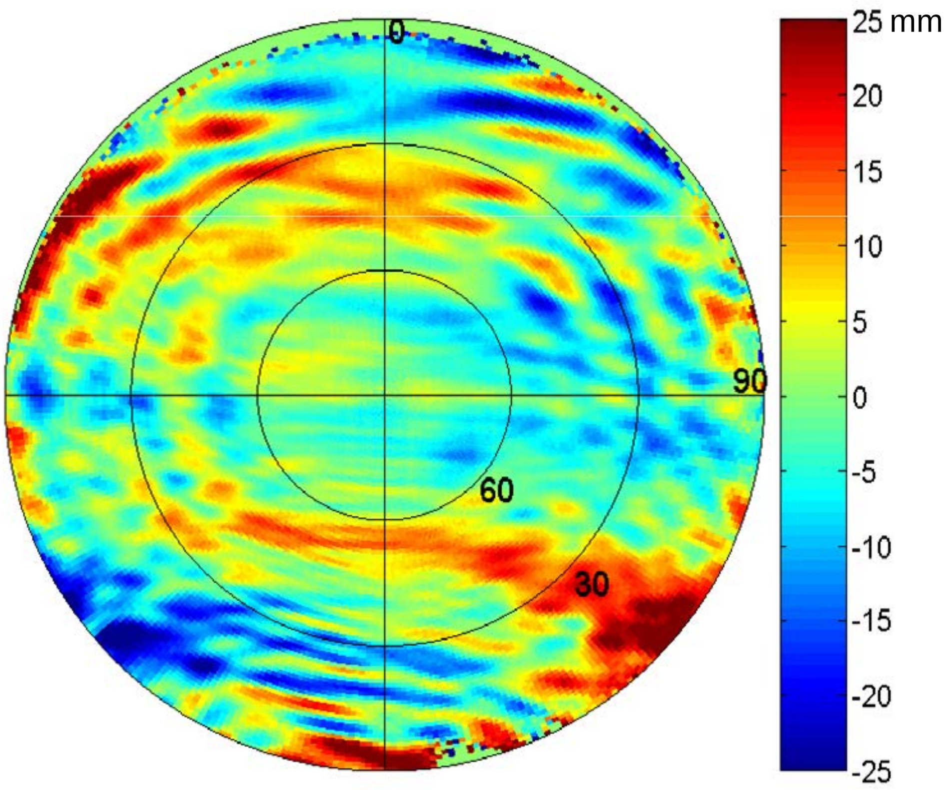

(Jäggi et al., 2009)

Improving LEO Orbit Determination (2)

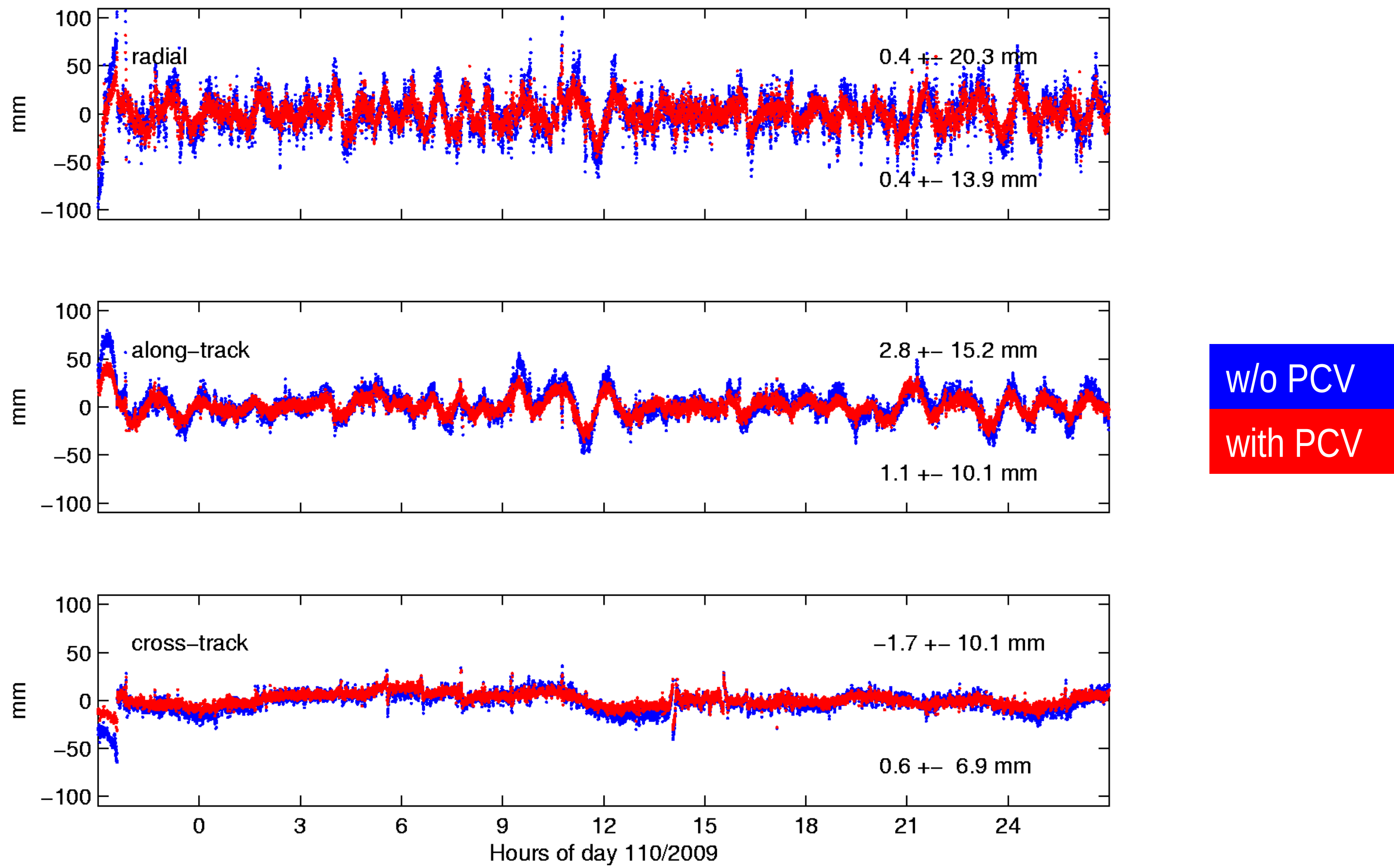

Orbit Differences KIN-RD (GOCE: entire mission)

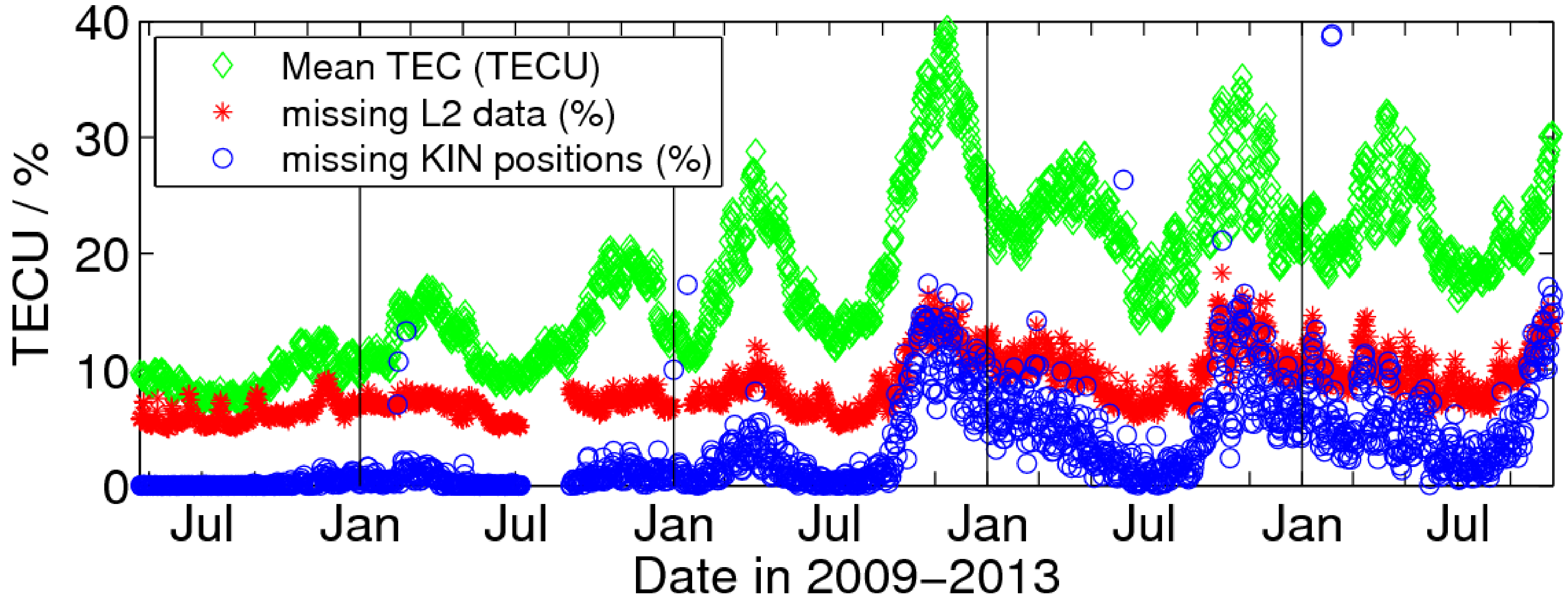

The result illustrates the **consistency** between both orbit-types. The level of the differences is usually given by the quality of the kinematic positions.

The differences are highly correlated with the **ionosphere activity** and with **data losses on L2**.

(Bock et al., 2014)

Orbit Differences KIN-RD (GOCE)

Ascending arcs (RMS)

Descending arcs (RMS)

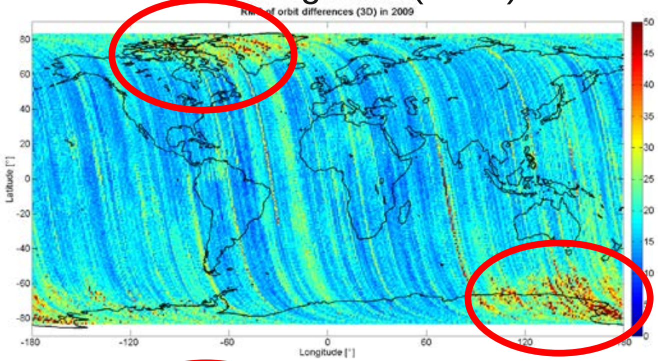

2009

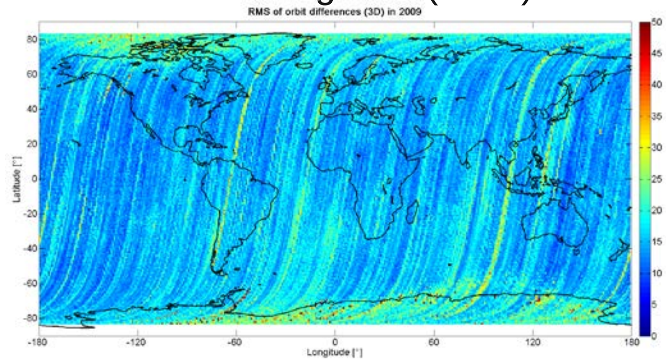

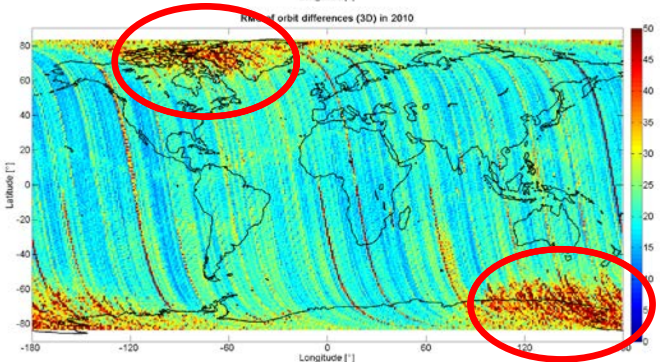

2010

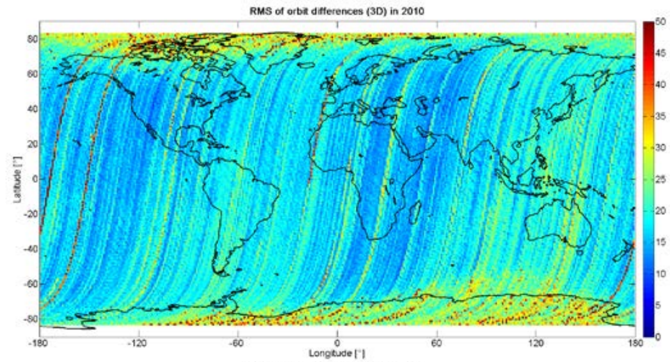

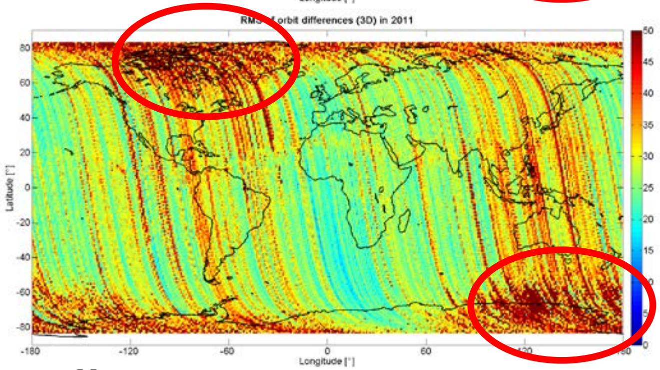

2011

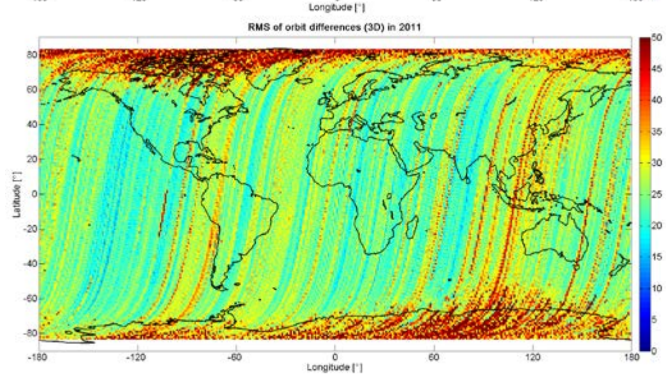

Wilhelm und Else Heraeus Autumn School
Global Gravity Field Modeling
from Satellite-to-Satellite Tracking Data

Orbit Validation with SLR (GOCE)

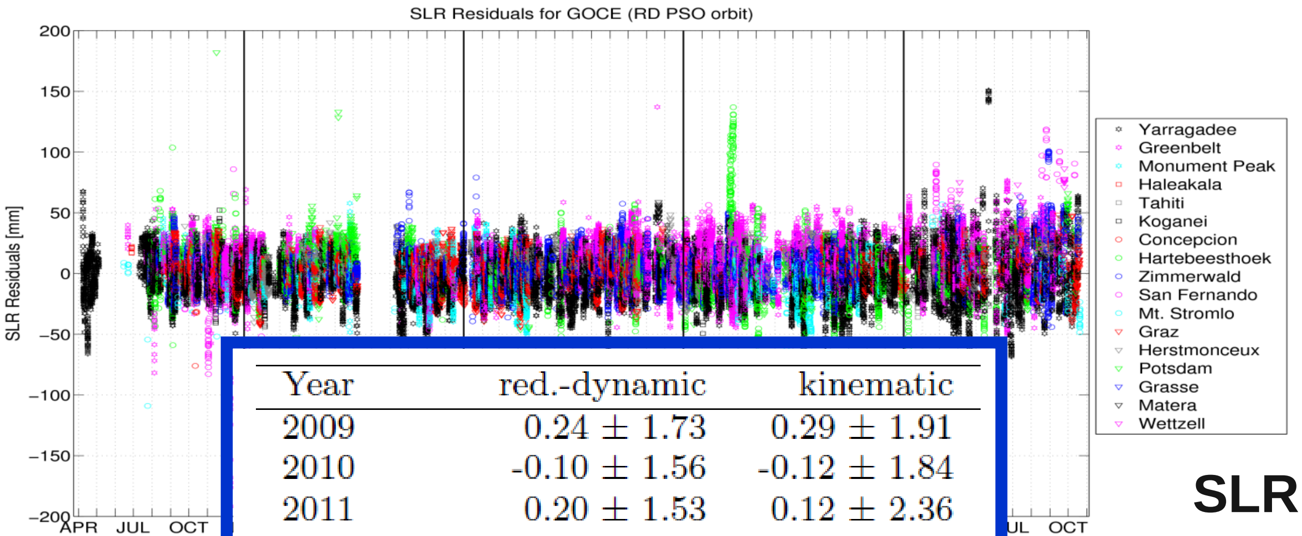

Reduced-dynamic

Year	red.-dynamic	kinematic
2009	0.24 ± 1.73	0.29 ± 1.91
2010	-0.10 ± 1.56	-0.12 ± 1.84
2011	0.20 ± 1.53	0.12 ± 2.36
2012	0.10 ± 1.94	-0.05 ± 2.78
2013	0.63 ± 2.62	0.45 ± 3.17
2009–2013	0.18 ± 1.84	0.10 ± 2.42

SLR statistics:

Mean ± RMS (cm)

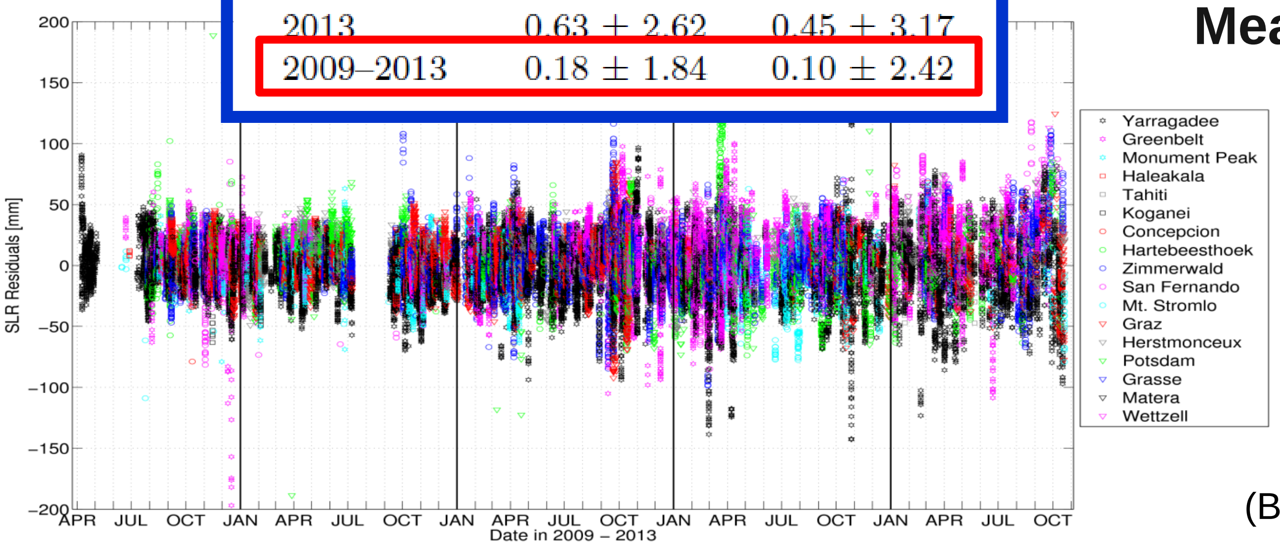

Kinematic

(Bock et al., 2014)

Orbit Validation with SLR (GOCE)

LEO orbits may be shifted up to several cm‘s in the cross-track direction by unmodeled PCVs.

Thanks to the low orbital altitude of GOCE it could be confirmed for the first time with SLR data that the PCV-induced cross-track shifts are real (see measurements from the SLR stations in the east and west directions at low elevations).

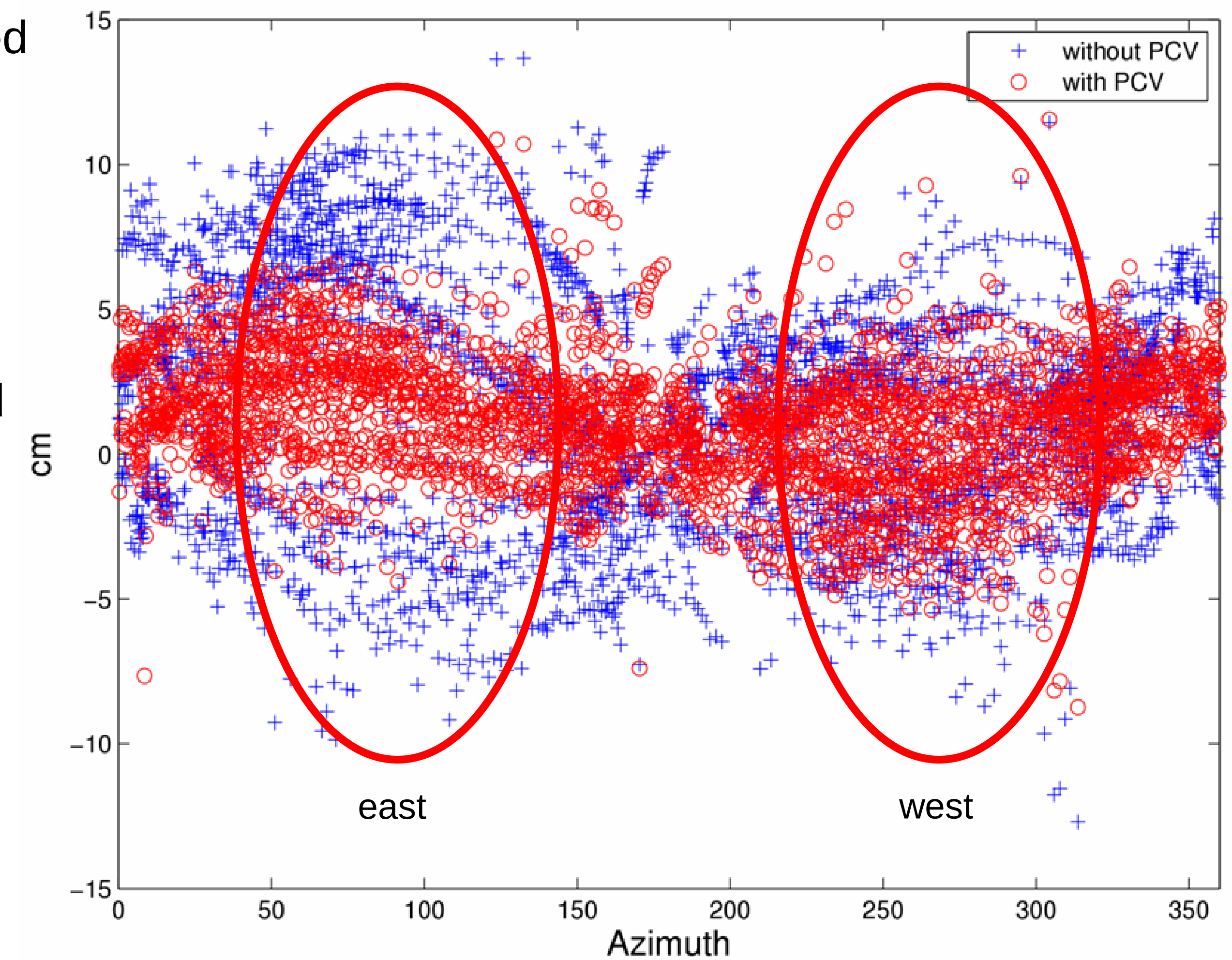

SLR validation concepts

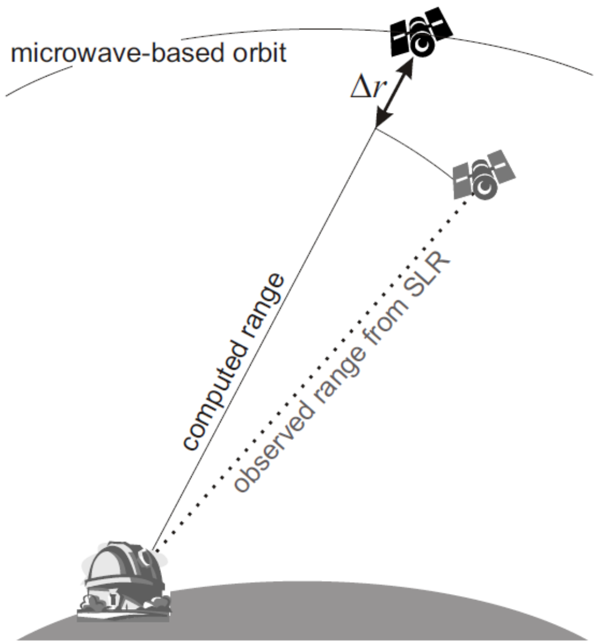

(Flohrer, 2008)

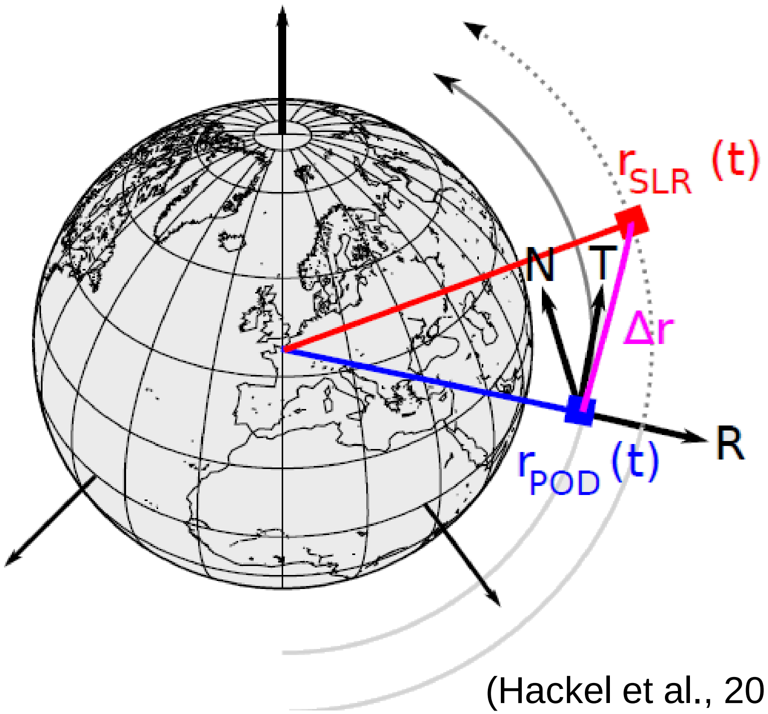

(Hackel et al., 2015)

Especially LEO satellites at **low orbital altitudes** allow not only for a validation of the orbit quality in the radial direction, but also in the other directions. Using long data spans, mean SLR biases may be determined in along-track and cross-track, as well.

Other Validation Concepts (1)

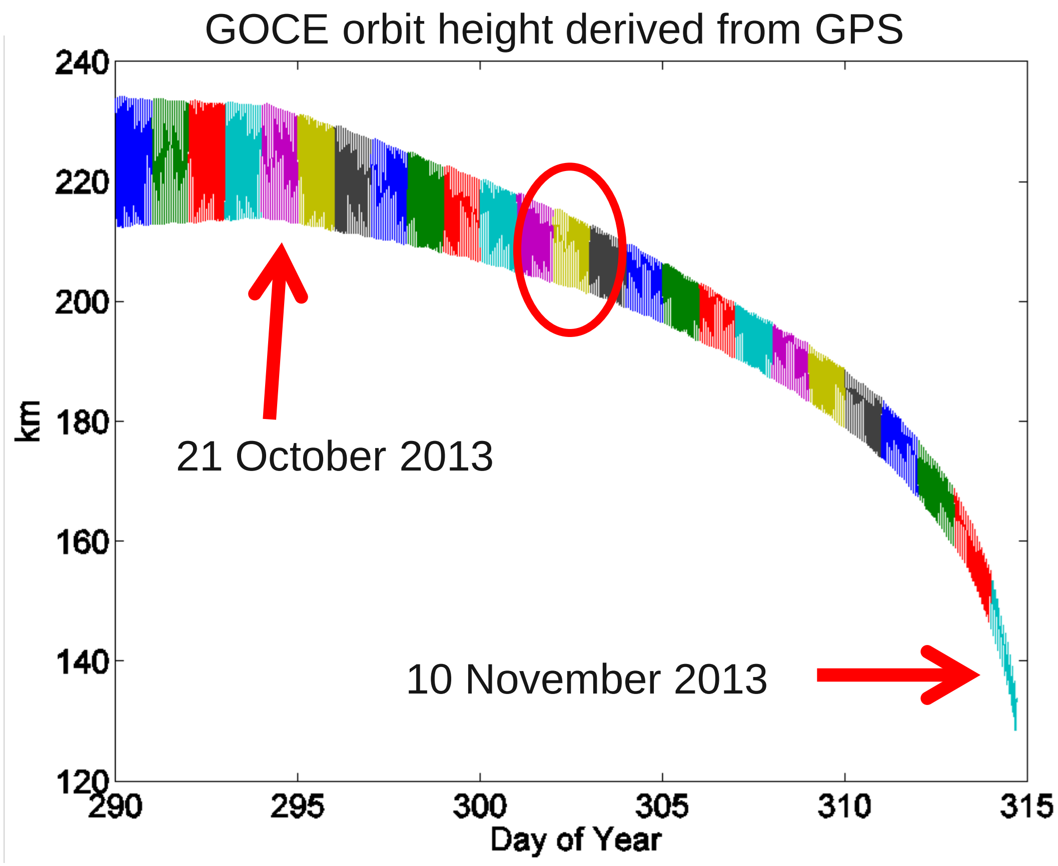

At extremely low orbital altitudes, the comparison between reduced-dynamic and kinematic orbits **rather** validates the quality of the reduced-dynamic orbits.

Wilhelm und Else Heraeus Autumn School
Global Gravity Field Modeling
from Satellite-to-Satellite Tracking Data

Other Validation Concepts (2)

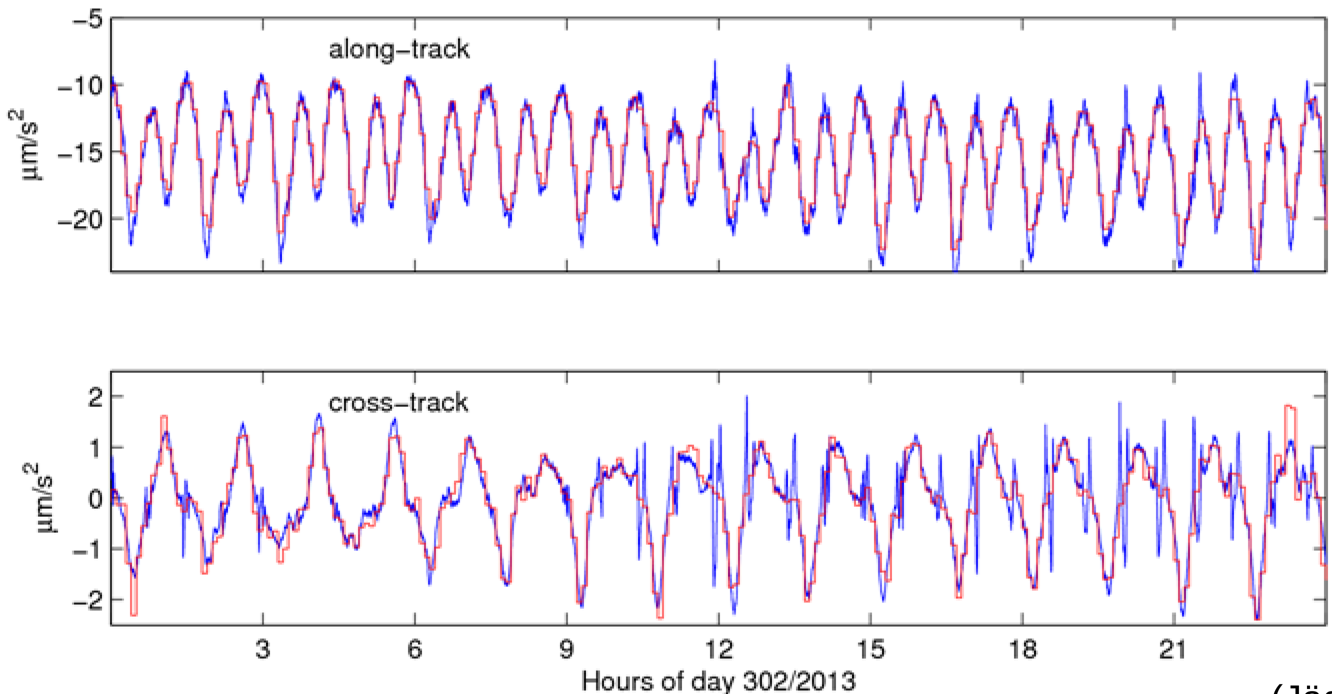

(Jäggi et al., 2014)

The comparison between **estimated accelerations** and measured data from onboard **accelerometers** may also provide an indication of the underlying orbit quality. If non-gravitational force models are taken into account, the **magnitude** of the estimated accelerations indicates the quality of the force modeling.

Non-gravitational Force Modeling (1)

Swarm orbit solutions derived from GPS

		ID0	ID7	ID8	
Ref. Frames	IERS1996	✓		kinematic only (KIPP)	[5]
	IERS2010		✓		[6]
Gravitation	GGM01S+TOP3.0	✓			[7]
	GOCO03S+FES4.0		✓		[8]
Radiation	SRP cannon-ball	✓			
	SRP macro		✓		
	ERP macro		✓		
Aerodyn.	Drag cannon-ball	✓			
	Drag macro				
	Drag, lift, molec.		✓		[3]
Atm. Density	Jacchia-71G	✓			[9]
	DTM-2012				[10]
	NRLMSISE-00		✓		[11]
Wind	HWM-07		✓		[12]

(Hackel et al., 2015)

Non-gravitational Force Modeling (2)

Swarm orbit solutions derived from GPS

ID	CD	CE	CR	a_R [nm/s^2]	a_T [nm/s^2]	a_N [nm/s^2]	SLR Residuals [mm]
id0	1.3 ± 0.3	n/a ± n/a	4.3 ± 0.9	9.4	36.9	24.3	-1.1 ± 16.7
id7	0.8 ± 0.2	0.7 ± 0.2	1.0 ± 0.2	1.5	22.2	14.0	0.7 ± 15.9
id8	n/a ± n/a	n/a ± n/a	n/a ± n/a	n/a	n/a	n/a	-0.7 ± 38.2

Quite an effort is needed to **actually improve** the quality of reduced-dynamic trajectories by taking into account non-gravitational force models. If dense and continuous tracking data (such as GPS) are available, the **pseudo-stochastic orbit modeling techniques are very powerful**.

But of course, a good modeling is always preferred. This guarantees that the trajectories have a **good dynamical stiffness** and are less prone to data problems and outages. But for results of highest quality, empirical parameters are usually nevertheless needed …

(Hackel et al., 2015)

Purely Dynamic LEO Orbit Modeling

GOCE orbit :

Acc.	CM[1]	Acc. 1
1-10 Nov. 2009[2]	5.18	5.20
1-10 Nov. 2009[3]	5.18	5.27
1-10 Nov. 2009[4]	5.18	5.17
Full mission[4,5]	6.87	6.89

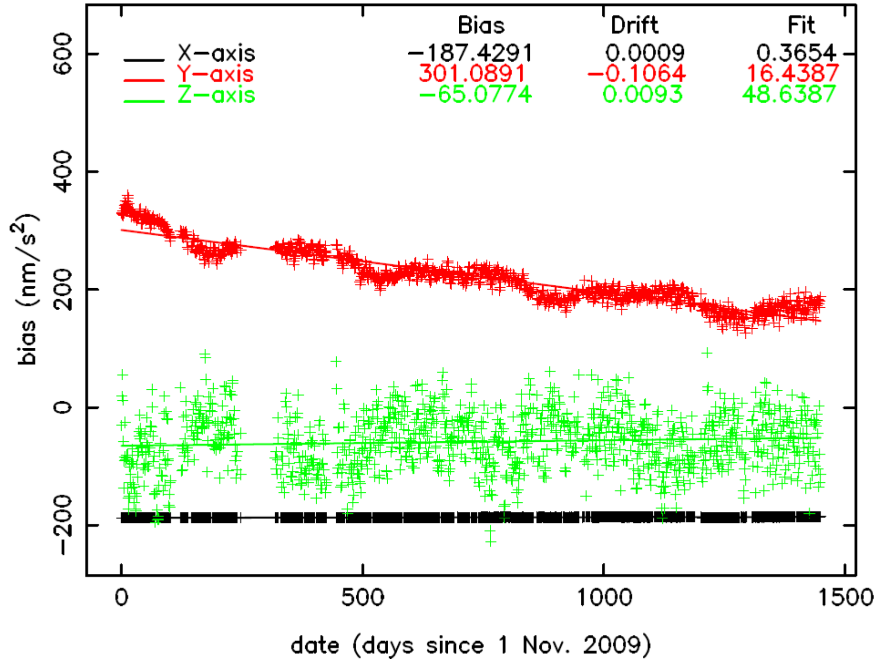

Thanks to the outstanding quality of the **GOCE accelerometers**, purely dynamic orbit determination is feasible. The table shows that the agreement with the official Precise Science Orbits is about 5cm when using the common-mode or even the individual accelerometer data. Accelerometer calibration parameters are estimated together with the initial conditions as the only additional parameters.

(Visser et al., 2015)

Wilhelm und Else Heraeus Autumn School
Global Gravity Field Modeling
from Satellite-to-Satellite Tracking Data

GRACE Orbit Validation with K-Band (1)

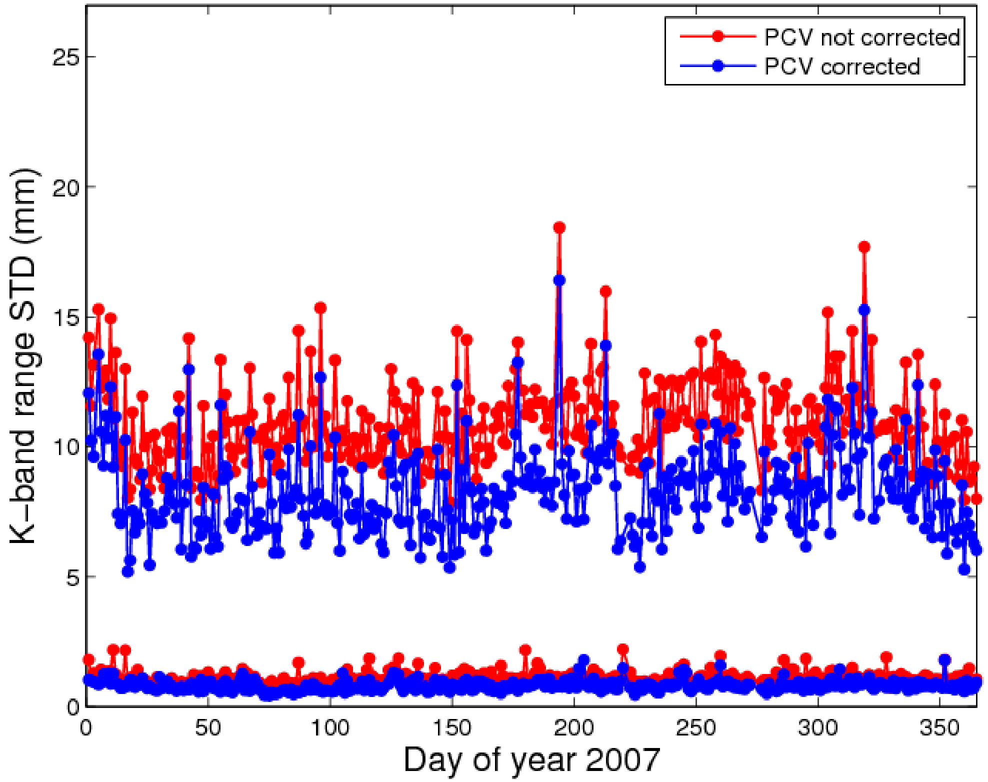

ZD solution
< 1cm

DD solution
(ambiguity-fixed)
< 1mm

The ultra-precise and continuously available K-Band data allow it to validate the **inter-satellite distances** between the GRACE satellites. Thanks to this validation, e.g., PCV maps were recognized to be crucial for high-quality POD.

(Jäggi et al., 2009)

GRACE Orbit Validation with K-Band (2)

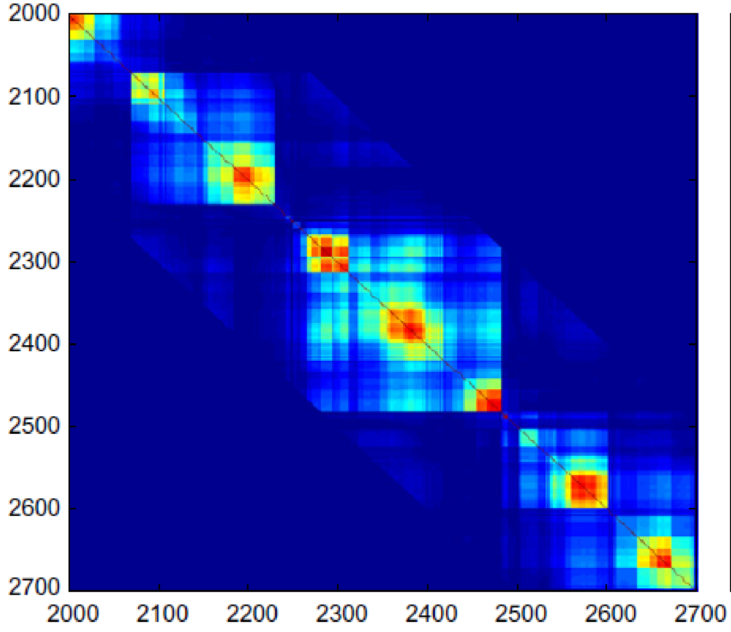

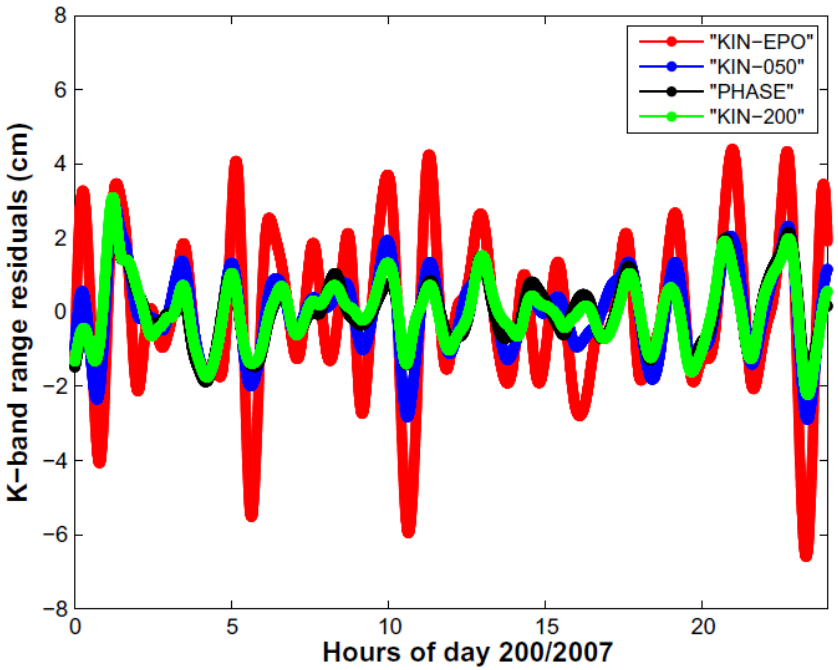

Reduced-dynamic fits through kinematic positions only then have the same quality as reduced-dynamic orbits directly derived from GPS carrier phase, if **covariance** information from the kinematic positioning is used over sufficiently long intervals to **properly weight** the kinematic pseudo-observations in the orbit determination.

(Jäggi et al., 2011b)

Generalized Orbit Determination

Generalized Orbit Determination (1)

The **actual orbit** $\boldsymbol{r}(t)$ is expressed as a truncated Taylor series:

$$\mathbf{r}(t) = \mathbf{r}_0(t) + \sum_{i=1}^{n_O} \frac{\partial \mathbf{r}_0(t)}{\partial O_i} \cdot o_i + \sum_{i=1}^{d} \frac{\partial \mathbf{r}_0(t)}{\partial Q_i} \cdot q_i$$

$\mathbf{r}_0(t)$	A priori orbit
$\frac{\partial \mathbf{r}_0(t)}{\partial O_i}, \frac{\partial \mathbf{r}_0(t)}{\partial Q_i}$	Partials w.r.t. arc-specific and dynamic (global) parameters
o_i, q_i	Corrections of arc-specific and dynamic (global) parameters

The variational equations of the dynamic parameters, e.g., gravity field coefficients, may be solved by the general methods as discussed earlier in this lecture. Their solutions may be reduced to definite integrals and efficiently solved by numerical quadrature.

Generalized Orbit Determination (2)

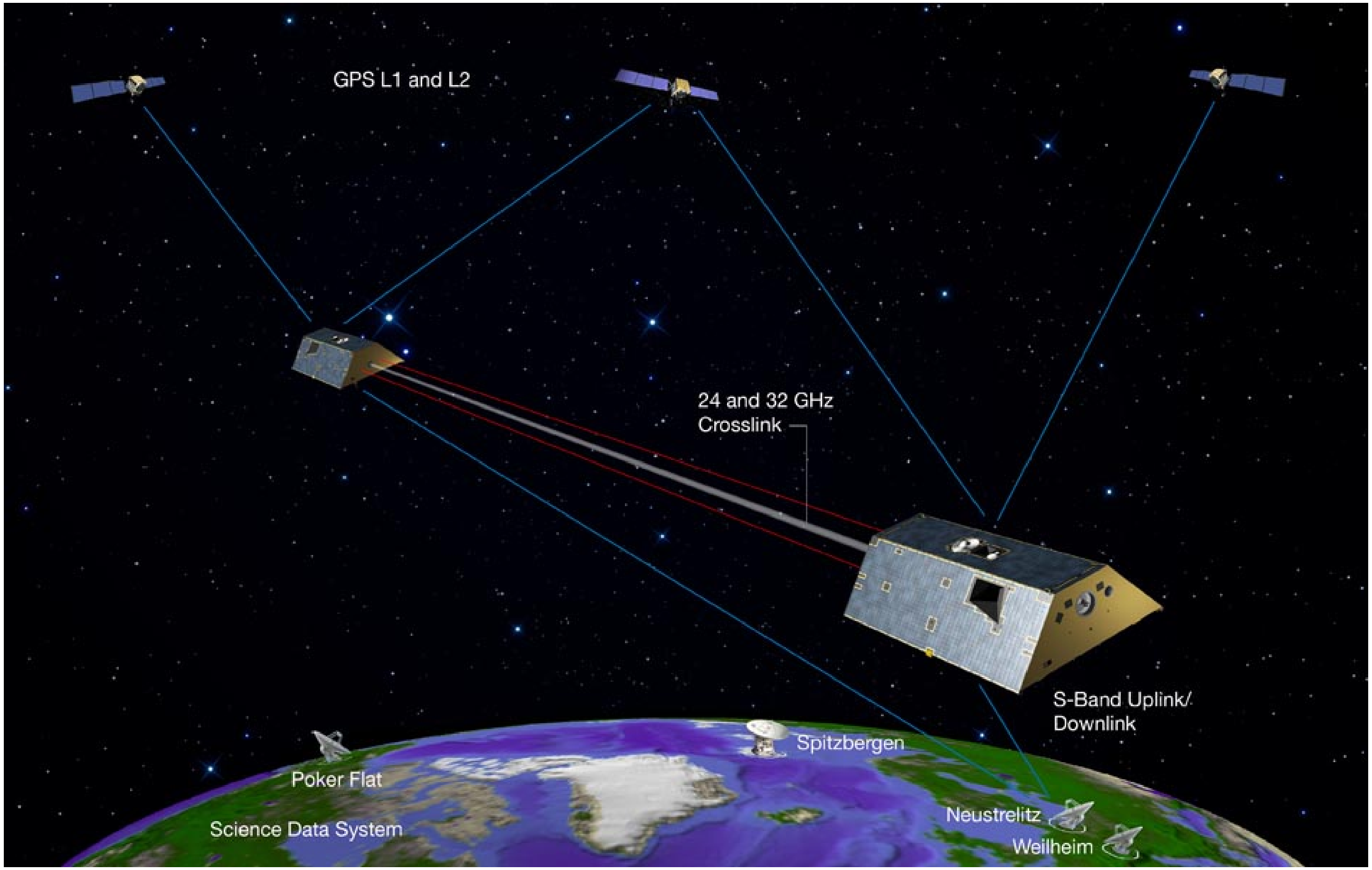

Generalized Orbit Determination (3)

The **actual orbit difference** $\mathbf{r}_a(t) - \mathbf{r}_b(t)$ is expressed as:

$$\begin{aligned}\mathbf{r}_a(t) - \mathbf{r}_b(t) = \quad & \mathbf{r}_{a0}(t) - \mathbf{r}_{b0}(t) \\ & + \sum_{i=1}^{n_{aO}} \frac{\partial \mathbf{r}_{a0}(t)}{\partial O_{ai}} \cdot o_{ai} \\ & - \sum_{i=1}^{n_{bO}} \frac{\partial \mathbf{r}_{b0}(t)}{\partial O_{bi}} \cdot o_{bi} \\ & + \sum_{i=1}^{d} \left(\frac{\partial \mathbf{r}_{a0}(t)}{\partial Q_i} - \frac{\partial \mathbf{r}_{b0}(t)}{\partial Q_i} \right) \cdot q_i\end{aligned}$$

In order to set-up the observation equations, the partial derivatives of the a priori orbits need to be related to the observables, e.g., by projecting the respective terms on the line-of-sight direction between GRACE-A and -B in the case of K-Band (biased) range observations.

Generalized Orbit Determination (4)

In case of **GPS-based gravity field determination**, the observation equations contain corrections for **arc-specific parameters** $\mathbf{o}$ and for (global) **dynamic parameters** $\mathbf{q}$

$$\varepsilon = \mathbf{A}_o\,\mathbf{o} + \mathbf{A}_q\,\mathbf{q} - \mathbf{l}$$

The corresponding normal equation system reads as

$$\begin{pmatrix} \mathbf{N}_{oo} & \mathbf{N}_{oq} \\ \mathbf{N}_{oq}^T & \mathbf{N}_{qq} \end{pmatrix} \cdot \begin{pmatrix} \mathbf{o} \\ \mathbf{q} \end{pmatrix} = \begin{pmatrix} \mathbf{b}_o \\ \mathbf{b}_q \end{pmatrix}$$

and, after pre-elimination of the arc-specific parameters, as

$$(\mathbf{N}_{qq} - \mathbf{N}_{oq}^T\,\mathbf{N}_{oo}^{-1}\,\mathbf{N}_{oq})\,\mathbf{q} = \mathbf{b}_q - \mathbf{N}_{oq}^T\,(\mathbf{N}_{oo}^{-1}\,\mathbf{b}_o)$$

Orbit Fixation

For didactic reasons, let us now **fix the arc-specific parameters** to previously determined values while estimating the corrections to the gravity field parameters in a second step. This implies that the sub-system

$$\mathbf{N}_{oo}\,\mathbf{o}' = \mathbf{b}_o$$

is solved **independently** from the remaining part of the correct normal equation system and that the parameters $\mathbf{o}'$ are introduced in the following gravity recovery step as known. The remaining normal equation system reads as

$$\mathbf{N}_{qq}\,\mathbf{q}' = \mathbf{b}_q - \mathbf{N}_{oq}^T\,\mathbf{o}' = \mathbf{b}_g - \mathbf{N}_{oq}^T\,(\mathbf{N}_{oo}^{-1}\,\mathbf{b}_o)$$

This yields a different (biased) solution as the orbit parameters $\mathbf{o}'$ fully depend **on the a priori gravity model** and the correlations between orbit and gravity field parameters are ignored.

(Meyer et al., 2015)

Relation to the Acceleration Approach (1)

Let us assume that the **second derivatives of the position vector** have been observed (derived by numerical differentiation from kinematic positions). The observation equations for one particular epoch read as

$$\varepsilon_r = \sum_{k=1}^{n_0} \frac{\partial \ddot{\mathbf{r}}(t_r)}{\partial O_k} \cdot o_k + \sum_{k=1}^{d} \frac{\partial \ddot{\mathbf{r}}(t_r)}{\partial Q_k} \cdot q_k - \Delta \ddot{\mathbf{r}}_r$$

where $\Delta \ddot{\mathbf{r}}_r$ represents the observed minus the computed acceleration. The partial derivatives in the second sum may be replaced by the right-hand sides of the variational equations, which read as

$$\frac{\partial \ddot{\mathbf{r}}(t_r)}{\partial Q_k} = \frac{\partial \mathbf{f}(t_r)}{\partial \mathbf{r}(t_r)} \cdot \frac{\partial \mathbf{r}(t_r)}{\partial Q_k} + \frac{\partial \mathbf{f}(t_r)}{\partial \dot{\mathbf{r}}(t_r)} \cdot \frac{\partial \dot{\mathbf{r}}(t_r)}{\partial Q_k} + \frac{\partial \mathbf{f}(t_r)}{\partial Q_k}$$

Wilhelm und Else Heraeus Autumn School
Global Gravity Field Modeling
from Satellite-to-Satellite Tracking Data

Relation to the Acceleration Approach (2)

The observation equations actually used in the acceleration approach read as

$$\varepsilon_r = \sum_{k=1}^{d} \frac{\partial \mathbf{f}(t_r)}{\partial Q_k} \cdot q_k - \Delta \ddot{\mathbf{r}}_r$$

From the point of view of orbit determination this implies that

$$\sum_{k=1}^{n_0} \frac{\partial \ddot{\mathbf{r}}(t_r)}{\partial O_k} \cdot o_k + \sum_{k=1}^{d} \left(\frac{\partial \mathbf{f}(t_r)}{\partial \mathbf{r}(t_r)} \cdot \frac{\partial \mathbf{r}(t_r)}{\partial Q_k} + \frac{\partial \mathbf{f}(t_r)}{\partial \dot{\mathbf{r}}(t_r)} \cdot \frac{\partial \dot{\mathbf{r}}(t_r)}{\partial Q_k} \right) = \mathbf{0}$$

It is thus assumed that the changes in the second derivatives of the orbit caused by the estimated gravity field parameters are counterbalanced by changes of the second derivatives of the orbit due to the changes in the arc-specific parameters. The assumption is met if the a priori orbit used to compute $\Delta \ddot{\mathbf{r}}_r$ in the acceleration approach equals the estimated a posteriori orbit from classical orbit determination.

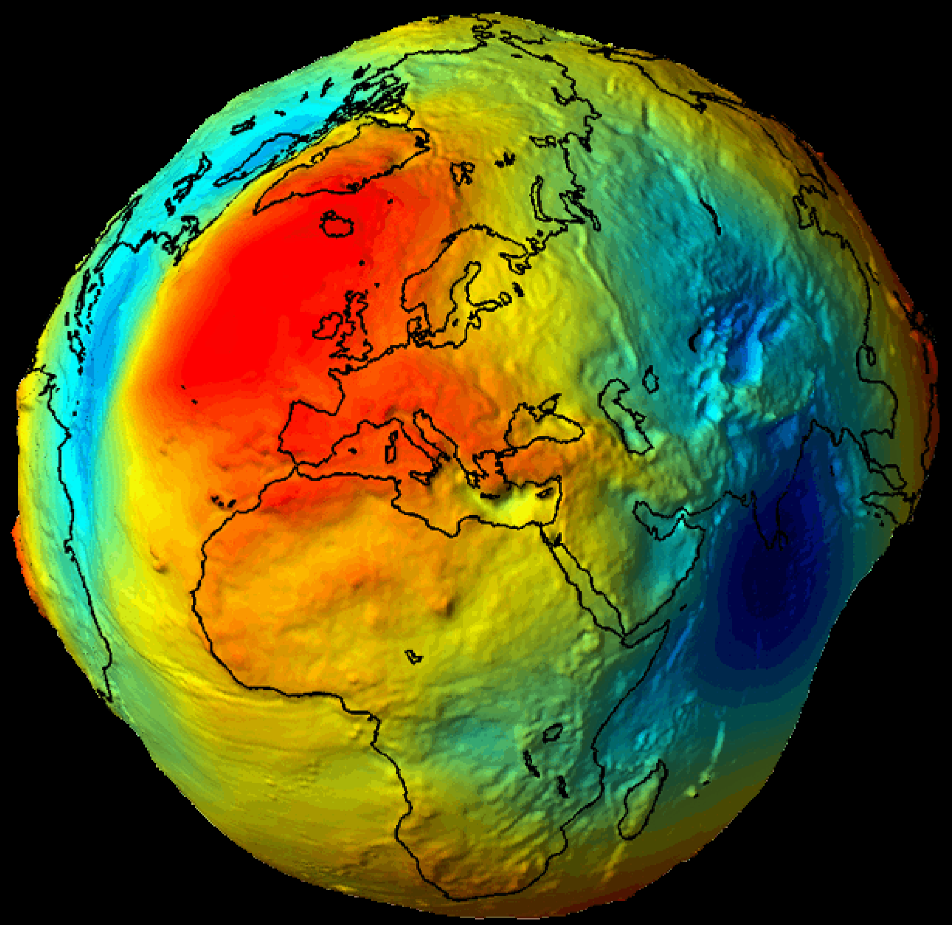

Gravity Fiel Solutions from Kinematic Positions

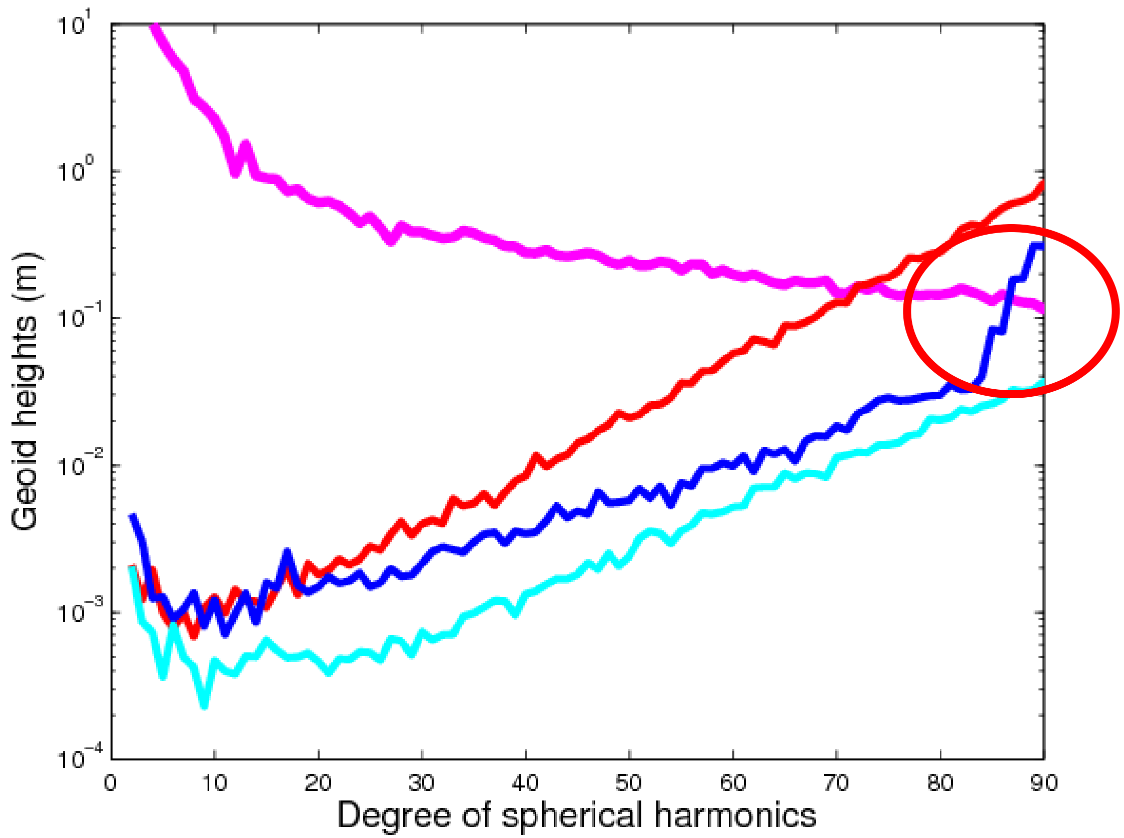

Reference field:
GRACE Solution

Differences:
1-year GRACE
0.7-years GOCE
8-years CHAMP

Different slopes of the difference degree amplitudes due to different LEO altitudes.

(Jäggi et al., 2011a)

Impact of PCVs on GPS-Based Gravity Field Recovery

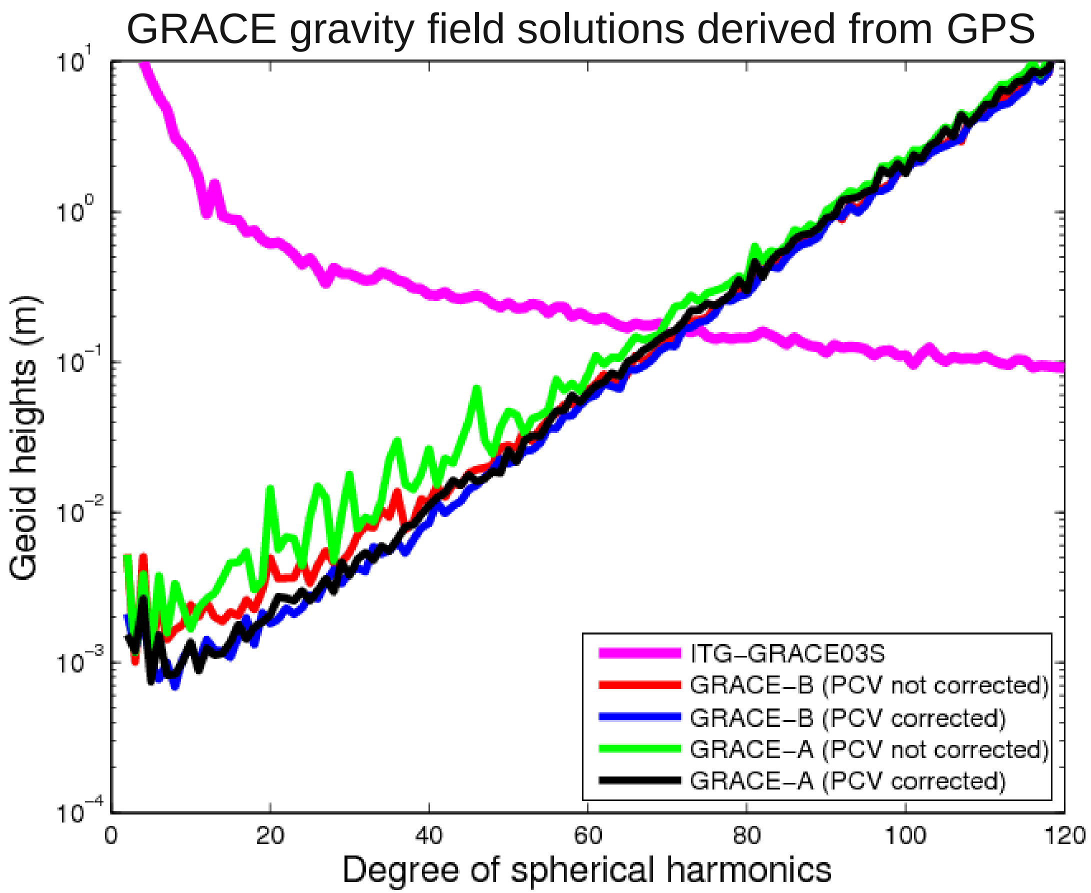

Mismodeled PCV maps may propagate via kinematic positions into the gravity field solutions. They represent a significant source for systematic POD errors.

(Jäggi et al., 2009)

Impact of PCVs on GPS-Based Gravity Field Recovery

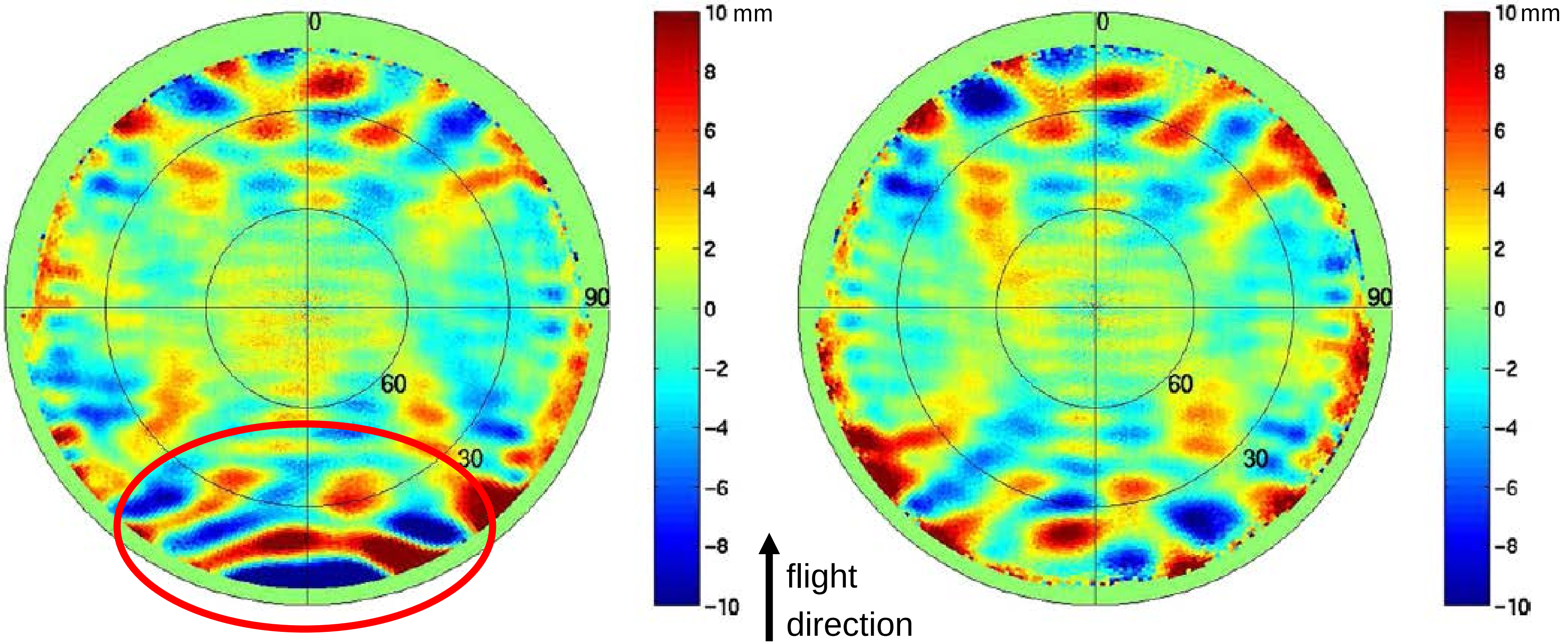

GRACE-A
(occultation antenna switched on)

GRACE-B

(Jäggi et al., 2009)

Other Sources of Systematic Errors

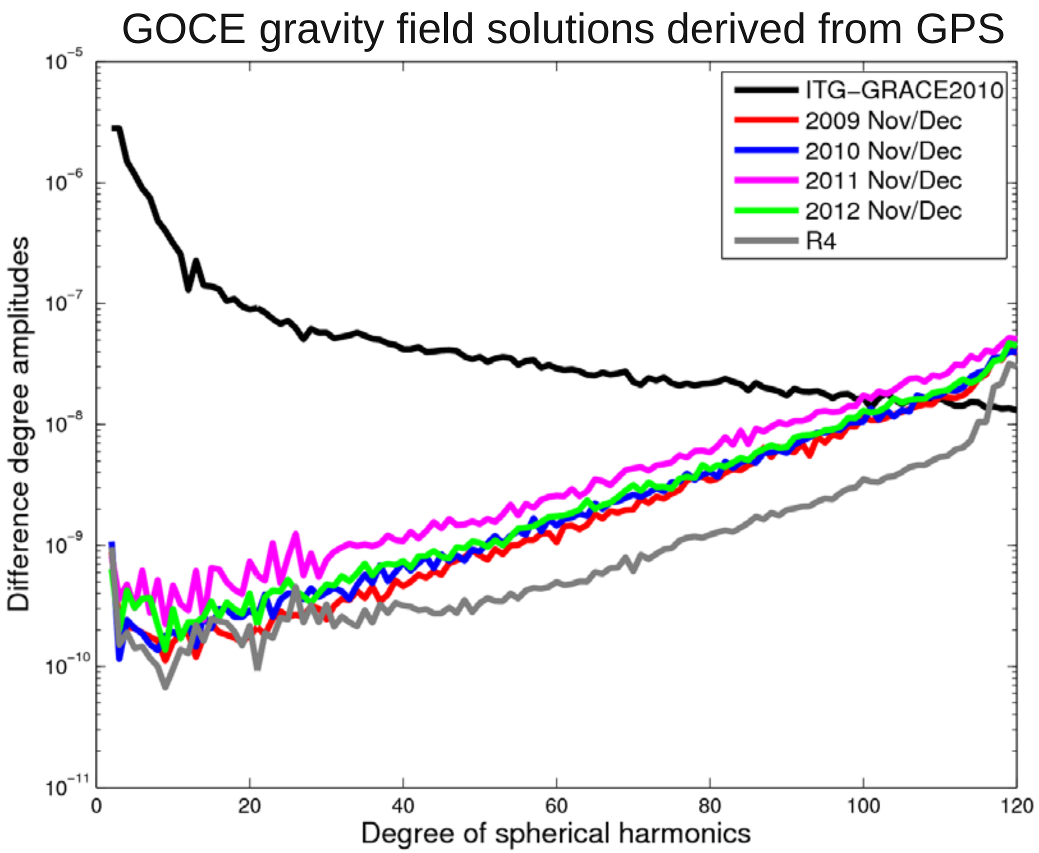

Significantly different qualities of various **bi-monthly** GOCE GPS-only solutions. The long-term solution R4 shows no significantly improved quality w.r.t. the bi-monthly solutions below degree 30.

(Jäggi et al., 2015)

Ionospheric Effects in the Orbits (1)

Systematic effects around the geomagnetic equator are present in the ionosphere-free GPS phase residuals **=> affects kinematic positions**

Degradation of kinematic positions around the geomagnetic equator propagates into gravity field solutions.

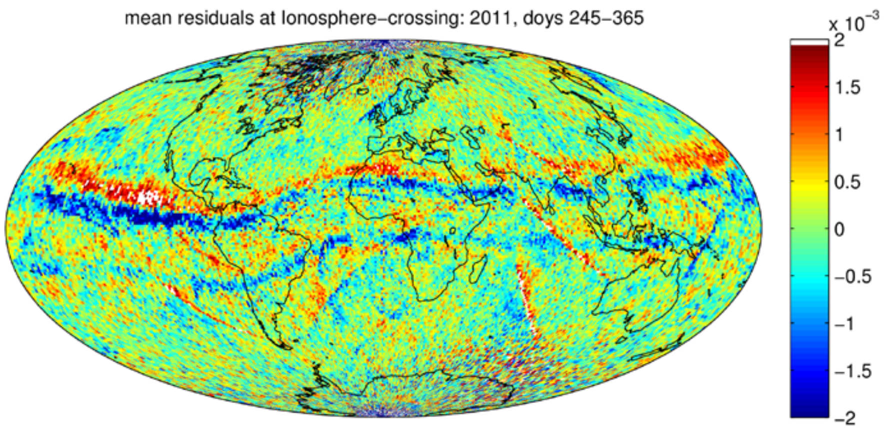

Phase observation residuals (- 2 mm … +2 mm) mapped to the ionosphere piercing point

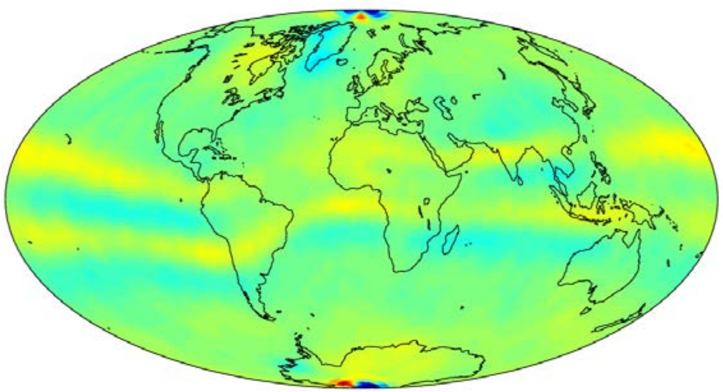

Geoid height differences (−5 cm … 5 cm); TIM-R4 model

(Jäggi et al., 2015a)

Wilhelm und Else Heraeus Autumn School
Global Gravity Field Modeling
from Satellite-to-Satellite Tracking Data

Ionospheric Effects in the Orbits (2)

One possible cause is the **neglection of the higher order ionosphere (HOI)** correction terms.

First tests using HOI correction terms did, however, **not** show any improvement in the results.

But an empirical approach can be adopted:

- Removal of observations, which have large ionosphere changes from one epoch to the next (e.g. >5cm/s).

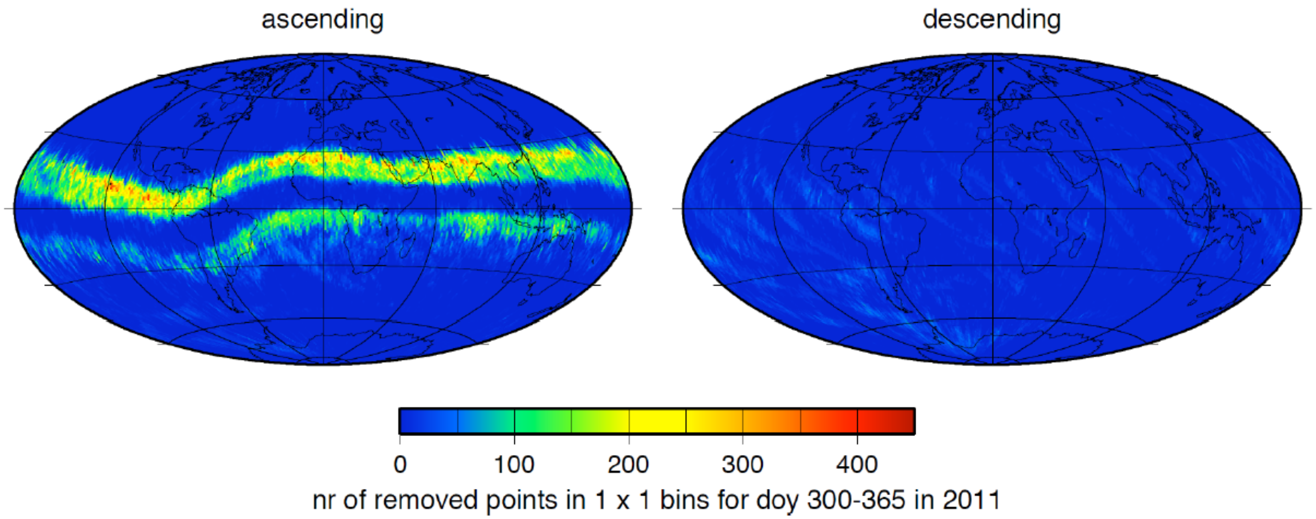

Ionospheric Effects in the Orbits (3)

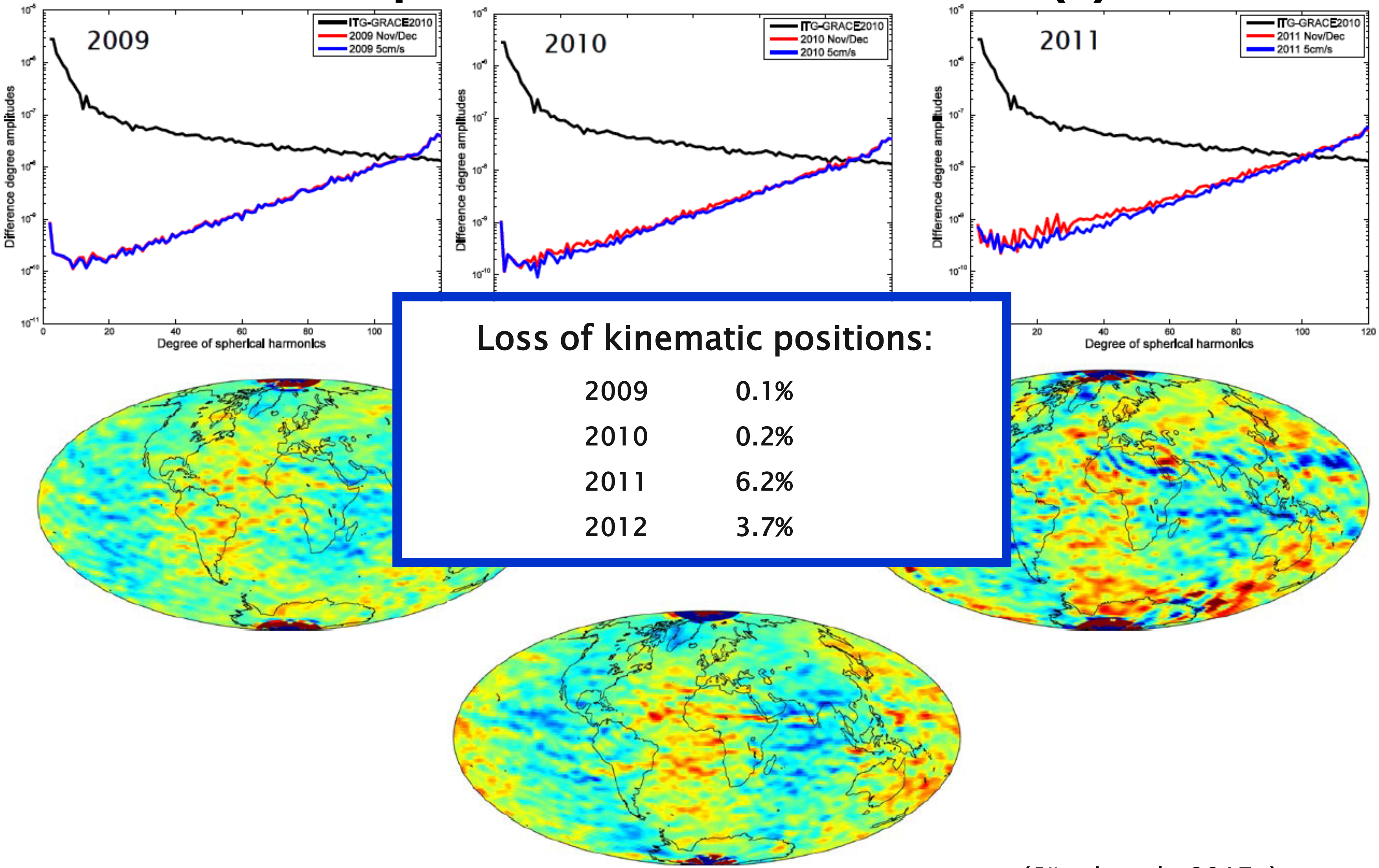

Loss of kinematic positions:

2009	0.1%
2010	0.2%
2011	6.2%
2012	3.7%

(Jäggi et al., 2015a)

Attempts to Model the Ionospheric Effects (1)

Conventional modeling of HOI correction terms does not show any improvements. Also the application of further HOI correction terms than recommended by the IERS Conventions 2010 does not bring any further improvements.

Ionosphere delays (= slant TEC) need to be directly derived from the geometry-free linear combination to compute more realistic HOI correction terms.

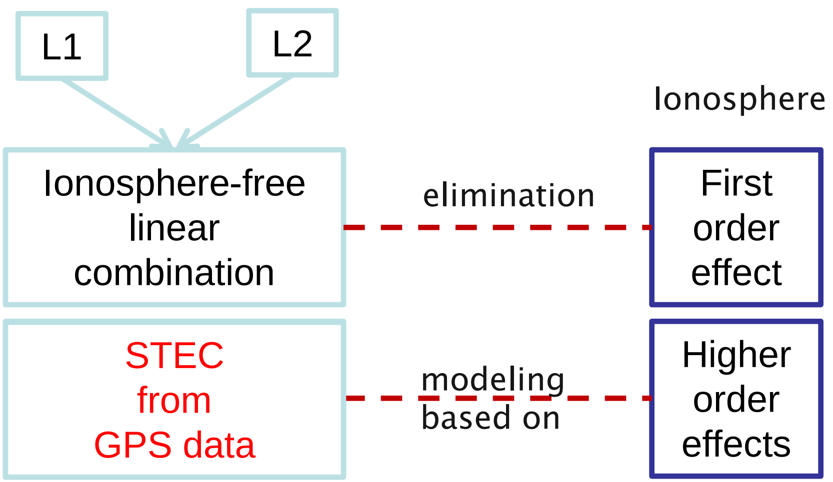

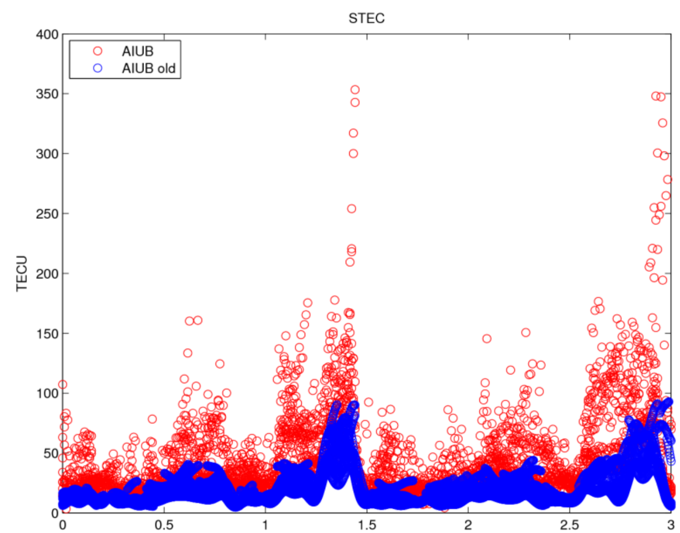

Attempts to Model the Ionospheric Effects (2)

STEC estimations are fed into the kinematic orbit determination instead of the global ionosphere map

HOI correction terms are computed based on the STEC estimations

Only partial reduction achieved so far in gravity field solutions

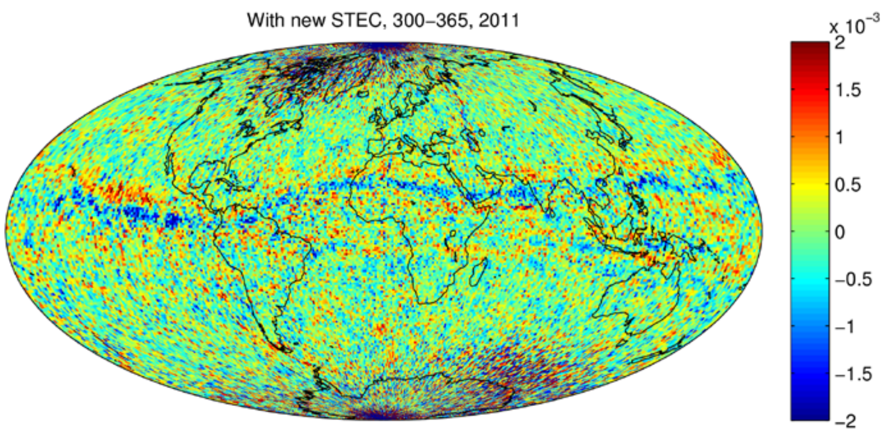

Phase observation residuals (-2 mm … +2 mm) mapped to the ionosphere piercing point

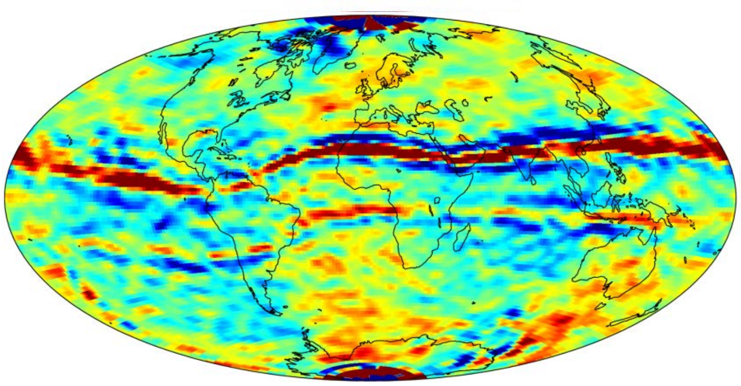

Geoid height differences (-5 cm … 5 cm); Nov-Dec 2011

Situation for other LEO Satellites (1)

Original GPS Data
(13 months)

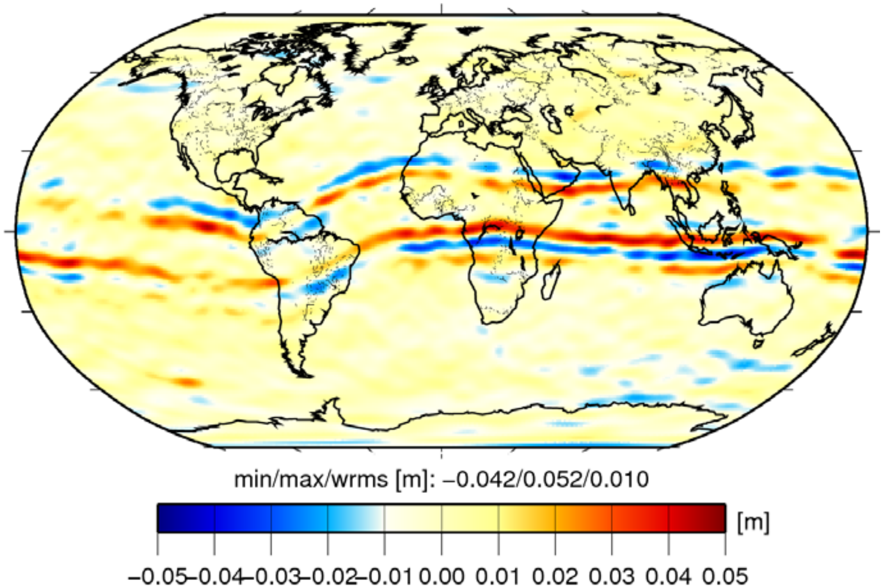

Screened GPS Data
(18 months)

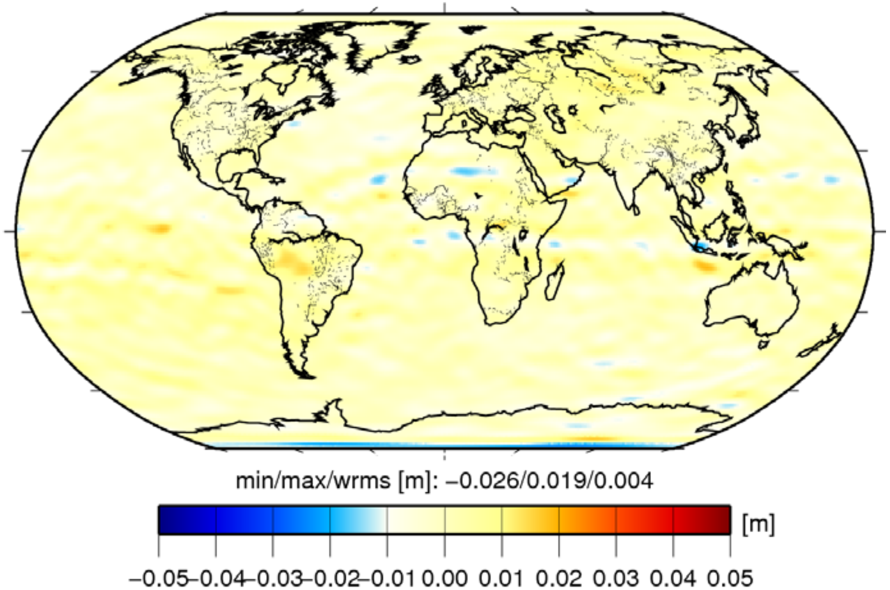

(Differences wrt GOCO05S, 400 km Gauss smoothing adopted)

Systematic signatures along the geomagnetic equator may be efficiently reduced for static Swarm gravity field recovery when screening the raw RINEX GPS data files with the dL4/dt criterion.

(Jäggi et al., 2015b)

Situation for other LEO Satellites (2)

Original GPS Data
(Swarm)

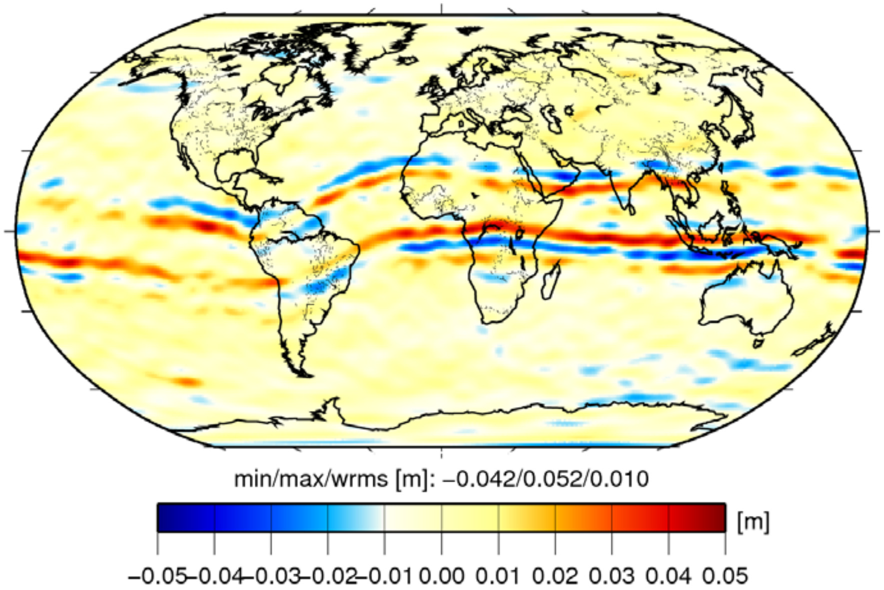

Original GPS Data
(GRACE)

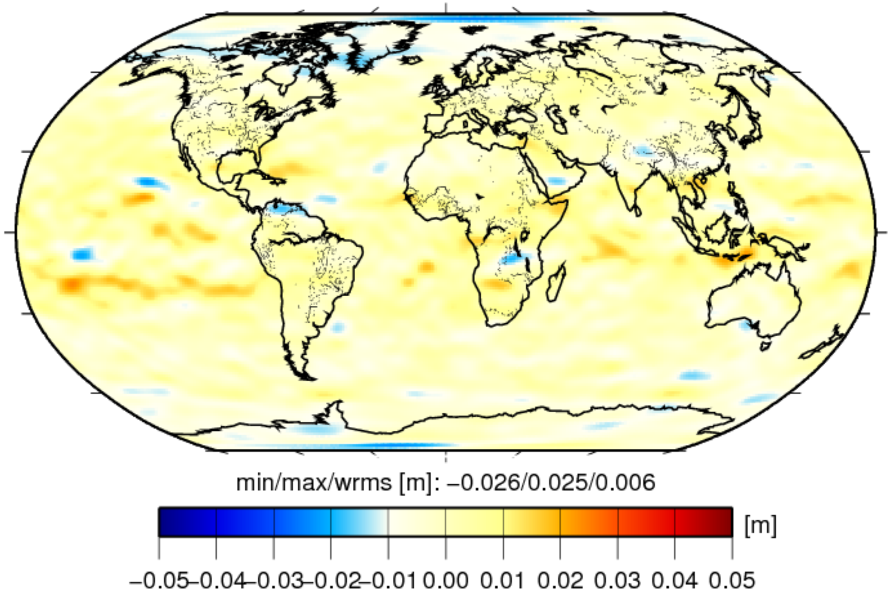

(Differences wrt GOCO05S, 400 km Gauss smoothing adopted)

Systematic signatures along the geomagnetic equator are not visible when using original L1B RINEX GPS data files from the GRACE mission.

Situation for other LEO Satellites (3)

GRACE-B, doy 060-090, 2014 (all arcs)

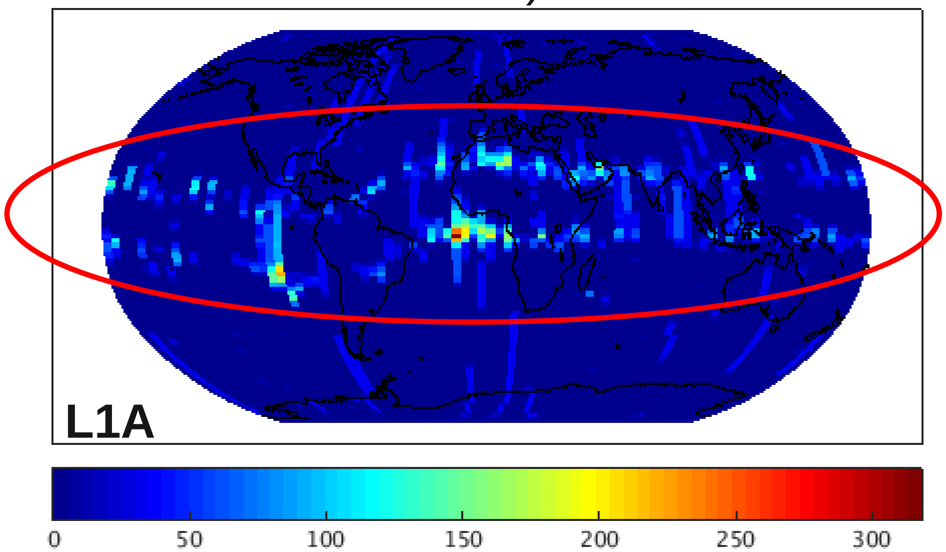

Swarm-A, doy 060-090, 2014 (all arcs)

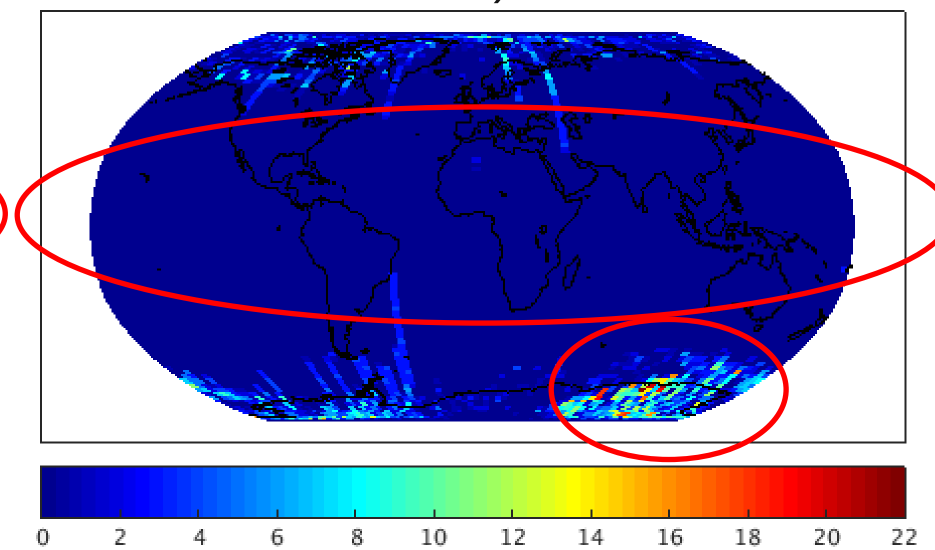

Significant amounts of data are missing in GRACE L1B RINEX files

=> problematic signatures cannot propagate into gravity field.

Swarm RINEX files are more complete (gaps only over the poles)

=> problematic signatures do propagate into the gravity field.

(Jäggi et al., 2015b)

Multi-Satellite SLR Solutions (1)

		SLR solutions
Estimated parameters		LAGEOS-1/2, Starlette, Stella, AJISAI, LARES, Blits, Larets, Beacon-C
Orbits	**Osculating elements**	a, e, i, Ω, ω, u_0 (LAGEOS: 1 set per 10 days, LEO: 1 set per 1 day)
	Dynamical parameters	LAGEOS-1/2 : S_0, S_S, S_C (1 set per 10 days) Sta/Ste/AJI : C_D, S_C, S_S, W_C, W_S (1 set per day)
	Pseudo-stochastic pulses	LAGEOS-1/2 : no pulses Sta/Ste/AJI : once-per-revolution in along-track only
Earth rotation parameters		X_P, Y_P, UT1-UTC (Piecewise linear, 1 set per day)
Geocenter coordinates		1 set per 30 days
Earth gravity field		**Estimated up to d/o 10/10** (1 set per 30 days)
Station coordinates		1 set per 30 days
Other parameters		Range biases for all stations (LEO) and for selected stations (LAGEOS)

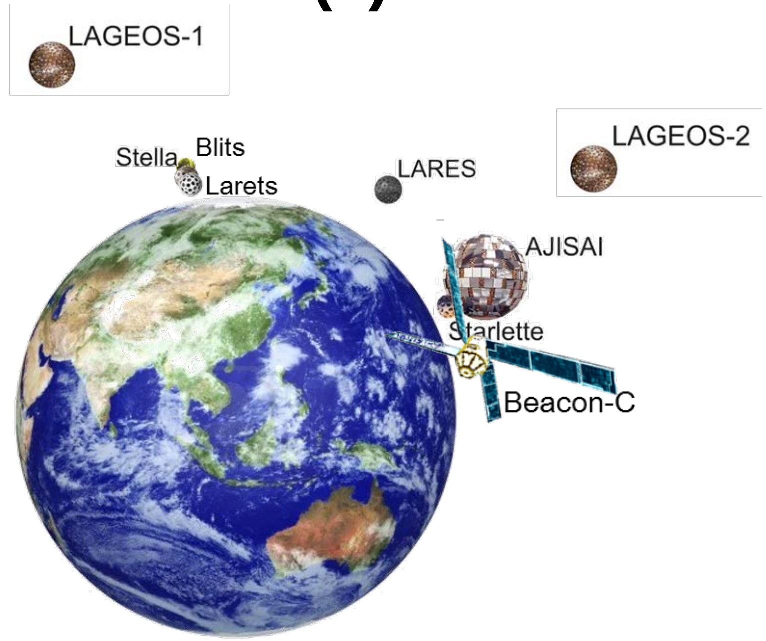

Up to 9 SLR satellites with different altitudes and different inclinations are used.

For LAGEOS-1/2: 10-day arcs are generated, for low orbiting satellites: 1-day arcs.

Different weighting of observations is applied: from 8mm for LAGEOS-1/2 to 50mm for Beacon-C.

Constraints introduced to regularize the normal equations (on GFC, pulses, EOPs).

(Sosnica, 2015)

Multi-Satellite SLR Solutions (2)

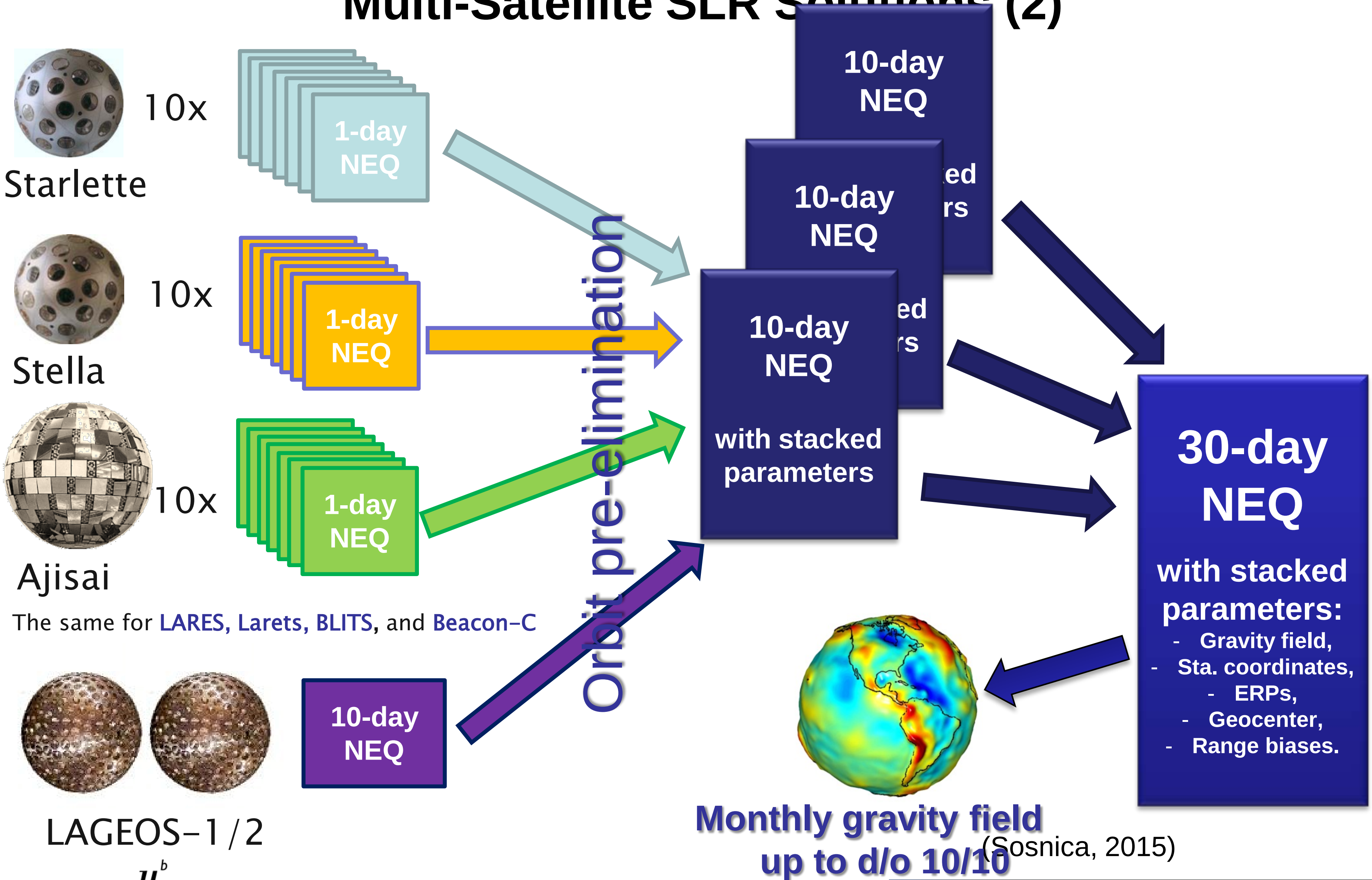

(Sosnica, 2015)

Multi-Satellite SLR Solution (3)

Table 5.9: Impact of different orbit parameterizations of LEO satellites on a posteriori sigma of unit weight and ERP (comparison w.r.t. IERS-08-C04).

Sol	Length of sol. [days]	Sets of oscul. elem.	Sets of dyn. par.	Stoch. pulses	RMS resid [mm]	X pole bias [μas]	X pole WRMS [μas]	Y pole bias [μas]	Y pole WRMS [μas]	LoD bias [μs/d]	LoD WRMS [μs/d]
A	7	1	7	S	7.78	57.7	269.8	-8.7	218.1	-3.6	106.5
B1	7	1	1	S	13.50	38.6	508.7	-6.8	442.3	-15.0	102.2
B2	7	7	7	S	13.42	20.7	395.7	4.4	400.1	-2.2	120.0
C1	7	1	7	S,R,W	7.52	57.7	269.8	-8.7	218.1	-3.7	116.5
C2	7	1	7	-	7.81	85.5	350.2	0.1	275.7	-36.3	140.4
D1	6	1	2	S	8.21	25.7	282.6	2.4	254.2	-25.4	119.7
D2	6	1	3	S	7.98	28.2	280.7	10.5	244.8	-13.5	115.1
D3	6	1	6	S	7.65	32.1	270.5	-4.3	217.9	-6.7	105.8

SLR only provides a **sparse coverage** of the orbits. In order to provide solutions of good quality, **most dynamic** solutions must be generated, e.g., by using long Arcs for the high orbiting LAGEOS satellite. Nevertheless, model deficiencies for the low orbiting satellites, e.g., due to air drag, need to be compensated by a small number of pseudo-stochastic parameters.

(Sosnica et al., 2014a)

Multi-Satellite SLR Solution (4)

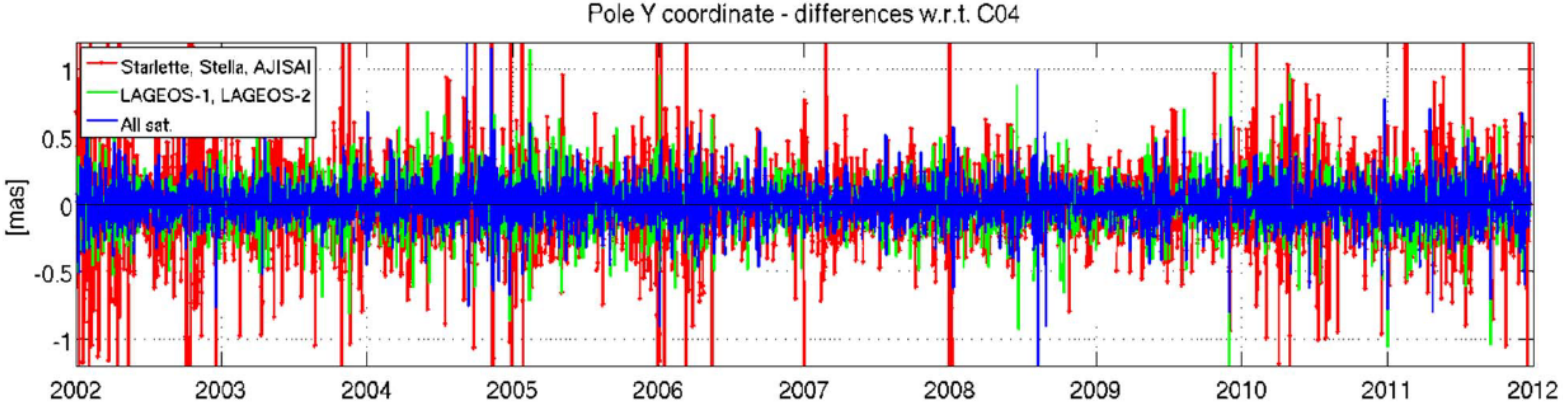

Solution type		X pole [μas] bias	X pole [μas] WRMS	Y pole [μas] bias	Y pole [μas] WRMS	LoD [μs] bias	LoD [μs] WRMS	Repeatability [mm] Up	Repeatability [mm] North	Repeatability [mm] East
LAGEOS-1/2	gravity up to 4/4	4.1	160.0	-8.0	155.2	6.1	57.0	11.1	10.2	12.3
LAGEOS-1/2	no gravity	45.8	168.5	-54.1	153.5	77.3	120.5	10.9	10.0	12.4
SLR-LEO	gravity up to 4/4	38.3	267.9	-7.8	217.6	-38.5	105.6	15.3	15.4	15.2
SLR-LEO	no gravity	190.1	437.5	-61.1	315.9	189.6	359.3	15.8	15.6	16.8
multi-SLR	gravity up to 4/4	6.4	148.9	8.5	140.3	6.3	56.3	11.3	11.2	11.7
multi-SLR	no gravity	83.7	153.1	63.3	156.7	75.8	121.7	11.1	11.3	11.8

SLR orbits are difficult to validate. The quality of the **geophysical parameters of interest**, which are co-estimated in the frame of the generalized orbit determination problem, provide the basis to assess the quality of the solution. Best results are obtained for a multi-satellite solution.

(Sosnica et al., 2014a)

Multi-Satellite SLR Solution (5)

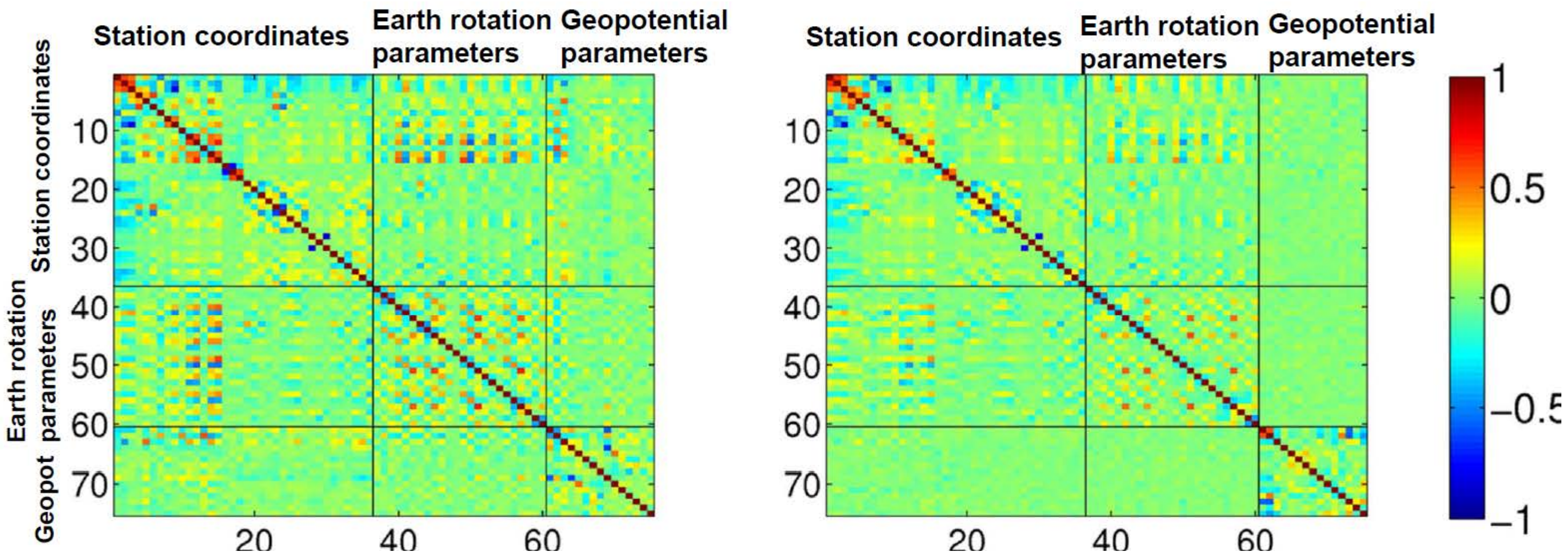

Multi-satellite solutions provide the advantage that the correlations between the estimated parameters (ERPs, geopotential coefficients, station coordinates) can be substantially reduced (better observation geometry due to the different orbital characterstics).

(Sosnica et al., 2014a)

Time-Variable Gravity from Non-Dedicated Satellites

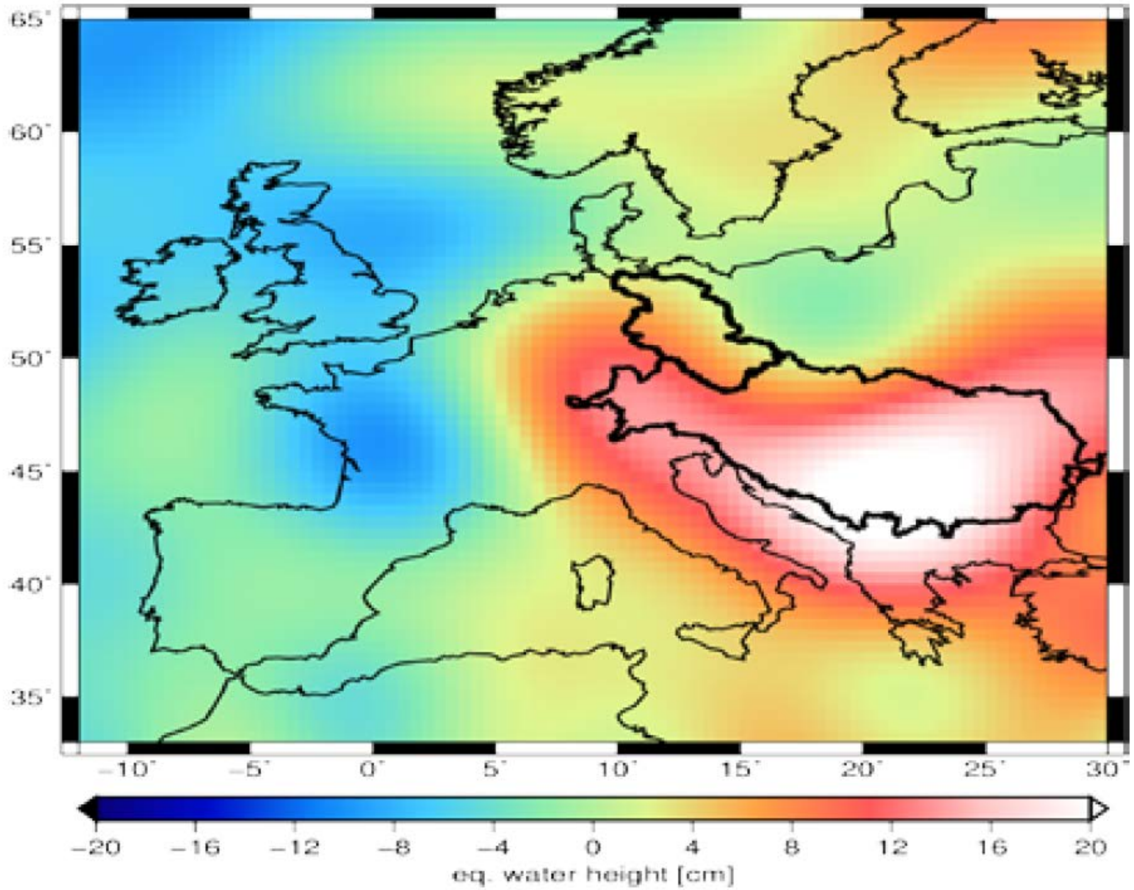

How well can time-variability by monitored by non-dedicated satellites tracked by SLR and GPS hl-SST?

Time-Variable Gravity from Non-Dedicated Satellites: SLR

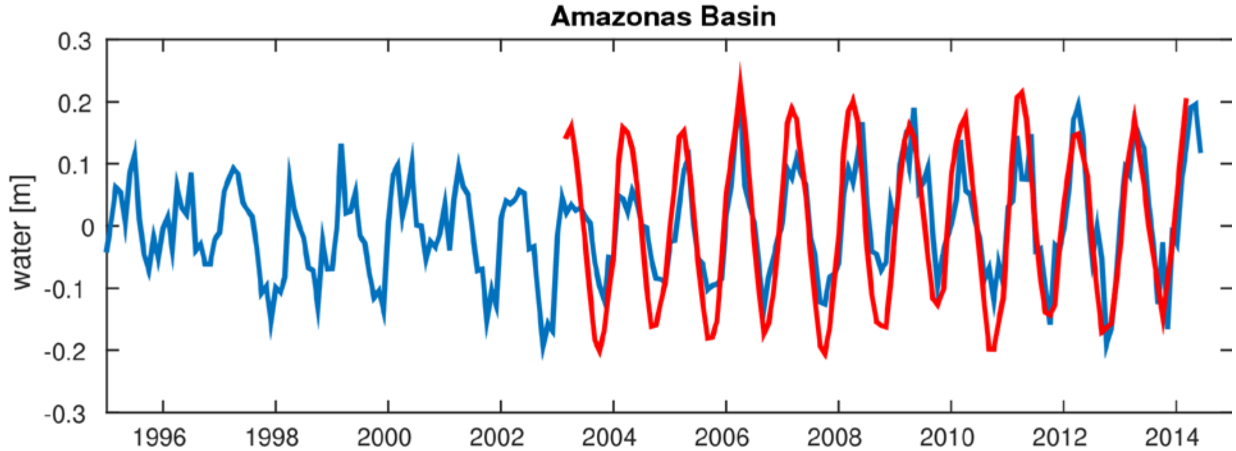

Up to d/o 10/10

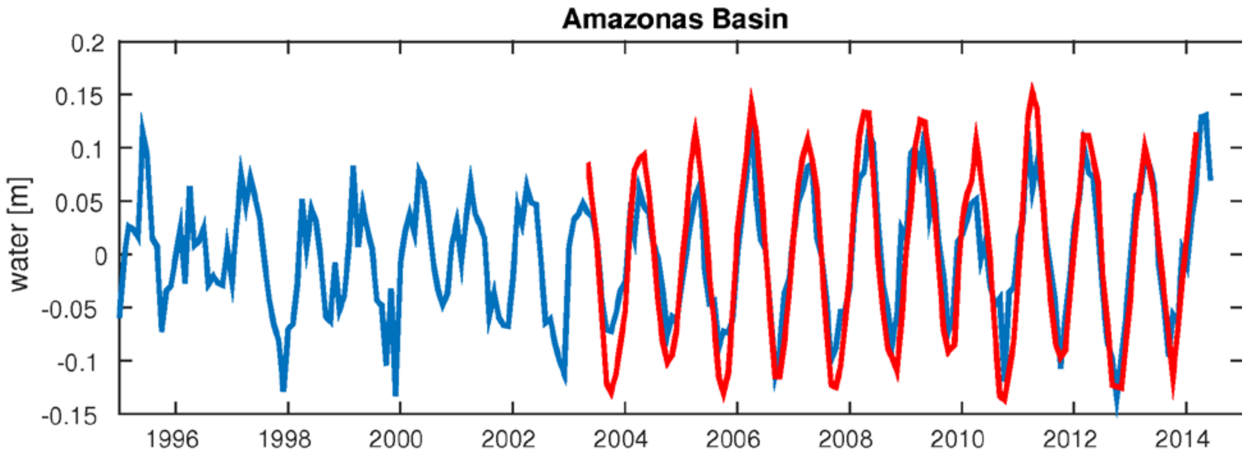

Up to d/o 6/6

(Sosnica et al., 2015b)

Time-Variable Gravity from Non-Dedicated Satellites: SLR

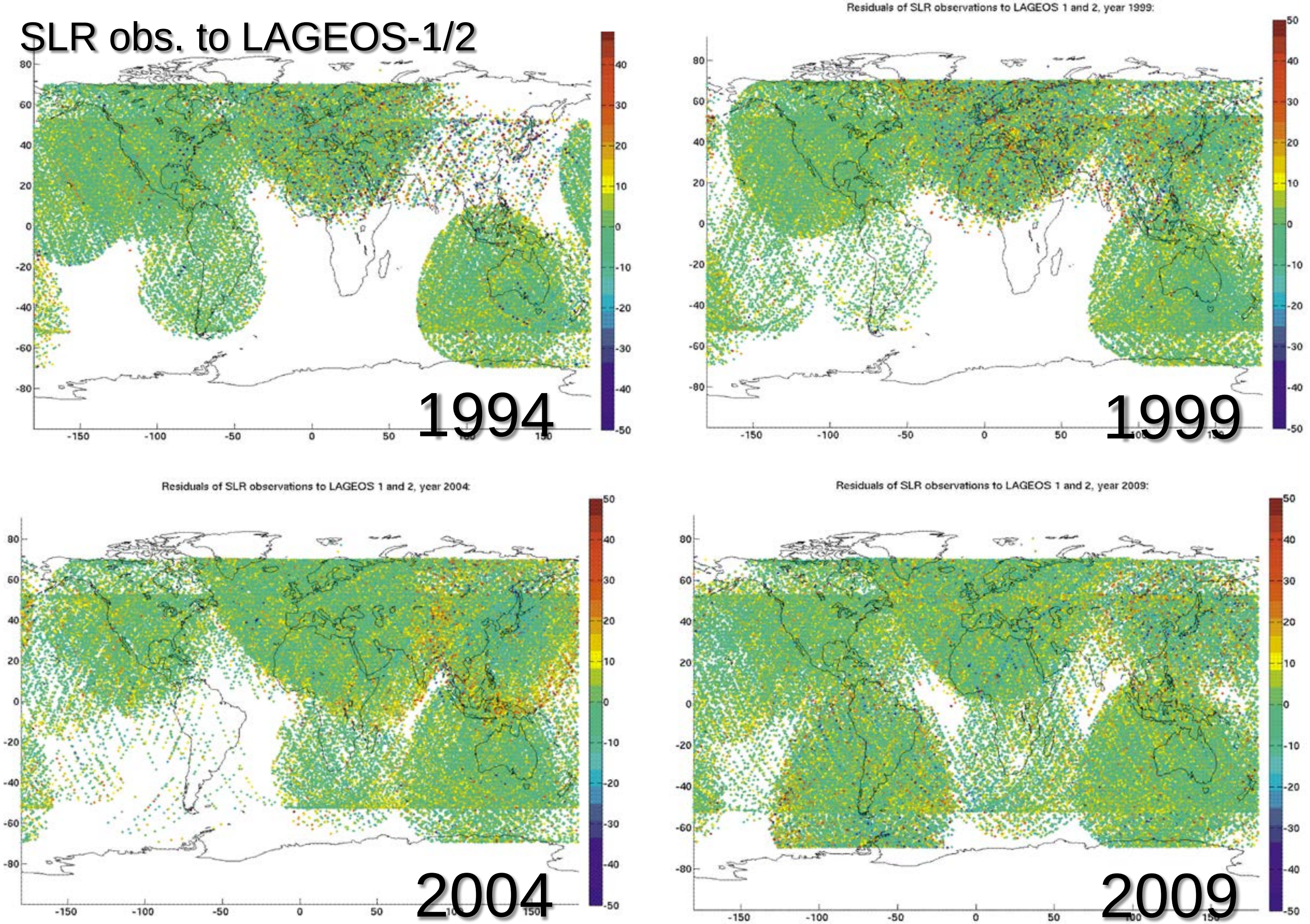

Wilhelm und Else Heraeus Autumn School
Global Gravity Field Modeling
from Satellite-to-Satellite Tracking Data

Time-Variable Gravity from Non-Dedicated Satellites: SLR

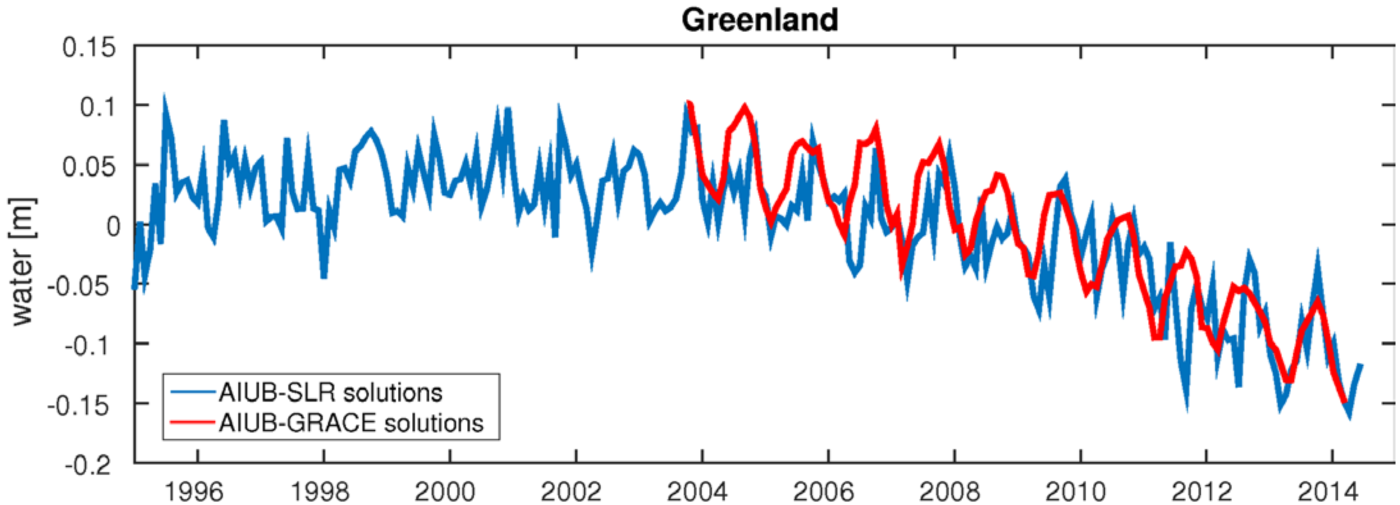

2005–2014: <u>accelerating</u> ice mass depletion

1995–2004
10 years without almost any changes

SLR and GRACE solutions up to d/o 6/6

1998

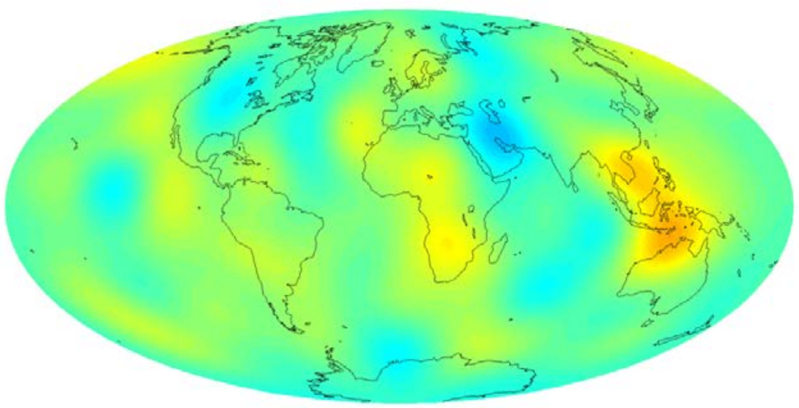

(Sosnica et al., 2015b)

Time-Variable Gravity from Non-Dedicated Satellites: GPS

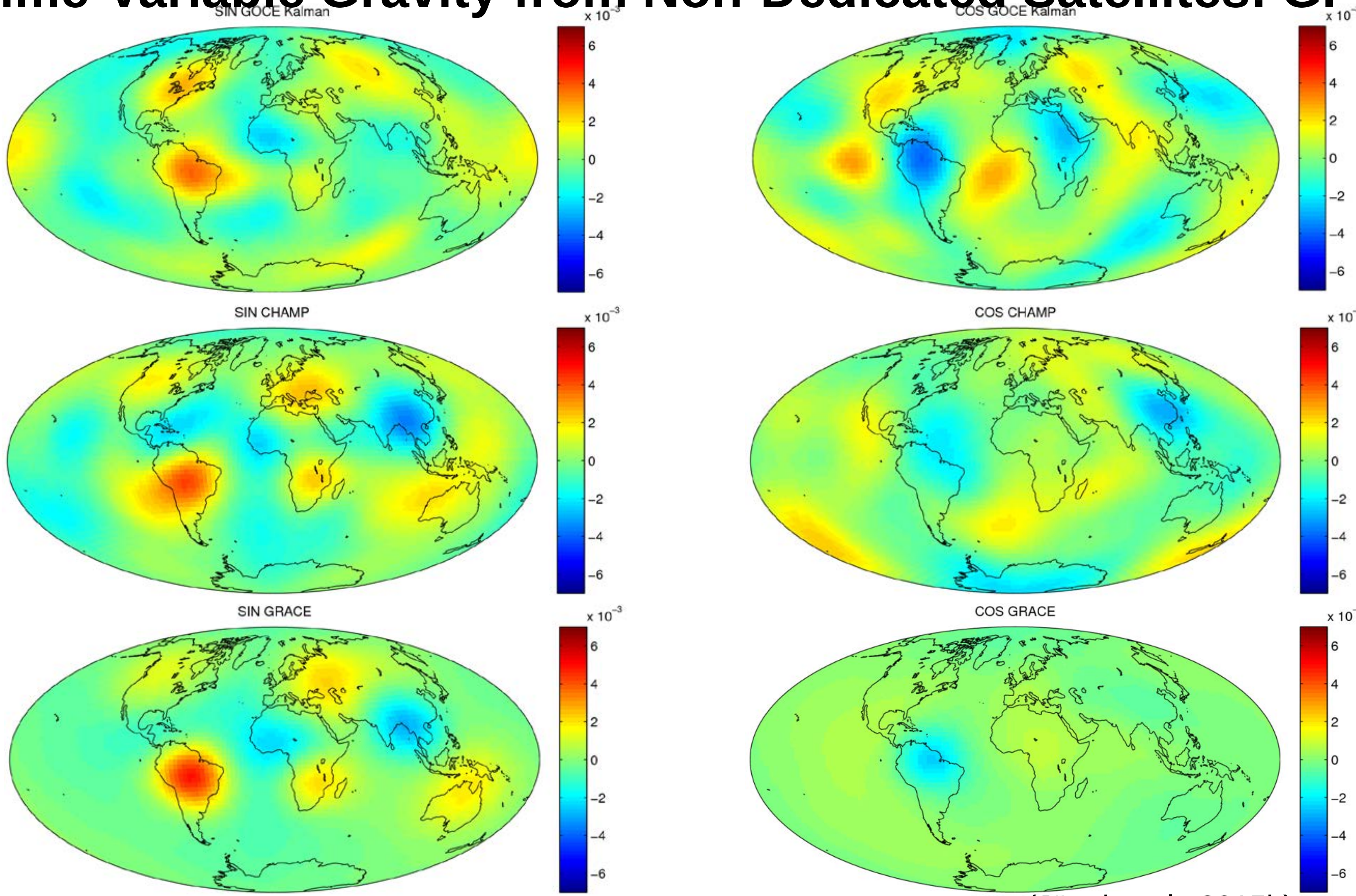

(Jäggi et al., 2015b)

Wilhelm und Else Heraeus Autumn School
Global Gravity Field Modeling from Satellite-to-Satellite Tracking Data

Time-Variable Gravity from Non-Dedicated Satellites: Swarm

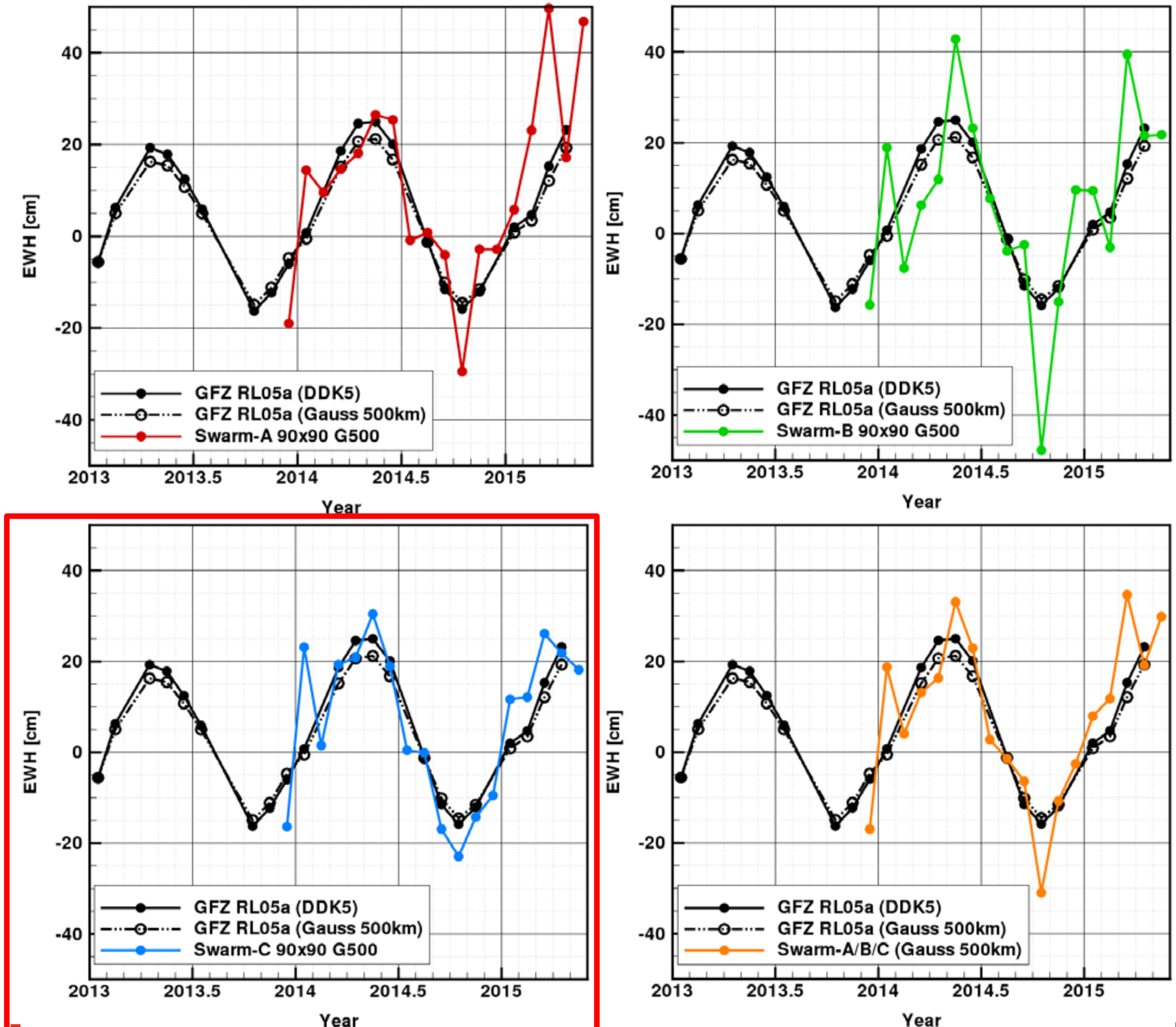

"True" signal:

- GFZ-RL05a (DDK5-filtered)

"Comparison" signal:

- GFZ-RL05a (500km Gauss)

Swarm signal:

- 90x90 solutions (Gauss-filtered)

Result:

- Best agreement for Swarm-C

(Jäggi et al., 2015b)

Time-Variable Gravity from Non-Dedicated Satellites: Combo

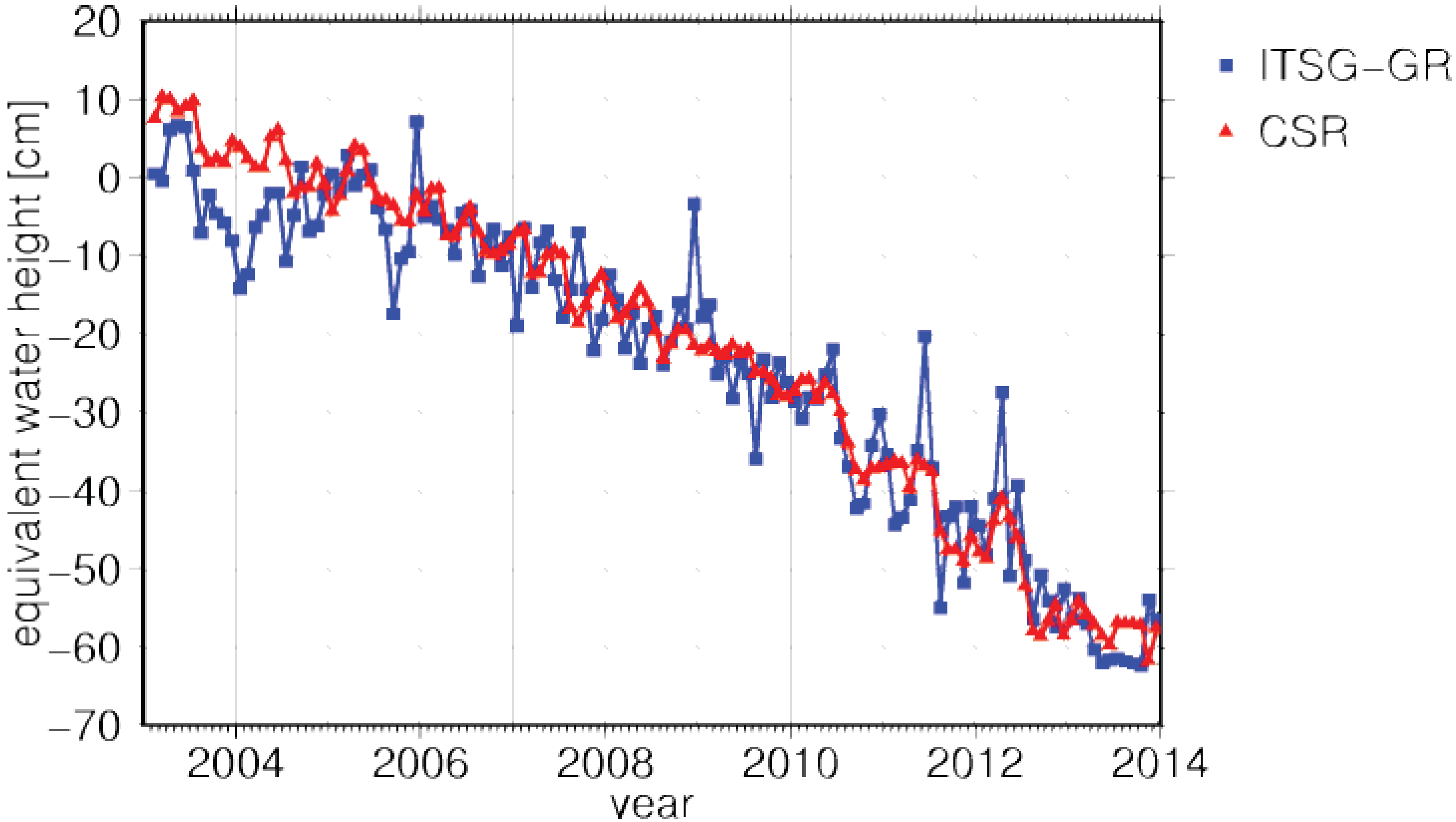

Combination of a multitude of LEO satellites tracked by GPS hl-SST provides
Promising recoveries also for smaller signals.

(Zehentner et al., 2015)

Time-Variable Gravity from Non-Dedicated Satellites: Combo

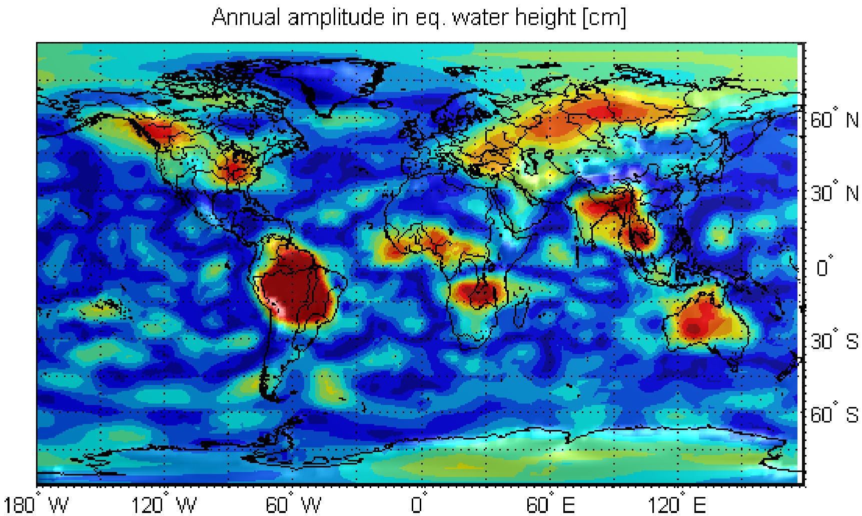

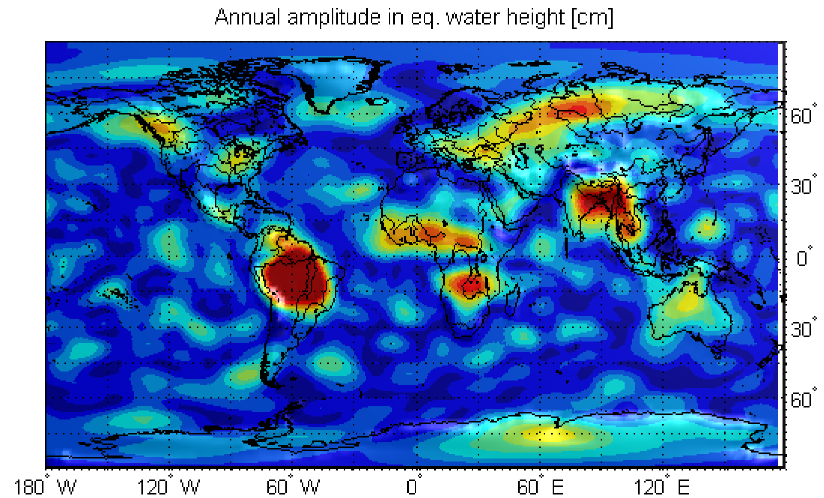

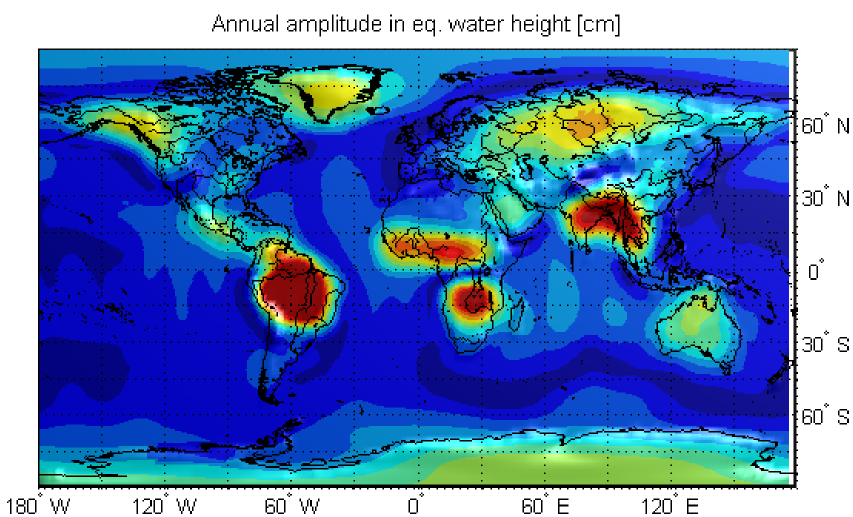

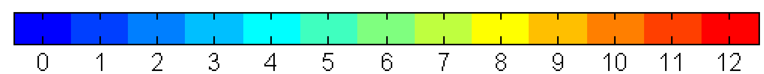

Combination of hl-SST solutions with SLR reduces the variations over oceans and some spurious signals.

(Sosnica et al., 2014b)

Time-Variable Gravity from Non-Dedicated Satellites: Combo

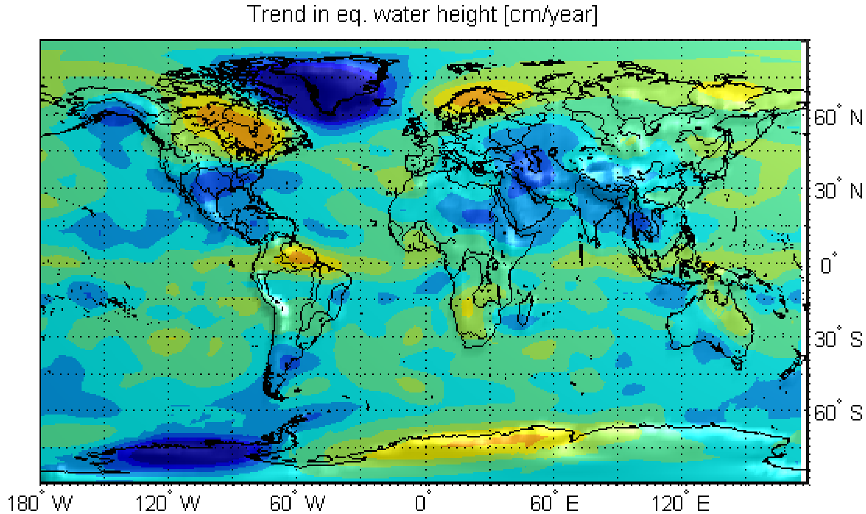

hl-SST

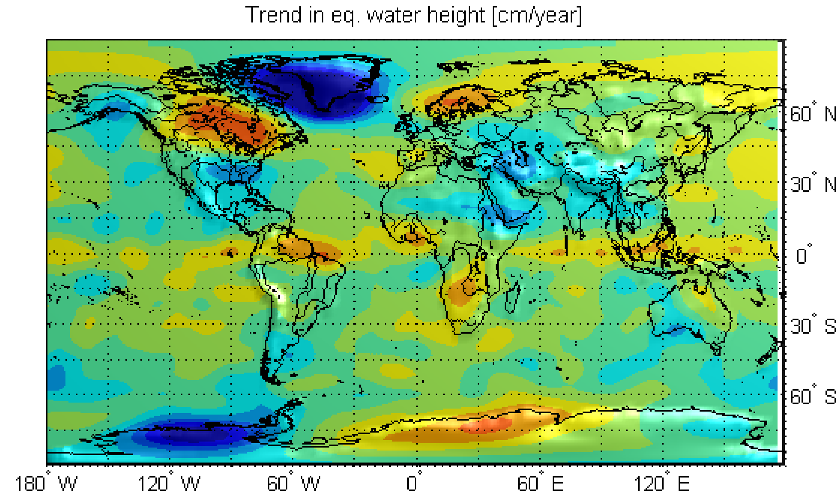

SLR+hl-SST

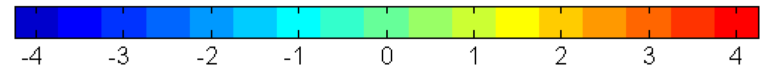

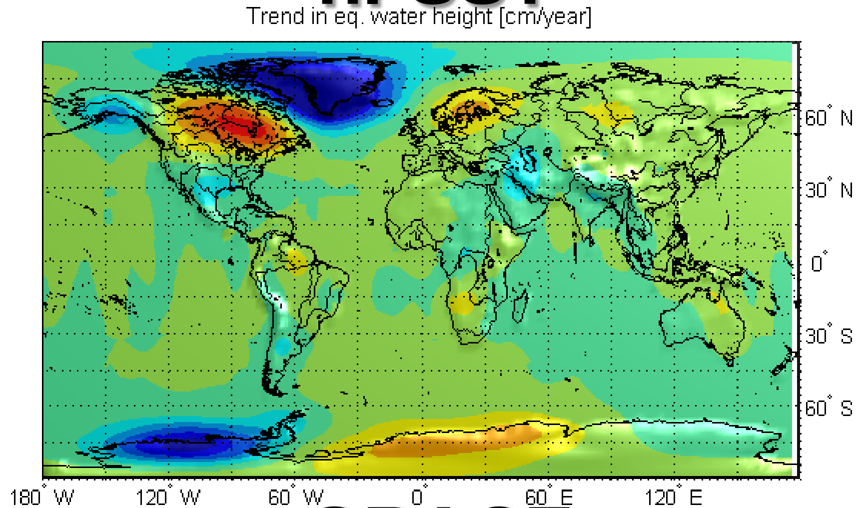

GRACE

(Sosnica et al., 2014b)


Thank you for your attention

Literature (1)

Beutler, G. (2005) Methods of Celestial Mechanics. Vol 1: Physical, Mathematical, and Numerical Principles. Springer, ISBN 3-540-40749-9

Blewitt, G. (1997): Basics of the GPS Technique: Observation Equations, in *Geodetic Applications of GPS*, Swedish Land Survey, pp. 10-54, available at http://www.sbg.ac.at/mat/staff/revers/lectures/2006_2007/GPS/GPSBasics.pdf

Bigazzi, A., B. Frommknecht (2010): Note on GOCE instruments positioning, XGCE-GSEG-EOPG-TN-09-0007, Issue 3.1, European Space Agency, available at http://earth.esa.int/download/goce/GOCE-LRR-GPS-positioning-Memo_3.1_[XGCE-GSEG-EOPG-TN-09-0007%20v3.1].pdf

Bock, H., R. Dach, A. Jäggi, G. Beutler (2009): High-rate GPS clock corrections from CODE: Support of 1 Hz applications. *Journal of Geodesy*, 83(11), 1083-1094, doi: 10.1007/s00190-009-0326-1

Bock, H., A. Jäggi, G. Beutler, U. Meyer (2014): GOCE: Precise orbit determination for the entire mission. *Journal of Geodesy*, 88(11), 1047-1060, doi: 10.1007/s00190-014-0742-8

Wilhelm und Else Heraeus Autumn School
Global Gravity Field Modeling
from Satellite-to-Satellite Tracking Data

Literature (2)

Dach, R., E. Brockmann, S. Schaer, G. Beutler, M. Meindl, L. Prange, H. Bock, A. Jäggi, L. Ostini (2009): GNSS processing at CODE: status report, *Journal of Geodesy*, 83(3-4), 353-366, doi: 10.1007/s00190-008-0281-2

Flohrer, C. (2008): Mutual Validation of Satellite-Geodetic Techniques and its Impact on GNSS Orbit Modeling. *Geodätisch-geophysikalische Arbeiten in der Schweiz*, 75, Schweizerische Geodätische Kommission, available at http://www.sgc.ethz.ch/sgc-volumes/sgk-75.pdf

Hackel, C., O. Montenbruck (2015): Impact of Improved Satellite Dynamics on Reduced-Dynamic Orbits, in preparation

Jäggi, A., U. Hugentobler, G. Beutler (2006): Pseudo-stochastic orbit modeling techniques for low-Earth satellites. *Journal of Geodesy*, 80(1), 47-60, doi: 10.1007/s00190-006-0029-9

Jäggi, A. (2007): Pseudo-Stochastic Orbit Modeling of Low Earth Satellites Using the Global Positioning System. *Geodätisch-geophysikalische Arbeiten in der Schweiz*, 73, Schweizerische Geodätische Kommission, available at http://www.sgc.ethz.ch/sgc-volumes/sgk-73.pdf

Literature (3)

Jäggi, A., R. Dach, O. Montenbruck, U. Hugentobler, H. Bock, G. Beutler (2009): Phase center modeling for LEO GPS receiver antennas and its impact on precise orbit determination. *Journal of Geodesy*, 83(12), 1145-1162, doi: 10.1007/s00190-009-0333-2

Jäggi, A., H. Bock, L. Prange, U. Meyer, G. Beutler (2011a): GPS-only gravity field recovery with GOCE, CHAMP, and GRACE. *Advances in Space Research*, 47(6), 1020-1028, doi: 10.1016/j.asr.2010.11.008

Jäggi, A., L. Prange, U. Hugentobler (2011b): Impact of covariance information of kinematic positions on orbit reconstruction and gravity field recovery. *Advances in Space Research*, 47(9), 1472-1479, doi: 10.1016/j.asr.2010.12.009

Jäggi, A., H. Bock, U. Meyer (2014): GOCE precise orbit determination for the entire Mission - challenges in the final mission phase. ESA Special Publications 728

Literature (4)

Jäggi, A., H. Bock, U. Meyer, G. Beutler, J. van den Ijssel (2015a): GOCE: assessment of GPS-only gravity field determination. *Journal of Geodesy*, 89(1), 33-48. doi: 10.1007/s00190-014-0759-z

Jäggi, A., C. Dahle, D. Arnold, H. Bock, U. Meyer, G. Beutler, J. van den IJSSel (2015b): Swarm kinematic orbits and gravity fields from 18 months of GPS data. *Advances in Space Research*, in review.

Mayer-Gürr, T., K.H. Ilk, A. Eicker, M. Feuchtinger (2005): ITG-CHAMP01: a CHAMP gravity field model from short kinematic arcs over a one-year observation period. *Journal of Geodesy*, 78(7-8), 462-480. doi: 10.1007/s00190-004-0413-2

Meyer, U., A. Jäggi, G. Beutler, H. Bock (2015): The impact of common versus separate estimation of orbit parameters on GRACE gravity field solutions. *Journal of Geodesy*, 89(7), 685-696. doi: 10.1007/s00190-015-0807-3

Wilhelm und Else Heraeus Autumn School
Global Gravity Field Modeling
from Satellite-to-Satellite Tracking Data

Literature (5)

Sośnica, K., A. Jäggi, D. Thaller, R. Dach, G. Beutler (2014a): Contribution of Starlette, Stella, and AJISAI to the SLR-derived global reference frame. *Journal of Geodesy*, 88(8), 789-804. doi: 10.1007/s00190-014-0722-z

Sośnica, K., A. Jäggi, U. Meyer, M. Weigelt, T. van Dam, N. Zehentner, T. Mayer-Gürr (2014b): Time varying gravity from SLR and combined SLR and high-low satellite-to-satellite tracking data. GRACE Science Team Meeting 2014, 29th September to 1st October 2014, Potsdam, Germany

Sośnica, K., D. Thaller, R. Dach, P. Steigenberger, G. Beutler, D. Arnold, A. Jäggi (2015a): Satellite laser ranging to GPS and GLONASS. *Journal of Geodesy*, 89(7), 725-743. doi: 10.1007/s00190-015-0810-8

Sośnica, K., A. Jäggi, U. Meyer, D. Thaller, G. Beutler, D. Arnold, R. Dach (2015b): Time variable Earth’s gravity field from SLR satellites. *Journal of Geodesy*, 89(10), 945-960. doi: 10.1007/s00190-015-0825-1

Literature (6)

Sośnica, K. (2015): Determination of Precise Satellite Orbits and Geodetic Parameters using Satellite Laser Ranging. *Geodätisch-geophysikalische Arbeiten in der Schweiz*, 93, Schweizerische Geodätische Kommission, available at http://www.sgc.ethz.ch/sgc-volumes/sgk-93.pdf

Svehla, D., M. Rothacher (2004): Kinematic Precise Orbit Determination for Gravity Field Determination, in *A Window on the Future of Geodesy*, edited by F. Sanso, pp. 181-188, Springer, doi: 10.1007/b139065

Visser, P., J. van den IJssel, T. van Helleputte, H. Bock, A. Jäggi, G. Beutler, D. Švehla, U. Hugentobler, M. Heinze (2009): Orbit determination for the GOCE satellite, *Advances in Space Research*, 43(5), 760-768, doi: 10.1016/j.asr.2008.09.016

Visser, P.N.A.M., J.A.A. van den IJssel (2015): Calibration and validation of individual GOCE accelerometers by precise orbit determination. *Journal of Geodesy*, in press, doi: 10.1007/s00190-015-0850-0

Zehentner, N., T. Mayer-Gürr (2015): Precise orbit determination based on raw GPS measurements. *Journal of Geodesy*, in review.